SIMULATING IRRADIANCE VARIABILITY IN AN URBAN ENVIRONMENT USING GEOGRAPHIC INFORMATION SYSTEMS AND QUANTIFYING IMPACTS ON THE ENERGY AND ECONOMIC PERFORMANCE OF ROOFTOP PHOTOVOLTAICS

by

Todd Gilbert Bowles

A thesis submitted to the faculty of
The University of Utah
in partial fulfillment of the requirements for the degree of

Master of Science

Department of Mechanical Engineering

The University of Utah

December 2017

The University of Utah Graduate School

STATEMENT OF THESIS APPROVAL

The thesis of **Todd Gilbert Bowles**
has been approved by the following supervisory committee members:

Amanda Smith,	Chair	**19 Oct 2017** Date Approved
Kuan Chen,	Member	**16 Oct 2017** Date Approved
Mathieu Francoeur,	Member	**16 Oct 2017** Date Approved

by **Tim Ameel**, Chair/Dean of
the Department/College/School of **Mechanical Engineering**
and by **David B. Kieda**, Dean of The Graduate School.

ABSTRACT

The transformation to urban living is becoming increasingly popular. The energy demand for these regions is continually increasing and is currently met with use of fossil fuels, at the expense of human health and well being. The implementation of renewable technology in these urban areas is necessary to alleviate low air quality and illness that result from fossil fuel consumption at a localized environment. Photovoltaic (PV) systems are a leading renewable technology adopted by many residents and property owners for use in small- and large-scale operations. Currently, irradiance data are estimated using macroscale models that are used to assess PV potential for a given region, while neglecting the local topography and its shading effects. This approach does not capture the solar availability at a localized level, which can be reflected in the anticipated PV power generation and system's Levelized Cost of Electricity (LCOE). With the implementations of Geographic Information System (GIS) software coupled with aerial Light Detection and Ranging (LiDAR) topography data, a model that captures the localized irradiance is achievable and essential for more accurate estimations while assessing the PV potential for a given region. Using this approach, a solar radiation model was created with inclusion of the local topography capturing the irradiation variability within Salt Lake Valley at a 3 meter resolution. With use of this model, better assessments regarding potential PV power generation systems are achievable, giving consumers confidence in their investment and the anticipated rate of return.

To my family, friends, and future engineers. Go Utes!

CONTENTS

ABSTRACT . . . . . **iii**

LIST OF FIGURES . . . . . **vi**

LIST OF TABLES . . . . . **ix**

ABBREVIATIONS AND SYMBOLS . . . . . **x**

ACKNOWLEDGEMENTS . . . . . **xi**

CHAPTERS

1. INTRODUCTION **1**

2. GRASS **4**

2.1 Generate Digital Elevation Model 4
2.2 R.Sun 5
2.2.1 Albedo 8
2.2.2 Linke Turbidity Coefficient 9
2.3 Photovoltaic Cell Efficiency 11
2.4 Inverter 12
2.4.1 String Inverter 12
2.4.2 Direct Current Power Optimizer 12
2.4.3 Micro Inverter 13
2.5 Tilt Angle 13

3. CASE STUDY SALT LAKE VALLEY **16**

3.1 Annual Irradiation Distribution Within Salt Lake Valley 16
3.1.1 Discussion 19
3.2 Tilt Angle Variance in Salt Lake Valley 19
3.2.1 Varying Tilt Angles at Winter Solstice 21
3.2.1.1 Winter Solstice Tilt Angle Results 22
3.2.2 Varying Tilt Angles at Summer Solstice 33
3.2.2.1 Summer Solstice Tilt Angle Results 33
3.2.3 Varying Efficiencies at Winter Solstice with Tilt Angle of **10º** and **40º** . . . 43
3.2.3.1 Efficiency at Winter Solstice Results 44
3.2.4 Varying Efficiency at Summer Solstice with Tilt Angle of **10º** and **40º** . . 59
3.2.4.1 Efficiency at Summer Solstice Results 60
3.3 Levelized Cost of Electricity 75

4. CONCLUSION AND FUTURE WORK **81**

REFERENCES **84**

LIST OF FIGURES

1.1 Figure showing the Salt Lake Valley as the region of interest. Courtesy of Google Earth. 3

2.1 Figure shown to demonstrate the quality of a DEM using LiDAR data points for the Merrill Engineering Building at the University of Utah. 6

2.2 Figure showing the DEM of Salt Lake Valley used for modeling irradiation. . . 7

3.1 Figure showing the irradiance distribution given by the NREL model with a color representing $4.5 - 5\frac{kWh}{m^2 day}$ 17

3.2 Figure showing the irradiance distribution throughout Salt Lake Valley 18

3.3 Figure showing the Salt Lake Valley PV electricity production at winter solstice using a tilt angle of 0^o. 23

3.4 Figure showing the Salt Lake Valley PV electricity production at winter solstice using a tilt angle of 5^o. 24

3.5 Figure showing the Salt Lake Valley PV electricity production at winter solstice using a tilt angle of 10^o. 25

3.6 Figure showing the Salt Lake Valley PV electricity production at winter solstice using a tilt angle of 15^o. 26

3.7 Figure showing the Salt Lake Valley PV electricity production at winter solstice using a tilt angle of 20^o. 27

3.8 Figure showing the Salt Lake Valley PV electricity production at winter solstice using a tilt angle of 25^o. 28

3.9 Figure showing the Salt Lake Valley PV electricity production at winter solstice using a tilt angle of 30^o. 29

3.10 Figure showing the Salt Lake Valley PV electricity production at winter solstice using a tilt angle of 35^o. 30

3.11 Figure showing the Salt Lake Valley PV electricity production at winter solstice using a tilt angle of 40^o. 31

3.12 Figure showing the Salt Lake Valley PV electricity production at summer solstice using a tilt angle of 0^o. 34

3.13 Figure showing the Salt Lake Valley PV electricity production at summer solstice using a tilt angle of 5^o. 35

3.14 Figure showing the Salt Lake Valley PV electricity production at summer solstice using a tilt angle of 10^o. 36

3.15 Figure showing the Salt Lake Valley PV electricity production at summer solstice using a tilt angle of 15^o. 37

3.16 Figure showing the Salt Lake Valley PV electricity production at summer solstice using a tilt angle of 20^o. 38

3.17 Figure showing the Salt Lake Valley PV electricity production at summer solstice using a tilt angle of 25^o. 39

3.18 Figure showing the Salt Lake Valley PV electricity production at summer solstice using a tilt angle of 30^o. 40

3.19 Figure showing the Salt Lake Valley PV electricity production at summer solstice using a tilt angle of 35^o. 41

3.20 Figure showing the Salt Lake Valley PV electricity production at summer solstice using a tilt angle of 40^o. 42

3.21 Figure showing the Salt Lake Valley PV electricity production at winter solstice with a 10^o tilt and $\eta_{PV} = 12\%$. 45

3.22 Figure showing the Salt Lake Valley PV electricity production at winter solstice with a 10^o tilt and $\eta_{PV} = 14\%$. 46

3.23 Figure showing the Salt Lake Valley PV electricity production at winter solstice with a 10^o tilt and $\eta_{PV} = 16\%$. 47

3.24 Figure showing the Salt Lake Valley PV electricity production at winter solstice with a 10^o tilt and $\eta_{PV} = 18\%$. 48

3.25 Figure showing the Salt Lake Valley PV electricity production at winter solstice with a 10^o tilt and $\eta_{PV} = 20\%$. 49

3.26 Figure showing the Salt Lake Valley PV electricity production at winter solstice with a 10^o tilt and $\eta_{PV} = 22\%$. 50

3.27 Figure showing the Salt Lake Valley PV electricity production at winter solstice with a 10^o tilt and $\eta_{PV} = 24\%$. 51

3.28 Figure showing the Salt Lake Valley PV electricity production at winter solstice with a 40^o tilt and $\eta_{PV} = 12\%$. 52

3.29 Figure showing the Salt Lake Valley PV electricity production at winter solstice with a 40^o tilt and $\eta_{PV} = 14\%$. 53

3.30 Figure showing the Salt Lake Valley PV electricity production at winter solstice with a 40^o tilt and $\eta_{PV} = 16\%$. 54

3.31 Figure showing the Salt Lake Valley PV electricity production at winter solstice with a 40^o tilt and $\eta_{PV} = 18\%$. 55

3.32 Figure showing the Salt Lake Valley PV electricity production at winter solstice with a 40^o tilt and $\eta_{PV} = 20\%$. 56

3.33 Figure showing the Salt Lake Valley PV electricity production at winter solstice with a 40^o tilt and $\eta_{PV} = 22\%$. 57

3.34 Figure showing the Salt Lake Valley PV electricity production at winter solstice with a 40^o tilt and $\eta_{PV} = 24\%$. 58
3.35 Figure showing the Salt Lake Valley PV electricity production at summer solstice with a 10^o tilt and $\eta_{PV} = 12\%$. 61
3.36 Figure showing the Salt Lake Valley PV electricity production at summer solstice with a 10^o tilt and $\eta_{PV} = 14\%$. 62
3.37 Figure showing the Salt Lake Valley PV electricity production at summer solstice with a 10^o tilt and $\eta_{PV} = 16\%$. 63
3.38 Figure showing the Salt Lake Valley PV electricity production at summer solstice with a 10^o tilt and $\eta_{PV} = 18\%$. 64
3.39 Figure showing the Salt Lake Valley PV electricity production at summer solstice with a 10^o tilt and $\eta_{PV} = 20\%$. 65
3.40 Figure showing the Salt Lake Valley PV electricity production at summer solstice with a 10^o tilt and $\eta_{PV} = 22\%$. 66
3.41 Figure showing the Salt Lake Valley PV electricity production at summer solstice with a 10^o tilt and $\eta_{PV} = 24\%$. 67
3.42 Figure showing the Salt Lake Valley PV electricity production at summer solstice with a 40^o tilt and $\eta_{PV} = 12\%$. 68
3.43 Figure showing the Salt Lake Valley PV electricity production at summer solstice with a 40^o tilt and $\eta_{PV} = 14\%$. 69
3.44 Figure showing the Salt Lake Valley PV electricity production at summer solstice with a 40^o tilt and $\eta_{PV} = 16\%$. 70
3.45 Figure showing the Salt Lake Valley PV electricity production at summer solstice with a 40^o tilt and $\eta_{PV} = 18\%$. 71
3.46 Figure showing the Salt Lake Valley PV electricity production at summer solstice with a 40^o tilt and $\eta_{PV} = 20\%$. 72
3.47 Figure showing the Salt Lake Valley PV electricity production at summer solstice with a 40^o tilt and $\eta_{PV} = 22\%$. 73
3.48 Figure showing the Salt Lake Valley PV electricity production at summer solstice with a 40^o tilt and $\eta_{PV} = 24\%$. 74
3.49 Figure showing the LCOE of Salt Lake Valley for the residential sector 78
3.50 Figure showing the LCOE of Salt Lake Valley for the commercial sector 79

LIST OF TABLES

3.1 Parametric analysis of Salt Lake Valley at winter and summer solstice 21

ABBREVIATIONS AND SYMBOLS

Abbreviation	Description
PV	Photovoltaic
DOE	Department of Energy
NREL	National Renewable Energy Laboratory
NSRD	National Solar Radiation Database
GIS	Geographic Information System
GRASS	Geographic Resource Analysis Support System
LiDAR	Light Detection and Ranging
DEM	Digital Elevation Model
MODIS	Moderate Resolution Imaging Spectroradiometer
LTC	Linke Turbidity Coefficient
PSM	Physical Solar Model
STC	Standard Test Conditions
DC	Direct Current
AC	Alternating Current
MPPT	Max Power Point

Symbol	Units	Description
α	Degrees	Sun Altitude Angle
β	Degrees	Tilt Angle
T_{L1}	-	Modified Turbidity Coefficient
B_{ncl}	W/m^2	Clear Sky Direct Normal Irradiance
η_{PV}	%	Relative PV Cell Efficiency
η_{In}	%	Inverter Efficiency
T_{amb}	^oC	Ambient Temperature
η_o	%	PV Cell Efficiency
E	Watt	Energy Rate
A	m^2	Area
L	Degrees	Latitude
n	#	Calender Day Number
I_o	W/m^2	Irradiation
V_{MPP}	Volt	Max Power Point Voltage
I_{MPP}	Amp	Max Power Point Current
C_i	$	Initial Cost
I_G	$	Government Incentives
LCOE	$/kWh	Levelized Cost of Electricity
d	%	Annual Degradation

ACKNOWLEDGEMENTS

Several faculty members and student peers offered up their time to help in the development of this thesis and to the success of my academic career. I would like to thank each professor who taught me mathematics and engineering concepts both at an undergraduate and graduate level. Additionally, I thank my committee members, especially Dr. Smith for the time and guidance efforts provided to assist in this successful outcome. Dr. Smith spent countless hours patiently listening to my frustrations and roadblocks while learning the GRASS software, and challenged me to figure out each step necessary to create the model presented in this work. She also funded a new high-end computer to support the massive data sets, without which computing the simulations would have been much more difficult. I would also like to thank each person in the Site Specific Energy Lab for their help in both research and coursework, especially Carlo, Zahra, Aowabin, and Thomas. I had valuable discussions with them and they were always willing to offer help when needed.

I also give thanks to Dr. Merryweather and Dr. Tan for trusting in my ability to be a TA and grader for their courses. I learned a great deal about best practices for conveying information in both written and verbal contexts. I enjoyed the student and faculty interaction, which was invaluable.

Finally, I would like to thank my family, wife, and children. My parents and siblings encouraged me throughout this process, which gave me confidence and will power. Most importantly, I thank my wife and children for their patience and understanding of my long days and stressful weeks. Their support and love was the most valuable contribution to this achievement. My success is completely dedicated to them, as they were the number one reason for enduring this long road.

CHAPTER 1

INTRODUCTION

The transformation to urban living is becoming increasingly popular. As of 2011, 52% of the global population lives within urban regions, which is expected to grow to 68% by 2050 [1]. These population dense areas are continuously growing, which necessitates an increase in energy demands. Currently, the energy demands are primarily met with the use of fossil fuels, as 40% of CO_2 emissions attributed to the U.S. are associated with urban living [2]. Because of the negative effects that result from burning fossil fuels, renewable technologies are becoming increasingly popular for both residential and commercial sectors.

Photovoltaic (PV) technology is one of the leading renewable energy resources due to its low maintenance and recent decline in equipment cost. The Department of Energy (DOE) set a goal in 2010 to reduce the installed PV system cost on a utility scale to \$1/Watt through incentives and programs by 2017 [3]. Currently, residential and commercial property owners are eligible for a 30% federal tax incentive on the total installation cost. Residential owners are also eligible for a state tax credit worth 25% of the installation cost, up to \$2,000. Commercial owners are offered a similar state tax credit worth 10% of the installation cost, up to \$50,000 [4]. Solar PV installations have exponentially increased in the past decade due to these incentives and installation affordability. Utah is now number six in the country for PV power generation with 2016 having the highest growth rate, taking installations to a capacity of over 1.4GW [5–7].

Currently, PV installation companies often rely on irradiation data provided by the National Renewable Energy Laboratory's (NREL's) National Solar Radiation Database [8] (NSRD), which is used for determining PV array sizing, based on the customer's electricity needs. This database contains irradiance data at a 4 kilometer resolution, of which the magnitude varies minimally throughout large regions: for the purpose of this thesis, most

of Salt Lake Valley. The local topography within an urban area plays a vital role in the availability of collectible solar radiation at a potential site, and the shadowing effects from buildings, trees, and mountain ranges are necessary factors for consideration. PV assessments may not account for these localized settings, which can dramatically affect the irradiation collected, resulting in lower than anticipated power generation and return on investment [9–13]. To alleviate the uncertainty of these shadowing effects, a localized model is necessary to address these factors, thereby allowing for optimized PV site layout and positioning. To address these issues, the objectives of this work are as follows:

- Develop a clear sky solar radiation model that accounts for the local topography of a given region.
- Assess a PV system's Levelized Cost of Electricity (LCOE) relative to current electricity pricing for commercial and residential sectors.
- Quantify the variability in annual irradiation, potential electricity production, and LCOE for a rooftop solar PV system in the Salt Lake Valley.

Geographic Information System (GIS) technology is a powerful tool used to analyze and process spacial or geographic data, which can be used to address these questions [9, 14–16]. For this assessment, Geographic Resource Analysis Support System (GRASS) [17] is the software tool package of choice. GRASS is an open sourced software suite originally directed and managed by the U.S. Army that is continually improved and updated. This software, coupled with aerial Light Detection and Ranging (LiDAR) [18] topography data, was used to create a model of the Salt Lake Valley to obtain more accurate irradiance estimations and determine the variability of solar radiation throughout the region; the model boundaries are shown in Figure 1.1. In general, this accuracy is dependent upon the topography data quality and resolution, which is 0.5m for the obtained data set. The method described in this manuscript can be used at any location for which LiDAR topography data are available, which can be used and modified accordingly to better address current PV system assessments [19].

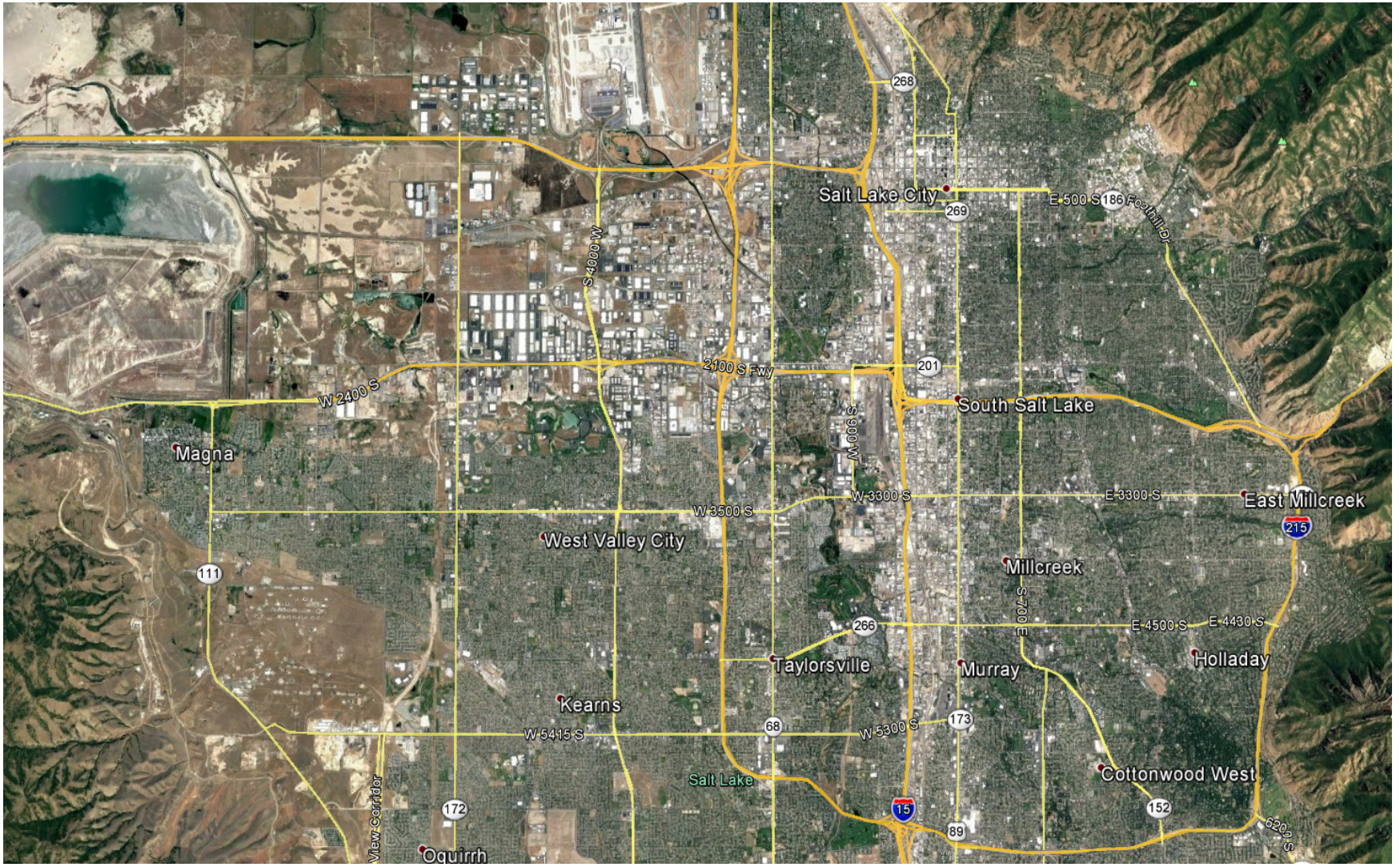

Figure 1.1. Figure showing the Salt Lake Valley as the region of interest. Courtesy of Google Earth.

CHAPTER 2

GRASS

Geographic Resource Analysis Support System (GRASS) is an open source GIS software package. The project is an international team effort consisting of scientists and developers participating from various fields. It has been under continuous development since 1982 and has involved Federal agencies, universities, and private companies. The software is used for geo-spatial data management and analysis, image processing, producing graphics and maps, spatial and temporal modeling, and visualizing in two and three dimensions. GRASS GIS contains over 350 modules to render maps and images; manipulate raster and vector data including vector networks; process multispectral image data; and create, manage, and store spatial data. It supports raster and vector data and offers a wide range of applications for research and engineering. For the application of this model, two-dimension raster data processing will be the primary use [9, 17, 20].

2.1 Generate Digital Elevation Model

To generate a digital elevation model (DEM), the LiDAR data are imported into the GRASS directory, which then must undergo two processes, spatial transformation and projection, to characterize the desired location. Projection refers to to an arbitrary designation for spatial data using a geographic coordinate system specific to a geo-spactial region. Once this is declared, the data are transformed to the region creating the desired location: for this application Salt Lake Valley. Because the LiDAR data are merely a collection of elevation data points, an interpolation method is necessary to create the surfaces that exist between these elevation points, thus creating the structures and landmarks within the region. Regularized spline with tension was the interpolation method used for this application, which approximates the surfaces between the surrounding points. A smoothing parameter is used to control the deviation between the given points and the desired surface. A buffer surrounding each data point is created and the interpolated map

is cropped to include only the areas near to its respective data points [21]. This process generates a detailed, high-quality DEM shown in Figure 2.1. The resolution at which these maps are generated is dependent upon the data source and the capabilities of the computer used. It is determined by taking the number of data points for the particular region and dividing it by the number of cells within the region. This is an approximation, as the data points are not uniformly distributed throughout the region. The LiDAR generated DEM is the basis for the irradiation model described in this manuscript, as it contains all surfaces of each structure and landmark within the region.

For the application of Salt Lake Valley, 15 LiDAR data regions were used. Each region was individually processed, taking careful note to define each region in a way that aligns cleanly to the others to avoid overlapping of data cells. Once each region was complete, the 15 regions were patched together to create the Salt Lake Valley floor DEM. To eliminate the possibility of null value cells existing, an additional regularized spline with tension was applied to the entire DEM. For computational purposes, the DEM was then resampled to a 3 meter resolution, again using a regularized spline with tension method.

Because the LiDAR data are only available for the valley floor, the eastern and western mountain ranges were developed using the World ALOS-3D data [18]. To create the mountain range DEMs, each region was carefully selected to capture the mountain range peaks that contribute to the valley floor shading: three eastern regions and five western regions. Each mountainous region was aligned to the Salt Lake Valley region and the data were imported and processed, eliminating null cells values, to a 3 meter resolution using the same method. Because only the mountain peaks were necessary to reproduce shading effects within the valley, and for computational reasons, lower elevation data points were eliminated from the regions when convenient to do so. Following the pre-processing of the mountain regions, the final DEM was created by patching the three eastern, five western, and the Salt Lake Valley regions together, giving the DEM necessary to capture the shadowing effects of the entire regional topography, shown in Figure 2.2.

2.2 R.Sun

R.sun is an internal function used by GRASS GIS that calculates solar irradiance at the specified resolution using a variety of input parameters. Input parameters consist of

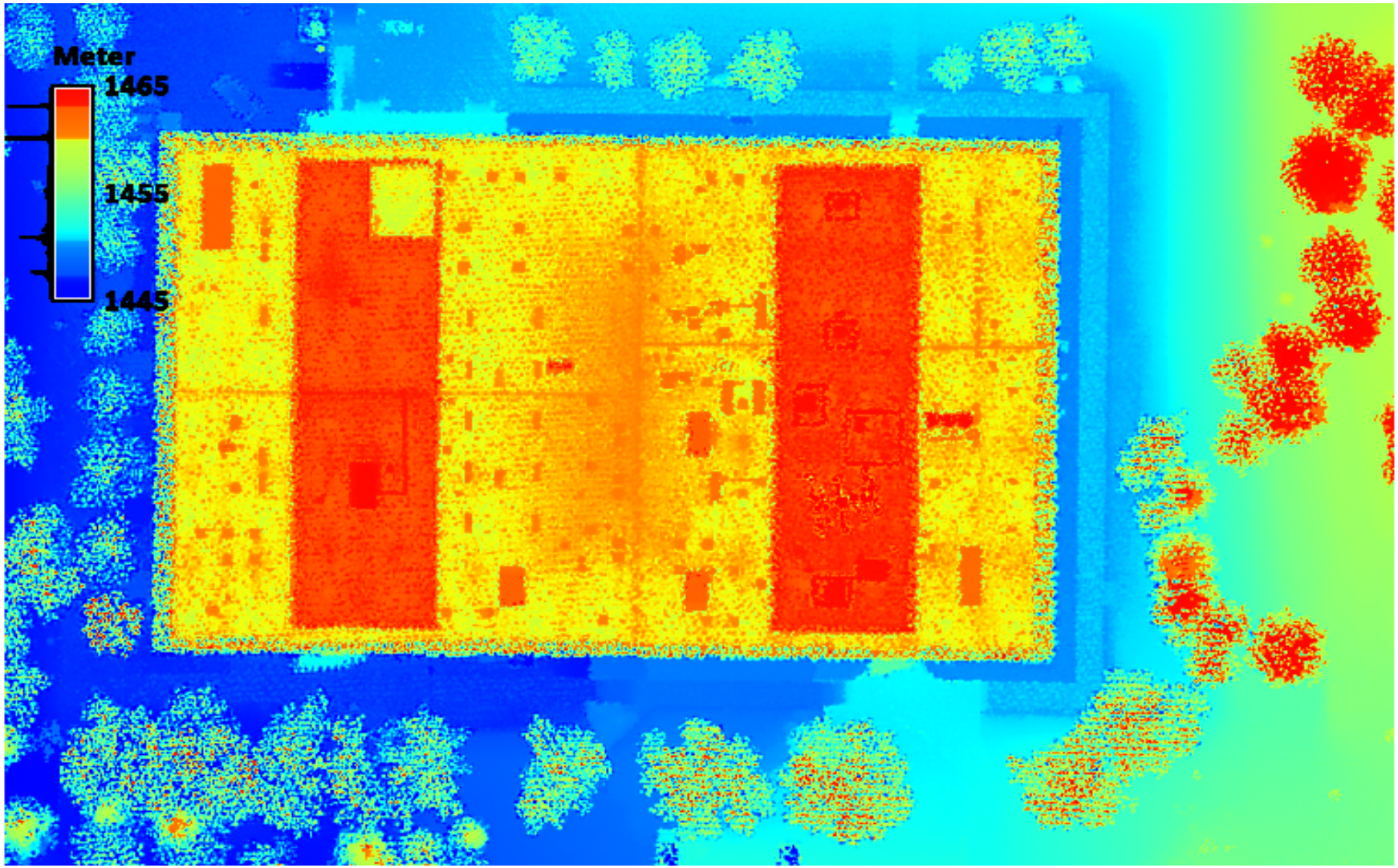

Figure 2.1. Figure shown to demonstrate the quality of a DEM using LiDAR data points for the Merrill Engineering Building at the University of Utah.

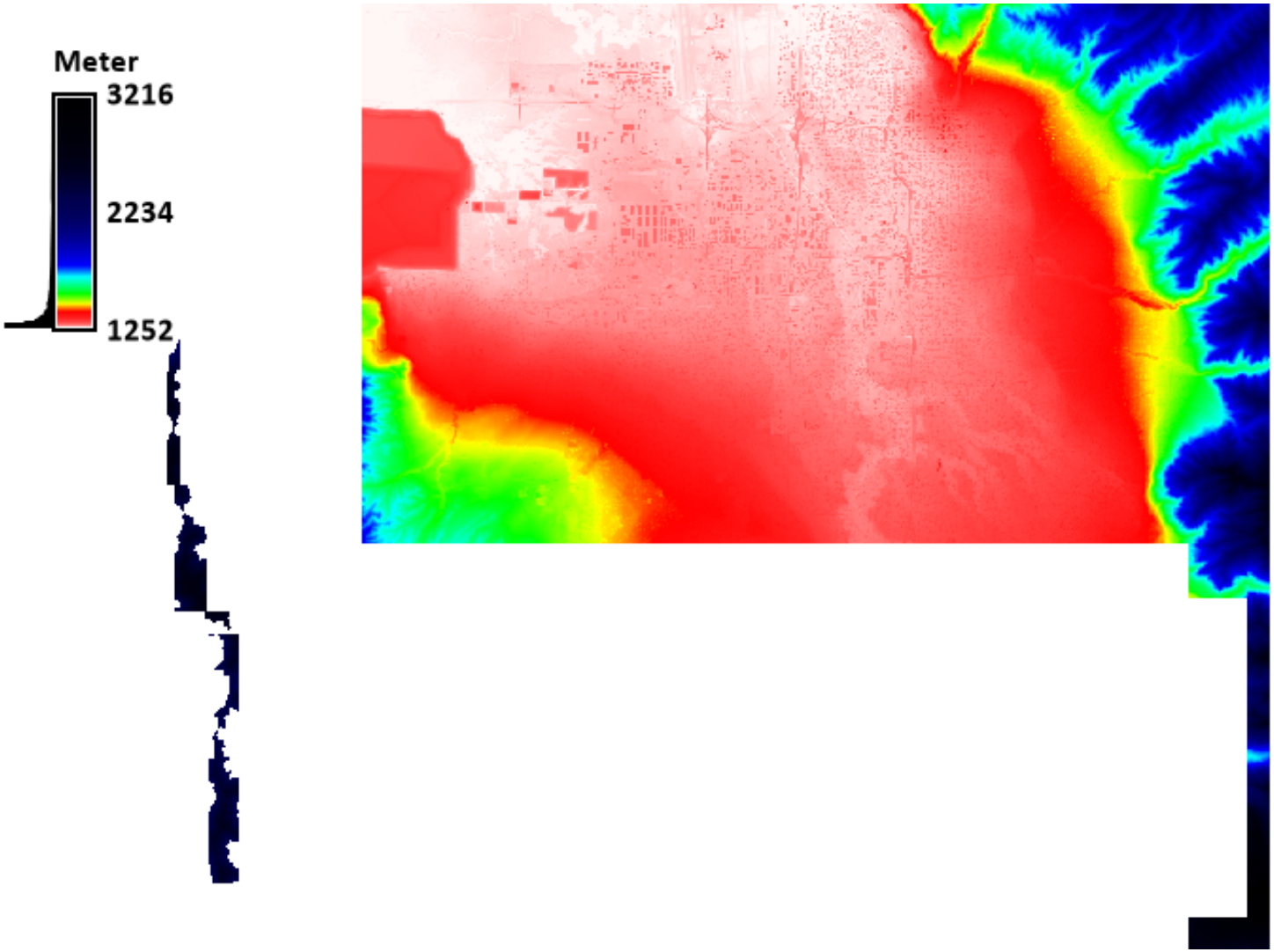

Figure 2.2. Figure showing the DEM of Salt Lake Valley used for modeling irradiation.

raster maps containing data for elevation, latitude, longitude, aspect, and slope, as well as input values for turbidity, albedo, time step, and civil time zone. The solar geometry of the model is based on the works of Krcho [22] and later improved by Jenco [23]. The equations describing sun-earth position as well as the interaction of solar radiation with atmosphere were originally based on the work of Kitler and Mikler [24]. This was then later updated by the work and suggestions by Scharmer and Grief (2000) [25]. The function has the ability to compute direct, diffuse, and reflected irradiance for clear sky conditions with the option to add annual cloud data retrieved from satellite data for real sky conditions [15, 26, 27]; this option was omitted as the presented model resembles clear sky conditions. The shadowing effect of the surrounding topography is taken into account with an algorithm that calculates the geometry of each data point relative to all others in the region. Solar irradiation maps for a given day are created by integrating the relevant irradiance from sunrise to sunset using a specified time step. The output raster map then gives irradiation data at the specified resolution in W/m^2 [17]. However, this is a computationally intensive process. The results shown in Chapter 3 were processed using a desktop computer with 64GB of RAM, consisting of a quad core processor with a maximum turbo frequency of 4.0GHz. The computation time to process the results was approximately 10 days.

2.2.1 Albedo

Land surface albedo is the fractional amount of short wave radiation reflected from the earth's surface or structures. Developing a model to accurately describe this is quite difficult, as different materials are spread throughout the visible spectrum. Previous models were typically created using empirical relations for the total shortwave radiation at a surface and satellite visuals or radiative transfer simulations. These approaches lacked the ability to accurately obtain albedo measurements due to the reflective spectral resolution and neglecting atmospheric conditions [28]. With advancements in technology, measurements are now being taken with remote sensing devices such as the Moderate Resolution Imaging Spectroradiometer (MODIS) [28–31], which consist of narrow band sensors, although the issue regarding the atmospheric conditions still remains.

The downward flux distribution at the bottom of the atmosphere is the weighting function used for spectral albedo conversion. Currently, little research is focused on iden-

tifying these atmospheric fluxes and implementing them into the conversion needed for high-resolution albedo measurement. Because different atmospheric conditions result in different fluxes, the measured albedo may not resemble the actual surface [28]. Studies do not typically involve this in-depth analysis because the researchers are generally less concerned with the high accuracy in a relatively small region, given the efforts needed to retrieve these fluxes [31–33]. The efforts are aimed at retrieving a relatively accurate albedo for large regions to address such issues as climate change.

The fraction of irradiation that is not absorbed is then reflected off the surface back to the atmosphere or onto neighboring surfaces. This radiation, which is projected onto the surface of a PV panel, is categorized as diffuse radiation. Diffuse radiation contributes minimally to the overall collection of irradiance, as the projected waves are once again a fraction of the reflected amount. Albedo measurements are currently taken using remote sensing devices such as MODIS, accounting for variability in time and space dependent upon the research group and its purpose.

Typical ground albedo values range from 0.15-0.2 [30, 34]. To determine the value used for this model, the approach was taken using data retrieved with MODIS and in-situ radiometric measurements [30]. Data were considered from each source across the U.S. with similar climate conditions as Utah, and statistically determined. The obtained value for the model is 0.17.

To assess the sensitivity of the model output with respect to albedo, an uncertainty analysis was conducted. Using albedo values of 0.15 and 0.2 as inputs to the model, the percent difference between the two scenarios was less than 1%. This is most likely due to the orientation of the surfaces of interest. PV panel mounting surfaces are typically directed at angles no larger than 40^o from the ground surface. The likelihood of radiation reflecting off a neighboring surface onto a surface that is directed between 0^o - 40^o is minimal outside of very dense urban areas.

2.2.2 Linke Turbidity Coefficient

The Linke Turbidity Coefficient (LTC) [35], an input parameter to the r.sun function, corresponds to how easily radiation is able to transport through the atmosphere. Aerosols and atmospheric gases both scatter and absorb solar radiation, which diminishes the direct

irradiance at the normal surface. This effect can drastically change the amount of irradiance that makes its way to the surface.

The LTC has its advantages as it has been widely used since 1922. The disadvantage is that it is dependent upon the air mass, which is difficult to quantify without measurement data [36]. Several approaches have been considered to better understand this work and improve the expression for better use in radiation models [36–39]. New studies have been conducted coupling LTC with newer relevant data, to retrieve a turbidity coefficient independent of air mass that also accounts for the local elevation. This is the approach taken in this manuscript and is referenced to the work of Ineichen that uses the variable T_{L1} [36].

NREL has developed a database for solar radiation across the U.S. and has been providing these data for over 25 years. Substantial improvements have been made throughout this time with their most recent update in 2014. This update includes their Physical Solar Model (PSM) [40], which uses a two-step process to retrieve cloud properties, aerosols, and various meteorological data which are used as input parameters to their model. This new physics-based model computes solar radiation for the United States at a 4 kilometer resolution using geostationary satellites and consists of a 30-minute temporal resolution. Using this tool, the clear sky direct normal irradiance (B_{ncl}) is retrieved, which can then be used to determine T_{L1} for Salt Lake Valley. Ineichen and Perez [36] use the modified approach to determine T_{L1} based on the original work done by Linke. The approach gives the following equation:

$$T_{L1} = [11.1 * Ln(b * I_o / B_{ncl}) / AM] + 1 \tag{2.1}$$

The parameters are defined as:

$$AM = 2$$

$$b = 0.664 + 0.163 / f_{h1}$$

$$f_{h1} = exp(-altitude/8000)$$

To validate this expression, twenty B_{ncl} samples within $320 km^2$ of Salt Lake Valley were taken at a 4 kilometer resolution. The calculated T_{L1} data ranged between 3.41 and 3.55.

These values are consistent with data corresponding to rural and city regions within the northern hemisphere consisting of a mild or temperate climate [41]. Taking the average T_{L1} of all 24 data points, a value of 3.5 was obtained and is used in the presented model.

2.3 Photovoltaic Cell Efficiency

PV cells have been developed using a wide range of semiconductors and sub categories within semiconductor grouping such as (mono)crystalline, poly-crystalline, and thin film. The efficiency assigned to a particular cell is correlated to how well the cell converts sunlight to electrical power. This is determined in standard test conditions (STC) by using a 1000 watt light (One Sun), replicating the sun's wavelength spectrum, while measuring the power output. Typical PV cell efficiencies currently used for residential and commercial production are 15-18%, but efforts and new developments are aimed at continuously increasing these efficiencies. The highest PV cell efficiencies have been documented since the early 1990s by "Progress in Photovoltaics". The criterion for these documented cells is to have been independently tested by a recognized test center. As of 2015, the highest tested commercial cell efficiency was 25.6% made by Panasonic and tested at AIST [42].

The efficiency of a PV cell is determined using STC at which the required temperature is set to be 25^oC. When conducting a site assessment, the ambient temperature must be taken into consideration, as it affects the panel efficiency. White [43] suggests the efficiency decreases 0.33% with each temperature degree above 25^oC and increases 0.33% with each degree below 25^oC. With inclusion of this component, the efficiency as a function of temperature [44] can be expressed as:

$$\eta_{PV} = \frac{25^oC - T_{amb}}{300^oC} + \eta_o \tag{2.2}$$

where η_o is the efficiency specified by the manufacturer and T_{amb} is the ambient temperature. Typical Meteorological Year (TMY) 3 weather data for Salt Lake City were obtained and used for this analysis [45].

Because the panel efficiency directly impacts the electricity production, the site must be assessed in great detail to maximize the economic benefit; as PV panel cost does not necessarily scale linearly with efficiency. With new technology such as micro inverters and

power optimizers, the assessment may consider using multiple efficiencies at a given site depending on the available rooftop area and orientation.

2.4 Inverter

Another major component of a PV system is the inverter, which is the device needed for converting direct current (DC) to alternating current (AC). The inverter chosen for a PV system is dependent upon the site and surrounding topography as well as the usable mounting surface area. The three most common inverter technologies used are string inverters, power optimizers, and micro inverters. Each technology is capable of performing the conversion, although associated cost, efficiency, and life cycle are different.

2.4.1 String Inverter

A basic string inverter system consists of PV panels wired in parallel using one or more strings [46]. Each string is then wired to the string inverter, typically mounted next to the utility power box for DC to AC conversion; which does so at usually a 95% efficiency. Because these are connected in parallel, the power output of the string is dependent upon each panel's performance. If power production decreases for an individual panel due to shading or cloud cover, the performance of each panel within the string will decrease accordingly. This lack of production necessitates a thorough assessment as to where the arrays are placed relative to the surrounding topography. However, the material cost for this type of system is the lowest because there is no additional equipment needed for conversion.

2.4.2 Direct Current Power Optimizer

PV systems consisting of power optimizers utilize a string inverter, yet each panel's power output is monitored and controlled. Each panel is designated a max power point voltage (V_{MPP}) and current (I_{MPP}) by the manufacturer. Each string consists of multiple panels wired in series, each consisting of an optimizer that constantly monitors the max power point (MPPT) of each panel. The optimizer is a DC to DC converter (98.8-99.5% efficiency) that alters each panel's output voltage according to the MPPT, producing a constant predetermined string voltage [47]. This allows for individual panel performance variation due to shading, as the optimizers adjust to hold a constant string voltage. How-

ever, because each panel consists of its own optimizer, the system cost is higher as it also consists of the string inverter necessary for DC to AC conversion.

2.4.3 Micro Inverter

Similar to power optimizers, each panel consists of a micro inverter wired in parallel within a string. The micro inverter performs the DC to AC conversion at the module with 96-98% efficiency [48]. Because of this, panels with different efficiencies can be oriented in such a way that is optimum for power production. This allows for a more creative approach to collect solar energy. This is the simplest and safest of all the inverter technologies as there is no need for DC string design, which contributes to a more timely installation, and the system does not consist of high voltage DC wires [46, 48]. However, micro inverters are relatively expensive, about twice that of a power optimizer, although a string inverter is not required.

When deciding which inverter to integrate within a PV system, a full economic assessment is crucial. The surrounding topography plays a vital role in determining this, as each site is unique with respect to the surroundings. If a potential site is relatively open with minimal shading, a stand-alone string inverter may be the most economic. However, considering residential and commercial rooftop PV systems, this is typically not the case and it is cost beneficial to implement either power optimizers or micro inverters into the system for optimum production. Each consist of their designated efficiencies and price points, which puts the necessity on the designer to provide the most economic system through a thorough assessment.

2.5 Tilt Angle

Panel tilt angle, usually expressed in degrees, is the angle between the surface of the earth and the mounting surface of the panel. For a fixed array, the tilt angle is typically optimal when equal to the location's latitude if an incentive program such as net metering is offered, but may vary more or less dependent upon the electricity pricing regime and intended power use [49, 50]. This differs from a tracking system where the panels are set up and controlled, intending to face normal to the sun at all times throughout the day, although these are typically only used in large-scale operations.

When considering a potential PV production site, the purpose is to convert solar energy to as much electrical energy as possible while minimizing cost. To do this, the electrical production potential is needed for the given site. This will allow for determination of panel array sizing, inverter technology, and the panel efficiency. Using the parameters previously discussed, the electrical energy per unit area that a site is capable of producing can be expressed as [51]:

$$\frac{E}{A} = \eta_{PV}\,\eta_{In}\,I_o\,sin(\alpha\ +\ \beta) \tag{2.3}$$

Combining with the module efficiency as a function of ambient temperature, shown by equation 2.3, gives:

$$\frac{E}{A} = \Big[\frac{25^oC - T_{amb}}{300^oC} + \eta_o\Big]\,\eta_{In}\,I\,sin(\alpha\ +\ \beta) \tag{2.4}$$

where α is the sun altitude angle, β is the PV tilt angle in degrees, η_{PV} is the panel efficiency, I_o is the incoming irradiation, and η_{In} is the inverter efficiency. The altitude sun angle is dependent on the Julian day n and the latitude L of the potential site. The following equations are used to express the maximum sun angle for any given day [52].

$$\alpha = 90 - |L - \delta_s| \tag{2.5}$$
$$Where \quad \delta_s = 23.45\,sin\Big[\frac{360\,(284+n)}{365}\Big]$$

Alternatively, the sun altitude angle can be expressed as a function of the Julian day and time.

$$\alpha = sin^{-1}\big[sin\,L\,sin\,\delta_s + cos\,L\,cos\,\delta_s\,cos\,h_s\big] \tag{2.6}$$
$$Where \quad h_s = \frac{15^o}{h}\cdot(hours\,from\,local\,solar\,noon)$$

The expressions and descriptions shown in Chapter 2, combined with the GRASS software and LiDAR data, can be used to better assess the PV potential for a given region. The

results of this combination are shown in Chapter 3, which describes the irradiance distribution within the Salt Lake Valley and how PV cell efficiency can increase the potential in areas that experience topographical shading.

CHAPTER 3

CASE STUDY SALT LAKE VALLEY

PV panel efficiency, system materials, and tilt angles are key components to photovoltaic power generation. The optimal tilt angle places the panel surface directly normal to the incoming irradiance, which maximizes the energy collected, and therefore produced. A panel's efficiency determines the amount of electrical power generated from the collected solar energy. These are dependent upon the semiconductor materials used and production process, among other constraints. Efficiencies have been improving over the last several years and are continually monitored and verified. Panel efficiency is partly responsible for the financial cost associated with the system, as more efficient panels are typically more expensive. PV panel tilt angle and efficiency must be carefully addressed when assessing the economics of a potential PV production site.

3.1 Annual Irradiation Distribution Within Salt Lake Valley

NREL has developed a clear sky solar radiation database for various regions within North and South America using their PSM, which gives the global horizontal irradiance for each region as a heat map. The database is widely used in the solar PV industry to assess potential PV systems and estimate the expected power generation; however, it currently exists at a coarse resolution of four kilometers. This macroscale model was developed using satellite imagery and weather data, yet lacks the inclusion of the local topography. Using NREL's model, the data for Salt Lake Valley was obtained and shown in Figure 3.1. Comparing with the model presented in this manuscript, Figure 3.2 describes the spatial distribution of annual irradiance at a 3 meter resolution, with inclusion of the local topography and its effects within Salt Lake Valley.

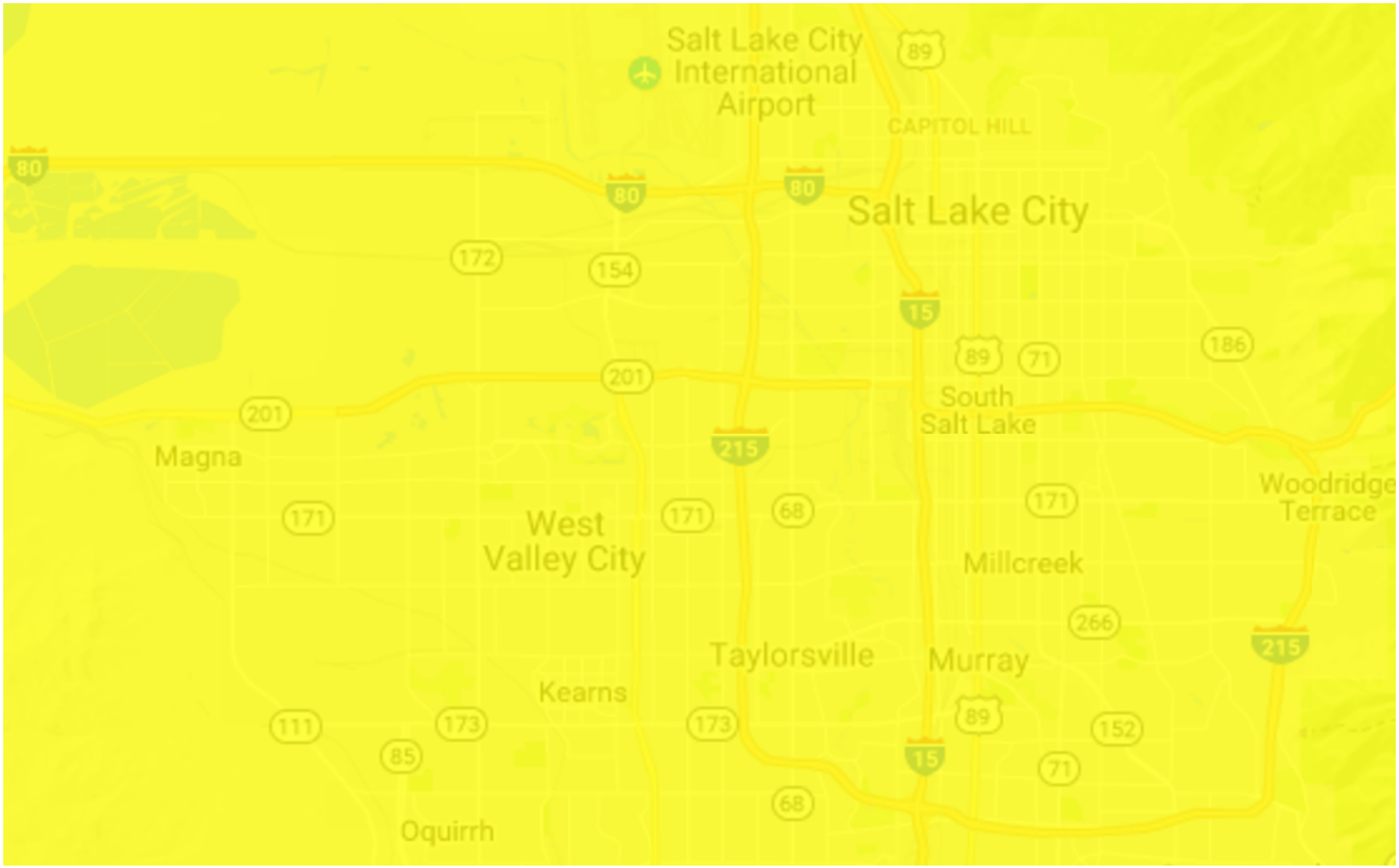

Figure 3.1. Figure showing the irradiance distribution given by the NREL model with a color representing $4.5 - 5 \frac{kWh}{m^2 day}$

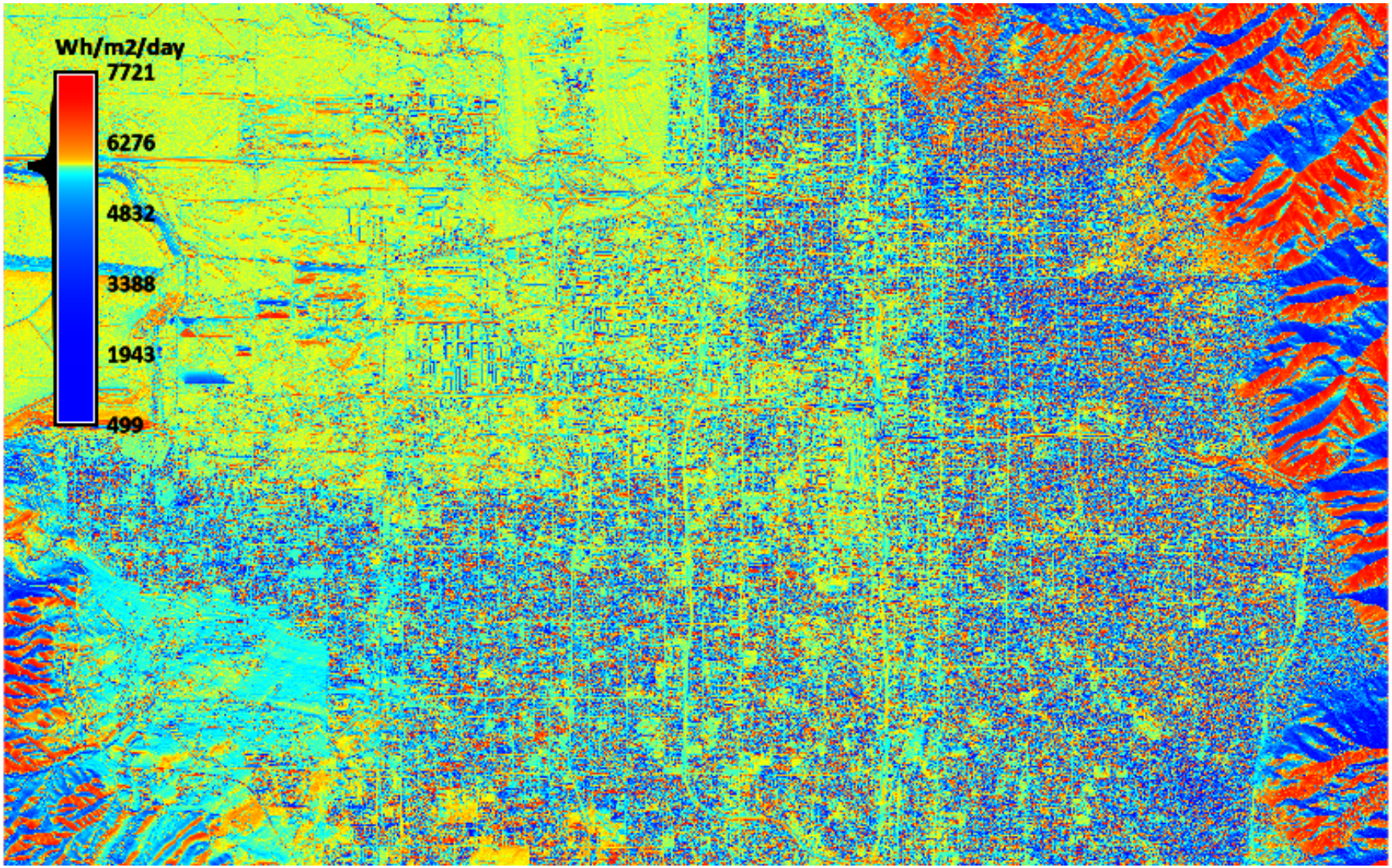

Figure 3.2. Figure showing the irradiance distribution throughout Salt Lake Valley

3.1.1 Discussion

As expected, the distribution of annual irradiation is highly dependent upon the local topography and its placement within the valley. The color coding used in the NREL model shown in Figure 3.1 represents 4.5-5$\frac{kWh}{m^2day}$ and is assigned to all locations within Salt Lake Valley. The results shown in Figure 3.2 indicate the irradiance varies between 0.49-7.7$\frac{kWh}{m^2day}$, having a mean value of 5595$\frac{kWh}{m^2day}$ and a standard deviation of 847$\frac{kWh}{m^2day}$, resulting in a coefficient of variation of 15.1%.

The center of Salt Lake Valley represents the data given by the NREL model well, but is not adequate for the eastern and western regions. The eastern region accumulates an average of roughly 3.5$\frac{kWh}{m^2day}$, while the northwestern region accumulates an average of 5.8$\frac{kWh}{m^2day}$, and the southwestern region accumulates an average of 4.3$\frac{kWh}{m^2day}$. Using the the NREL model for potential PV power generation may result in less than anticipated irradiance availability, which would extend the payback period for a PV system and may not be a reasonable economical investment. Likewise, the evaluation of a potential PV site in the northwestern region may result in a larger than needed PV system, therefore producing excess electricity while creasing the initial cost of the larger system. The NREL model may be adequate for a zeroth-order analysis, but a model similar to the one presented is necessary for a more thorough analysis of Salt Lake Valley and for a better understanding of site differences within the valley.

3.2 Tilt Angle Variance in Salt Lake Valley

Rooftop PV power generation is constrained to the mountable area of the rooftop; fire code requires a 3 foot perimeter space between PV array and rooftop edges [53]. Rooftops throughout the valley consist of different surface areas and orientations, both of which affect the potential for power generation. Non-shaded PV panels mounted on south facing roof slopes will produce more electricity on an annual basis than if positioned in alternate directions [54, 55]. This is due to Salt Lake Valley residing in the northern hemisphere, so the irradiance is directed toward southern facing surfaces. East or west facing roof tops have greater potential for electricity production with increasing tilt angle, which account for the lower sun angle. Because of the high energy demands in the afternoon, especially during the summer months, systems that are oriented slightly to the west may not gen-

erate as much power on an annual basis, but may better addresses the building's energy demands, which also relieves the grid from additional power supply [54–56]. Depending on the utility's program, an east or west facing system may be a better option, as people tend to use more electricity during the morning and evening hours in their residences.

Currently, Rocky Mountain Power offers a net metering program. This program allows the PV system to send unused power back into the grid for a credit. This credit is then available for use for up to 1 year [57, 58]. Regions with similar programs do not necessarily benefit from east or west facing systems as the unused credit throughout the day is usable to supplement the morning and evening hours; this is solely on a cost benefit standpoint. However, regions without similar programs will benefit by producing power when they are more likely to consume it.

Roof pitch angles vary throughout the valley and typically range between 25^o - 40^o for the residential sector and 0^o - 40^o for the commercial sector. While the lower pitched roof tops could produce more energy during summer months, the opposite occurs during winter months; the alternate trend occurs with steeper pitched rooftops. Due to city codes and standard installation practices [53, 59], residential property owners do not typically have the option to alter the roof structure to adjust the tilt angle. If the option is available, it is usually not economic or cosmetically pleasing to do so. This is the benefit to the net metering program for property owners, as system designs can include energy production on an annual basis, therefore supplementing the power usage by the credits accumulated. However, the commercial sector typically has the ability to alter the PV tilt angle, by utilizing tilted racking systems, which is beneficial to do so. Depending on the facility's electricity needs and the utility programs available, an optimum tilt angle will minimize the system payback period.

Power production in the valley is not only dependent upon roof geometries, but also varies within sub-regions of the valley. Figure 3.2 shows that PV systems near the east bench collect less irradiance on an annual basis due to the mountain range causing morning shadows, but also because of the mature vegetation found within. On the west side of the valley, sites will accumulate more irradiance because of the less developed vegetation and relatively low building structures. Sites near the downtown region collect smaller amounts of irradiance due to the large surrounding building structures causing shade at

various times throughout the day. The northwestern region receives the most irradiance due to the lack of vegetation and undeveloped area.

A parametric analysis has been performed addressing various tilt angles and cell efficiencies for the Salt Lake Valley. The analysis was performed at both extreme sun positions during the year, Summer and Winter solstice. Table 3.1 presents each parametric analysis and the varying parameter, while the following subsections present and describe the results.

3.2.1 Varying Tilt Angles at Winter Solstice

Understanding the PV power generation potential at various tilt angles allows for a better analysis of the region. This analysis shows the potential of utilizing a tilted mounting structure at 5^o increments across the valley ranging from 0^o - 40^o. The following results describe how the topography of each sub-region affects the potential PV power generation with respect to its magnitude and spatial distribution.

During the winter months, the sun altitude angle is lower in the northern hemisphere due to the earth's tilt. At the winter solstice, the altitude angle and ideal PV tilt angle at solar noon are approximately given as:

$$\alpha = 90^o - Latitude + Earth's\ Tilt$$

$$\beta = Latitude + Earth's\ Tilt$$

considering Salt Lake Valley with an estimated latitude of 40.75^o. Accounting for the earth's tilt of 22.5^o, the sun altitude angle is expected to be roughly 26.75^o, indicating

Table 3.1. Parametric analysis of Salt Lake Valley at winter and summer solstice

Parametric Analysis			
Study	PV Efficiency (η_{PV})	Tilt Angle (β)	Increment
Winter Solstice, β	15%	0^o - 40^o	5^o
Summer Solstice, β	15%	0^o - 40^o	5^o
Winter Solstice, η_{PV}	12-24%	10^o	2%
Winter Solstice, η_{PV}	12-24%	40^o	2%
Summer Solstice, η_{PV}	12-24%	10^o	2%
Summer Solstice, η_{PV}	12-24%	40^o	2%

an ideal PV tilt angle of 63.25^o. To validate equation 2.5, the method was used and a sun altitude angle at solar noon was determined to be 25.8^o. This is similar to the rough estimate of 26.75^o and is the chosen method for the following analyses.

Because the sun altitude angle is a function of the earth's rotation, α varies between 0^o and 25.8^o. Considering the surrounding mountain ranges, the relative altitude angle is assumed to vary between 15^o and 25.8^o. The average altitude angle was determined with equation 2.5 using 1^o incremental steps in the earth's rotation and was determined to be 22.1^o, indicating the ideal tilt angle for a south facing system at winter solstice is roughly 68^o. Although this is the ideal tilt angle for the day, it is not practical in most applications, although as α approaches 68^o, the potential electricity generation will increase appropriately. The following figures show the electrical power generation potential of a PV system in the valley with tilt angles varying from 0^o - 40^o, which is a typical range for most applications, and a conservative PV cell efficiency of 15%. This was done by calculating the irradiance at each data cell using the corresponding tilt angle.

3.2.1.1 Winter Solstice Tilt Angle Results

Figures 3.3 - 3.11 show the results of various tilt angles in Salt Lake Valley at winter solstice. In general, it is shown that as the tilt angle increases, the electricity generation potential increases accordingly. The PV potential is high in nearly all of the northwestern region, yet the sub-regions within the southern and eastern regions show much less potential due to the shadowing from the local topography. With a low sun altitude angle, which is experienced during the winter months in the northern hemisphere, structures create longer shadows that project onto neighboring PV surface areas, resulting in less PV potential for that surface. As the tilt angle increases, PV surface areas exposed to the sun collect more incident irradiance. Likewise, PV surfaces that are normally covered by a cast shadow may extend beyond the shadows, thus exposing the surface to incoming irradiation. As such, areas that consist of a dense topography may benefit an increased tilt angle to suffice the building electricity demands. Because the northwestern region is far less populated and developed in comparison to the other regions in the valley, and its positioning with respect to the mountain ranges, the PV potential is much higher at each given tilt angle.

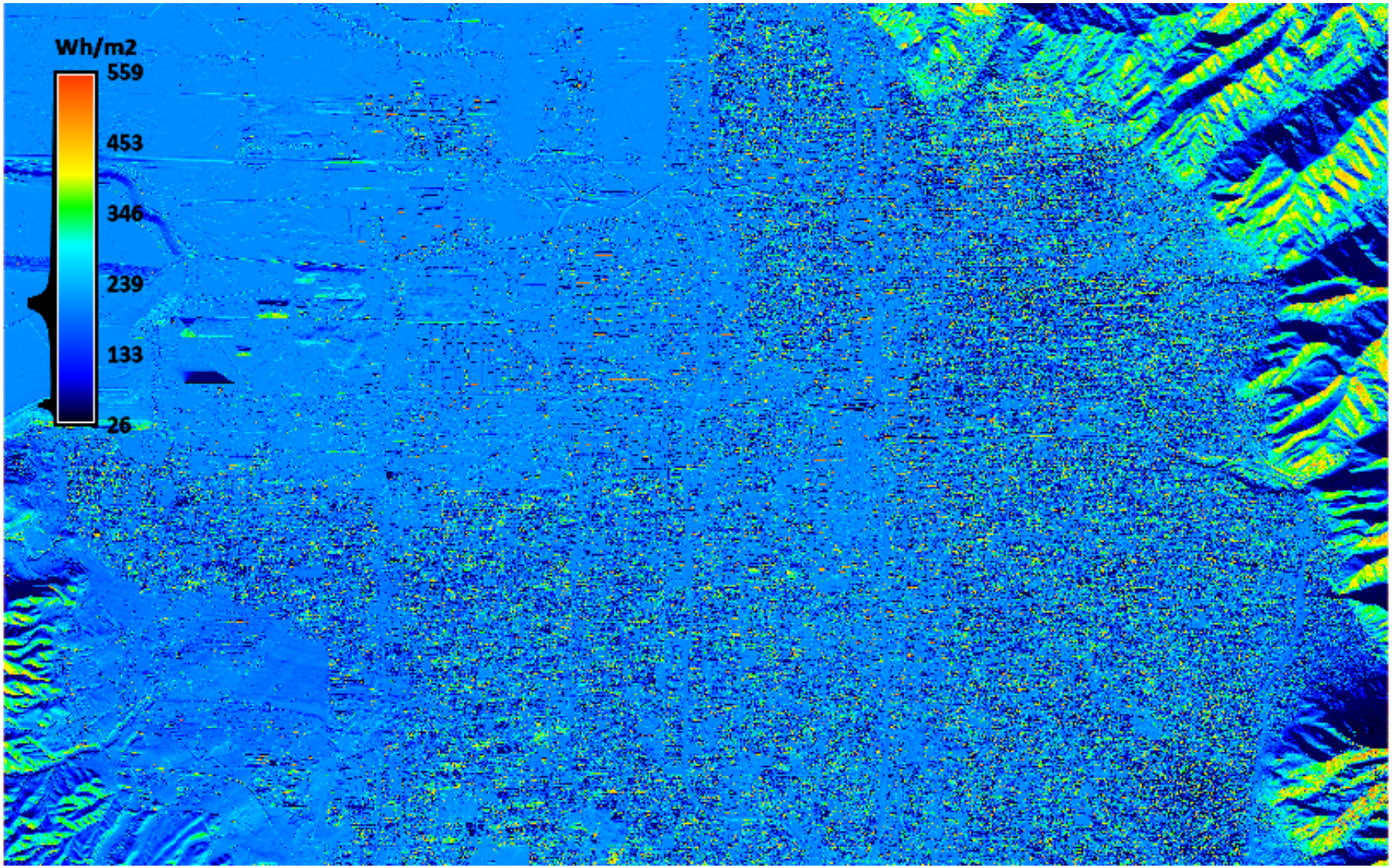

Figure 3.3. Figure showing the Salt Lake Valley PV electricity production at winter solstice using a tilt angle of 0^{o}.

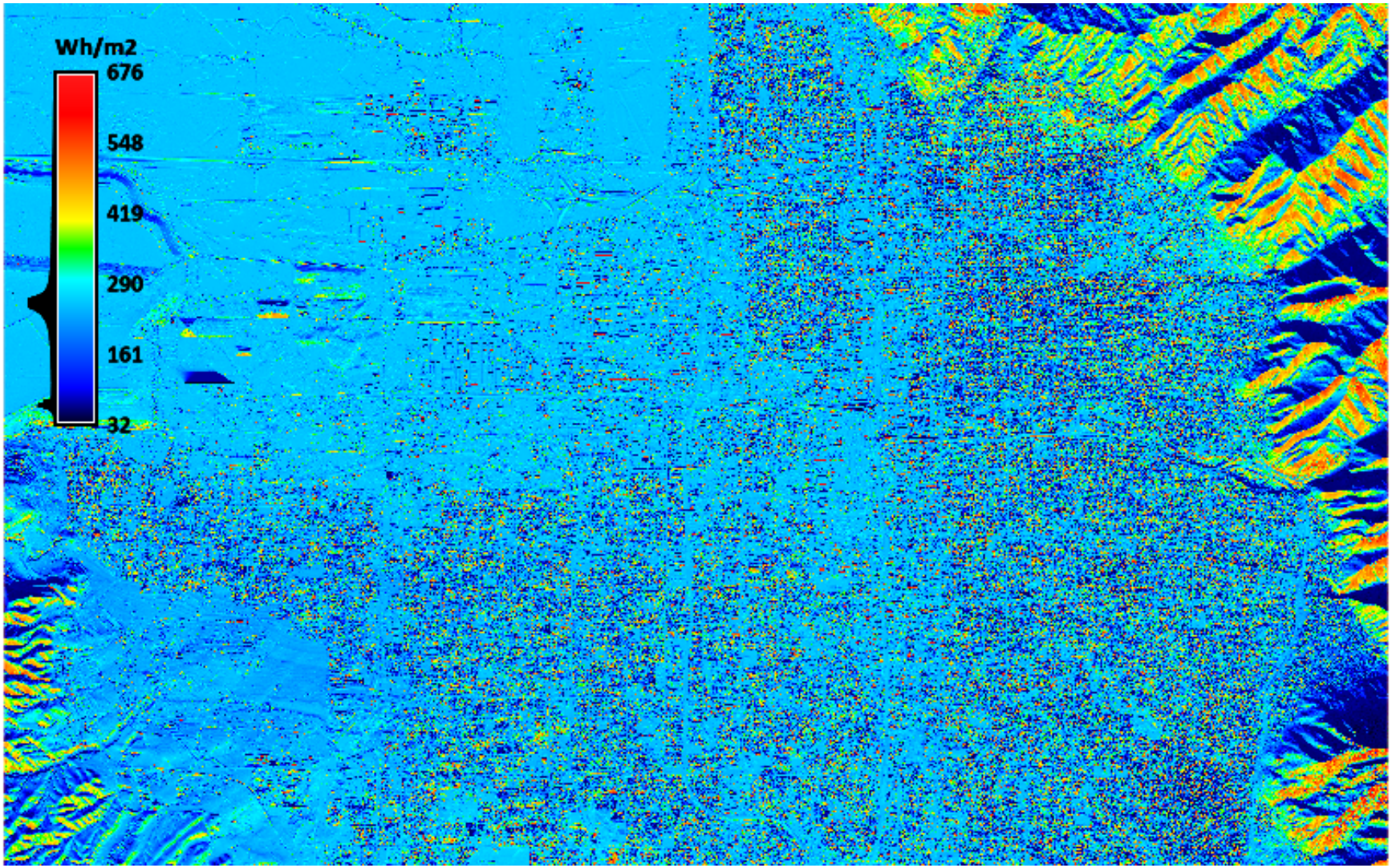

Figure 3.4. Figure showing the Salt Lake Valley PV electricity production at winter solstice using a tilt angle of 5^0.

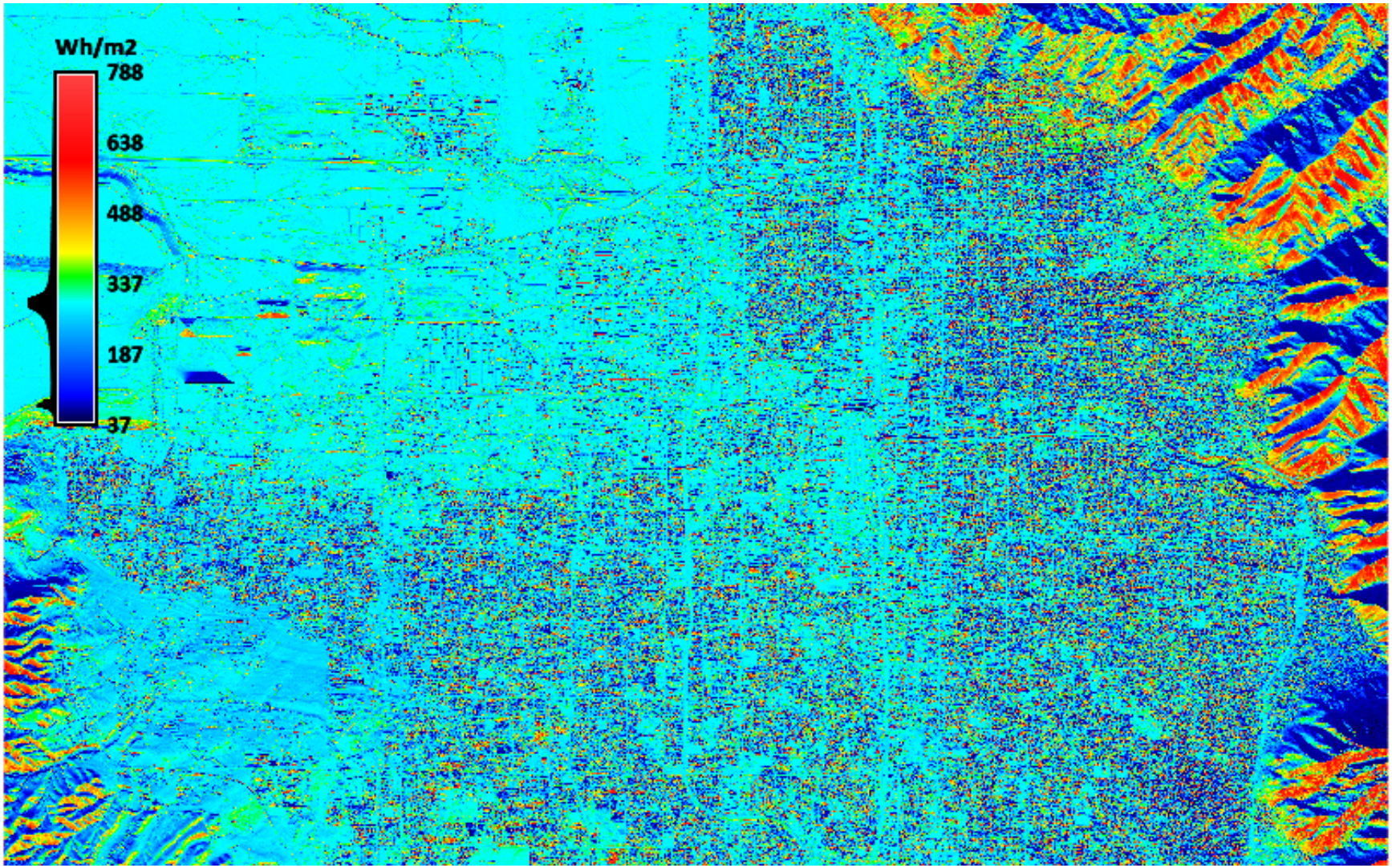

Figure 3.5. Figure showing the Salt Lake Valley PV electricity production at winter solstice using a tilt angle of 10^0.

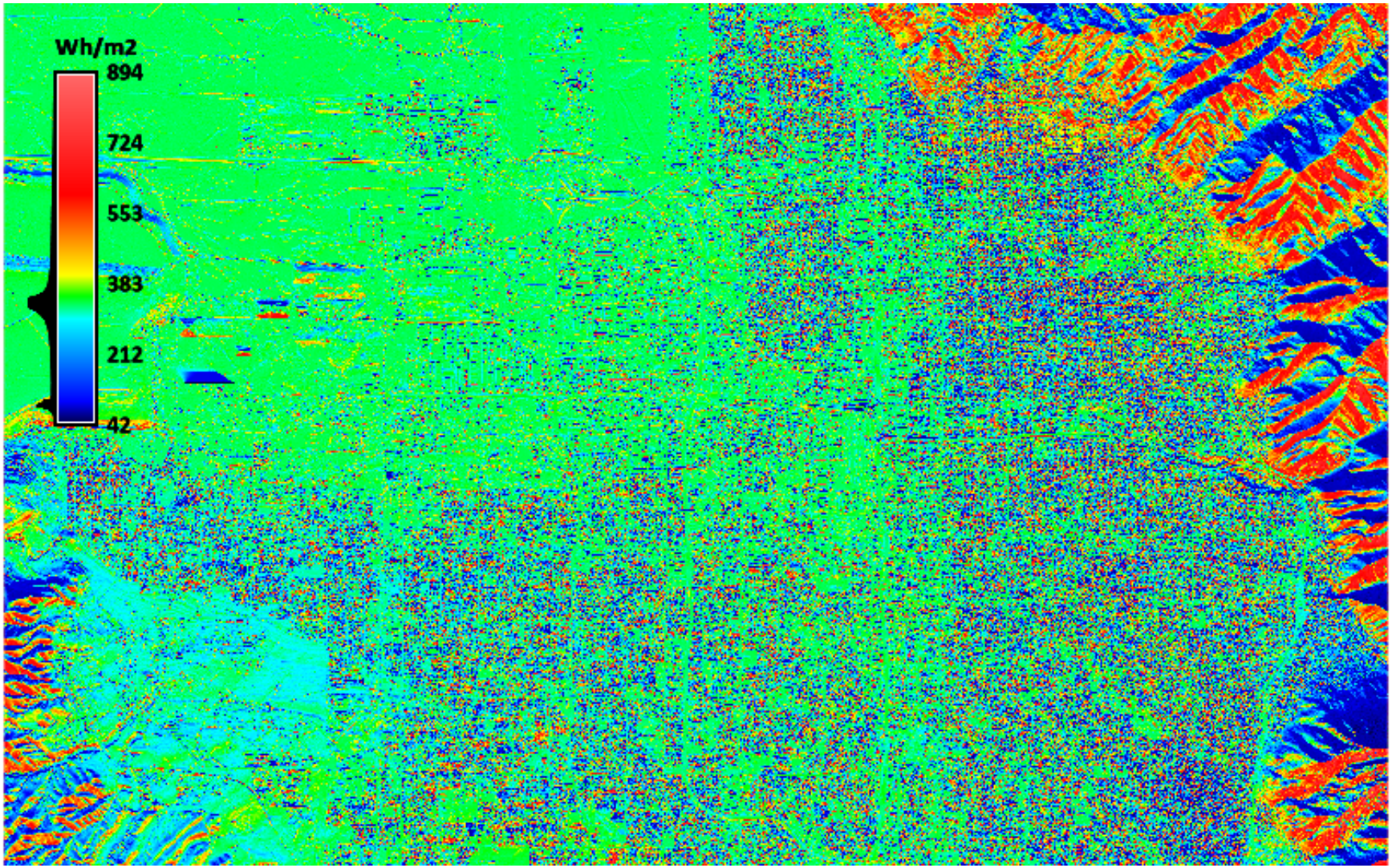

Figure 3.6. Figure showing the Salt Lake Valley PV electricity production at winter solstice using a tilt angle of 15^0.

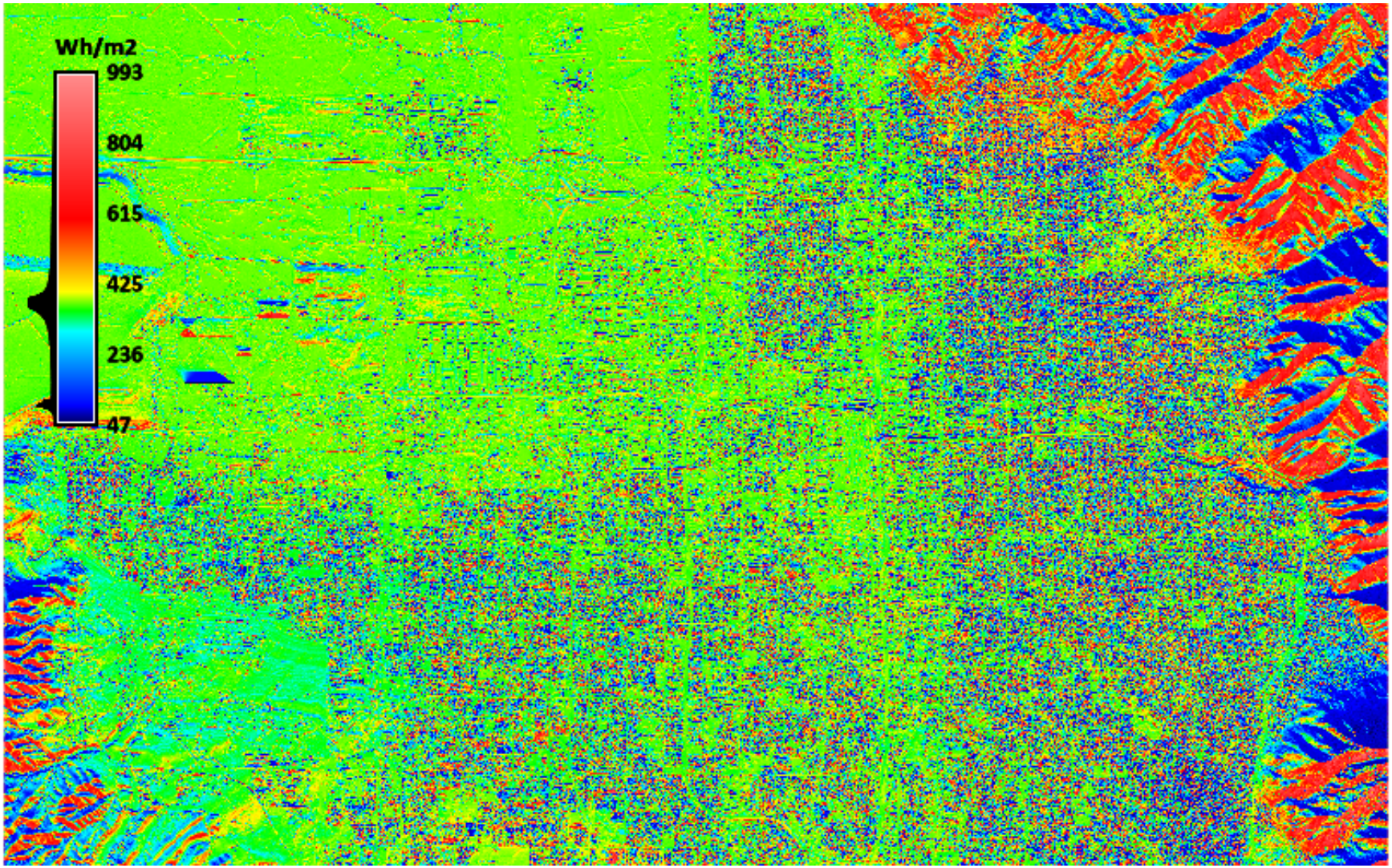

Figure 3.7. Figure showing the Salt Lake Valley PV electricity production at winter solstice using a tilt angle of 20^0.

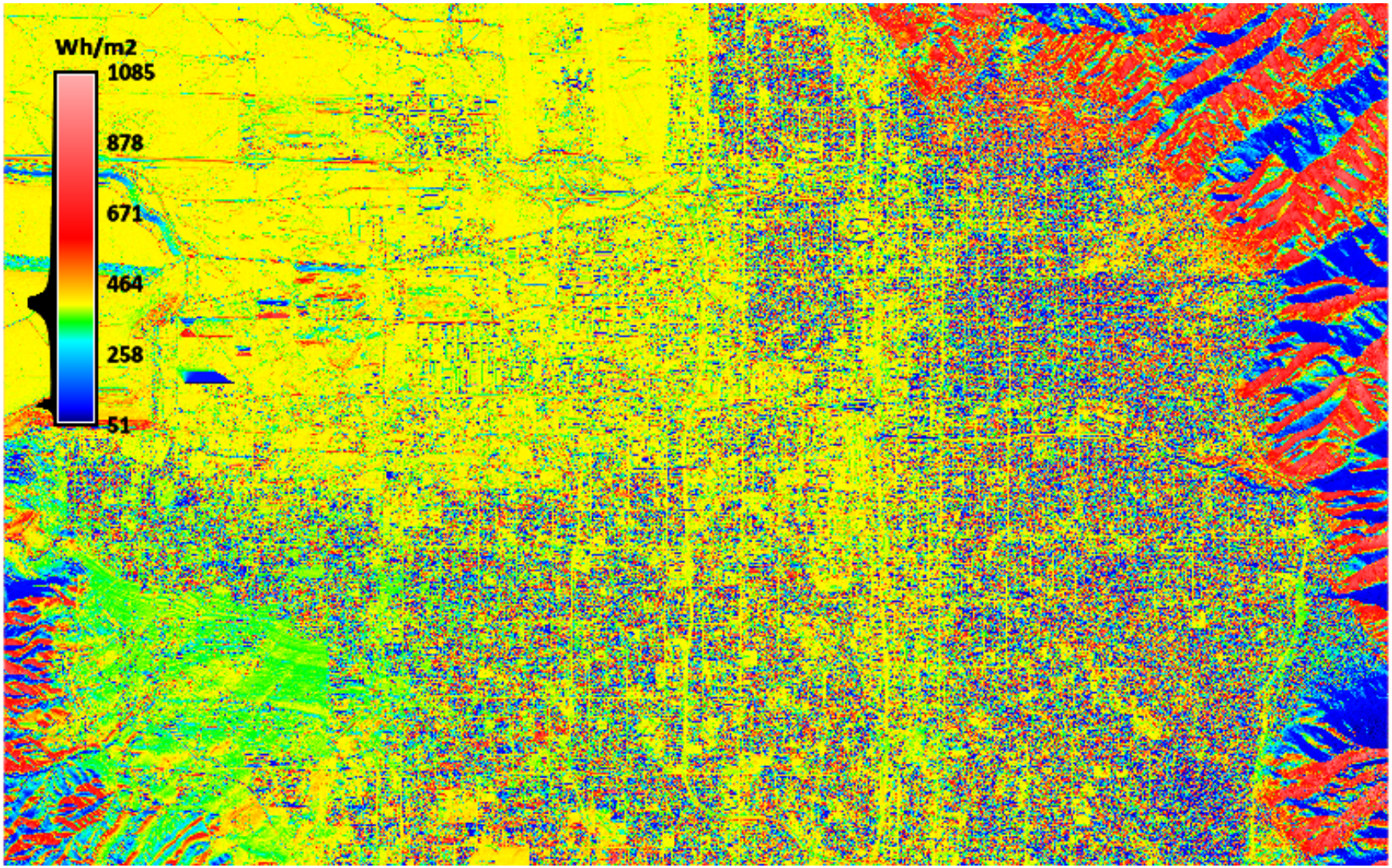

Figure 3.8. Figure showing the Salt Lake Valley PV electricity production at winter solstice using a tilt angle of 25^0.

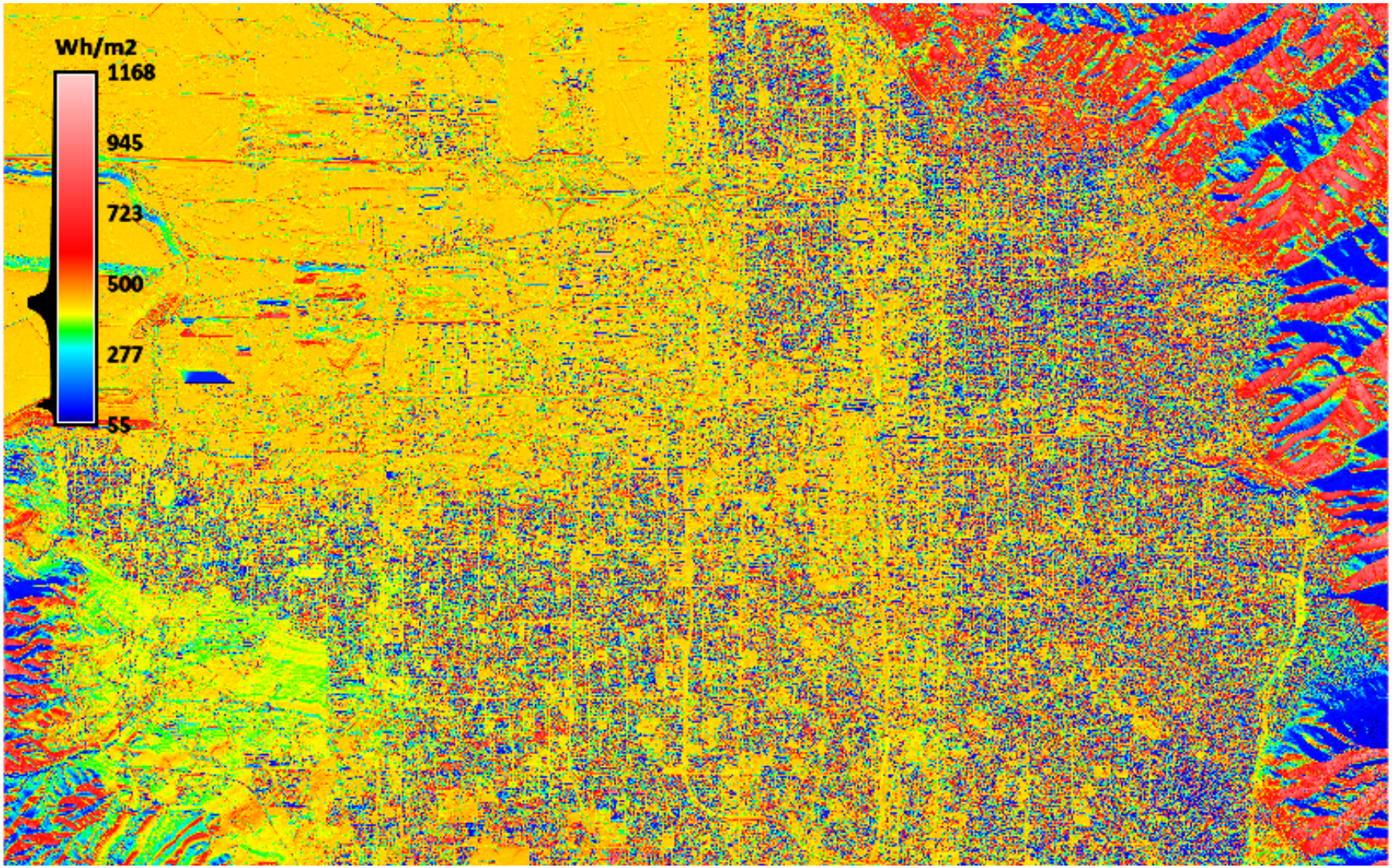

Figure 3.9. Figure showing the Salt Lake Valley PV electricity production at winter solstice using a tilt angle of 30^0.

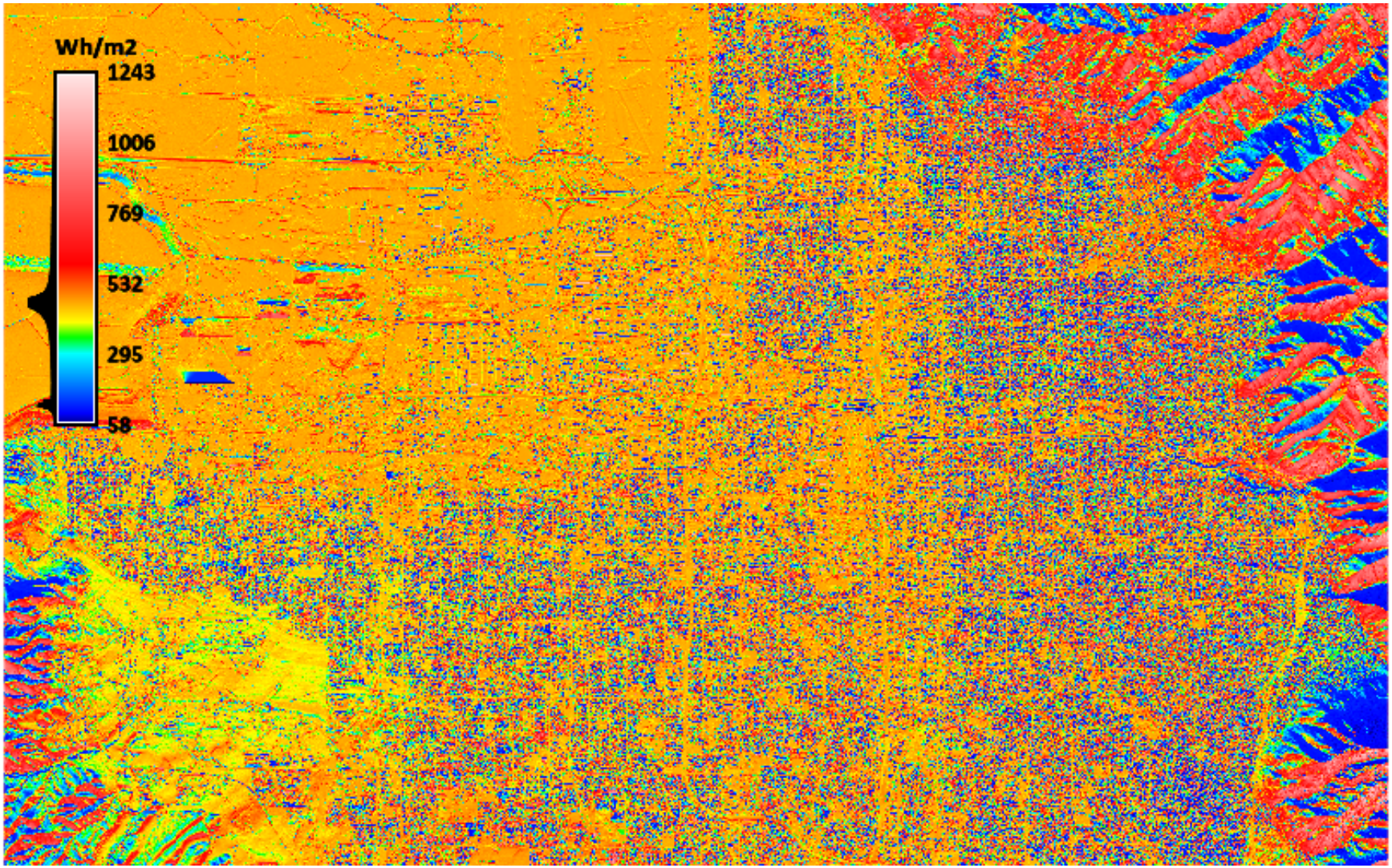

Figure 3.10. Figure showing the Salt Lake Valley PV electricity production at winter solstice using a tilt angle of 35^0.

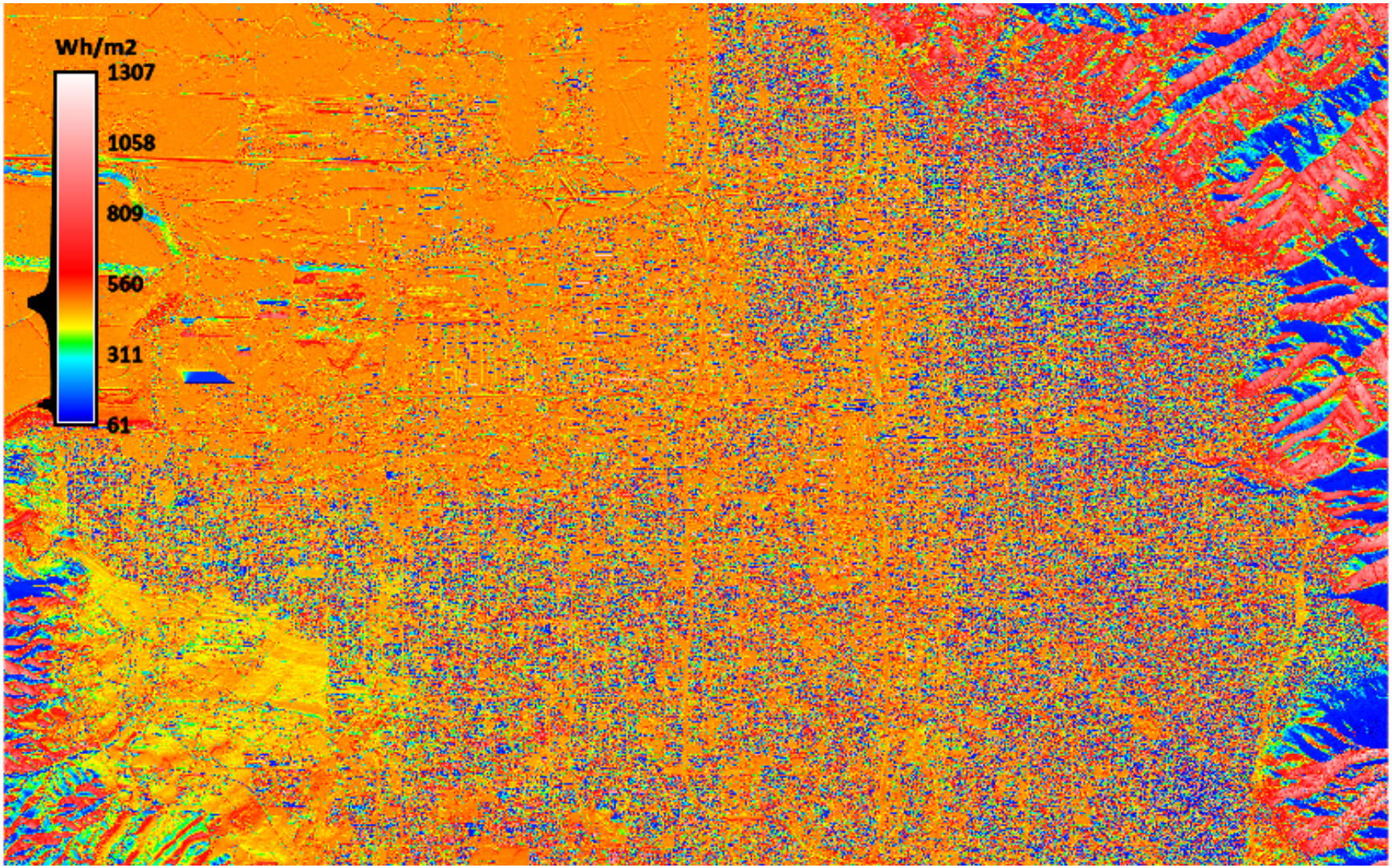

Figure 3.11. Figure showing the Salt Lake Valley PV electricity production at winter solstice using a tilt angle of 40^{0}.

As the tilt angle is increased, the irradiance in the northwestern region continually increases with each incremental step, while the sub-regions within the eastern and southern regions show smaller increases. This again is because the northwestern region is far more open and less developed. The industrial and commercial sectors within the northwestern region consist of buildings with a more uniform height distribution, which are spaced farther apart. This results in less roof top shadowing due to the trigonometry between the buildings and the sun altitude angle. Each of these characteristics contributes to the better PV potential for the region. However, this is not the case within the more densely populated regions as they are developed with buildings and vegetation that consist of random heights and closer spacing.

The irradiation magnitude at sub-regions within the eastern region increases much less with each incremental step. Development areas such as East Millcreek utilize the natural ecosystem by building homes within the native vegetation, rather than clearing the trees and replanting. This results in larger and a more dense collection of trees that cast shadows onto the intended PV surface area that the increased tilt angle cannot address. Likewise, because of its location with respect to the mountain range, the area is covered by the mountainous shadow until late morning. A similar case is experienced in more developed and populated areas such as Cottonwood, Holladay, and the eastern Salt Lake areas. Much of the land developments and buildings within these areas were constructed several years ago. The native and non-native landscape has overgrown many of the buildings and structures over the years, resulting in more shadowing on the intended PV areas. These areas are also relatively close to the eastern mountain range, although the morning shadow isn't quite as long as it is in the Millcreek area. Various sub-regions within the southwestern region experience similar topographical effects with respect to shading, yet are less severe. Areas such as Taylorsville, West Valley, and Magna contain building developments consisting of more uniform building heights and relatively low vegetation heights, which lessens the shadowing. This contributes to a better area regarding PV potential in comparison to the previously discussed areas. Although these densely populated sub-regions show relatively low potential in some areas, they do consist of areas experiencing similar irradiation magnitude as the northwestern region. Likewise, with increase in tilt angle, the length scale of these sub-regions grows with each incremental step, describing the benefit

of utilizing a tilt angle in less desirable areas. Downtown Salt Lake City consists of several buildings and structures that are closely spaced consisting of nonuniform heights. Within this area, the surrounding vegetation doesn't contribute much to the shadowing; however, the closely spaced buildings cast shadows onto surrounding buildings throughout much of the day, causing lower PV potential within the city regardless of PV tilt angle, except for on these few structures that are taller than their surroundings.

3.2.2 Varying Tilt Angles at Summer Solstice

Applying the previous method used to analyze tilt angles at winter solstice in section 3.2.1 with the inclusion of equation 2.5, the average sun altitude angle at the summer solstice was determined to be 46.5^o, indicating the ideal tilt angle for a south facing systems during the summer solstice is 43.5^o. Again, it is not typical for property owners to vary tilt angles according to seasonal changes, yet as α approaches 43.5^o, the potential for PV electricity generation increases. The following figures show the electrical power generation potential of a PV system in Salt Lake Valley at tilt angles varying from 0^o - 40^o and a PV array efficiency of 15%.

3.2.2.1 Summer Solstice Tilt Angle Results

Figures 3.12 - 3.20 show the potential for PV electricity generation in Salt Lake Valley as a function of tilt angle at the summer solstice. As expected, the magnitude of the electricity generation potential within the valley increases in comparison to that at winter solstice, which is due to the increased sun altitude angle and duration of exposure. With an increased altitude angle, more incident irradiation is obtainable at the surface, only increasing with each incremental step in tilt angle. Likewise, less shadowing area is cast by the surrounding topography. Again, the northwestern region shows the most potential at any given tilt angle, whereas the eastern and southern regions of the valley show lower potential. Similar to the winter solstice scenario, as the tilt angle is increased, the irradiance in the northwestern region continually increases with each incremental step; however, only a few sub-regions within the eastern and southern regions show smaller increases. This again is because the northwestern region is far more open and less developed, and because of its positioning with respect to the mountain ranges. The same reasoning holds to the previous discussion of better PV potential in the northwestern region during winter

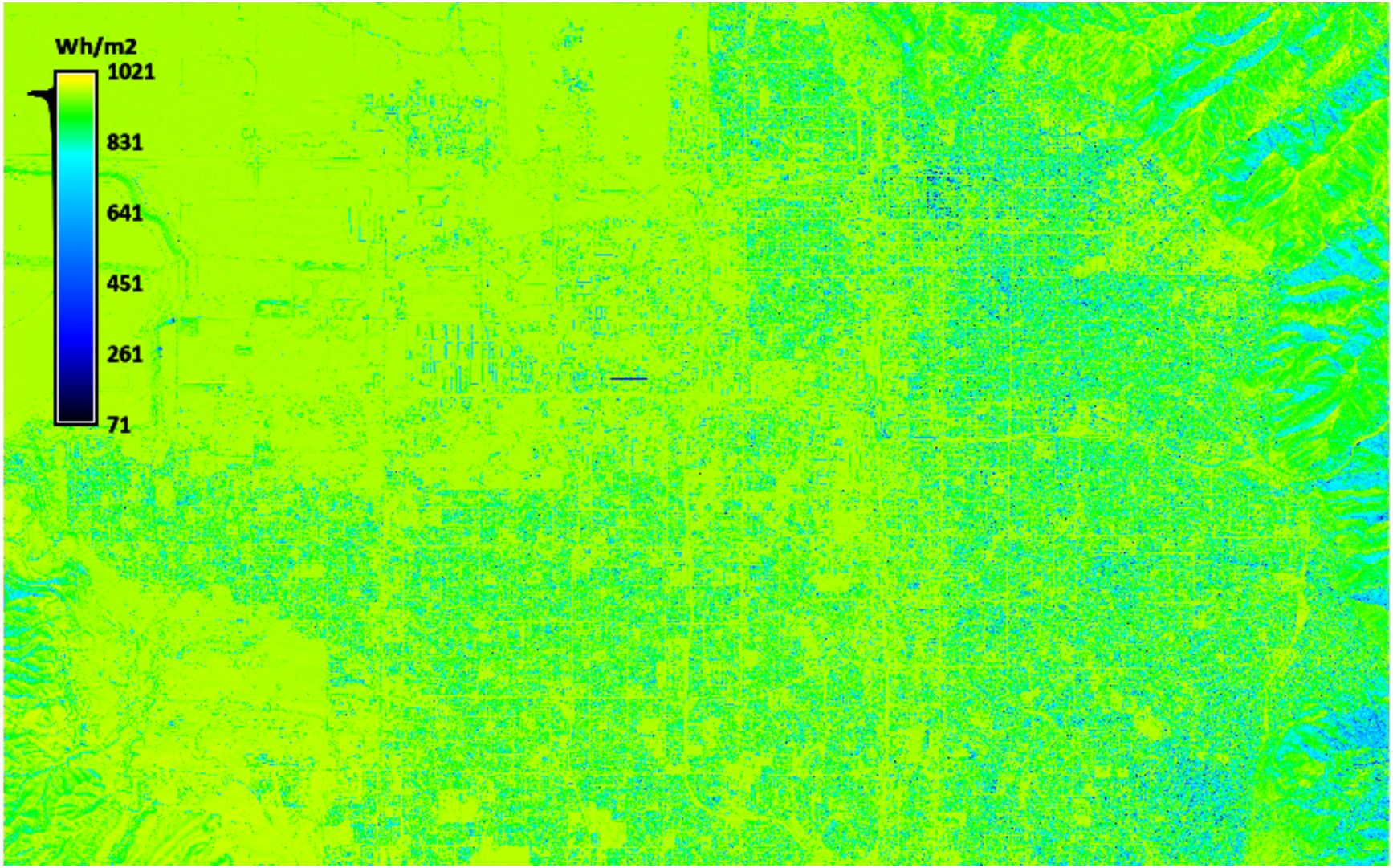

Figure 3.12. Figure showing the Salt Lake Valley PV electricity production at summer solstice using a tilt angle of 0^o.

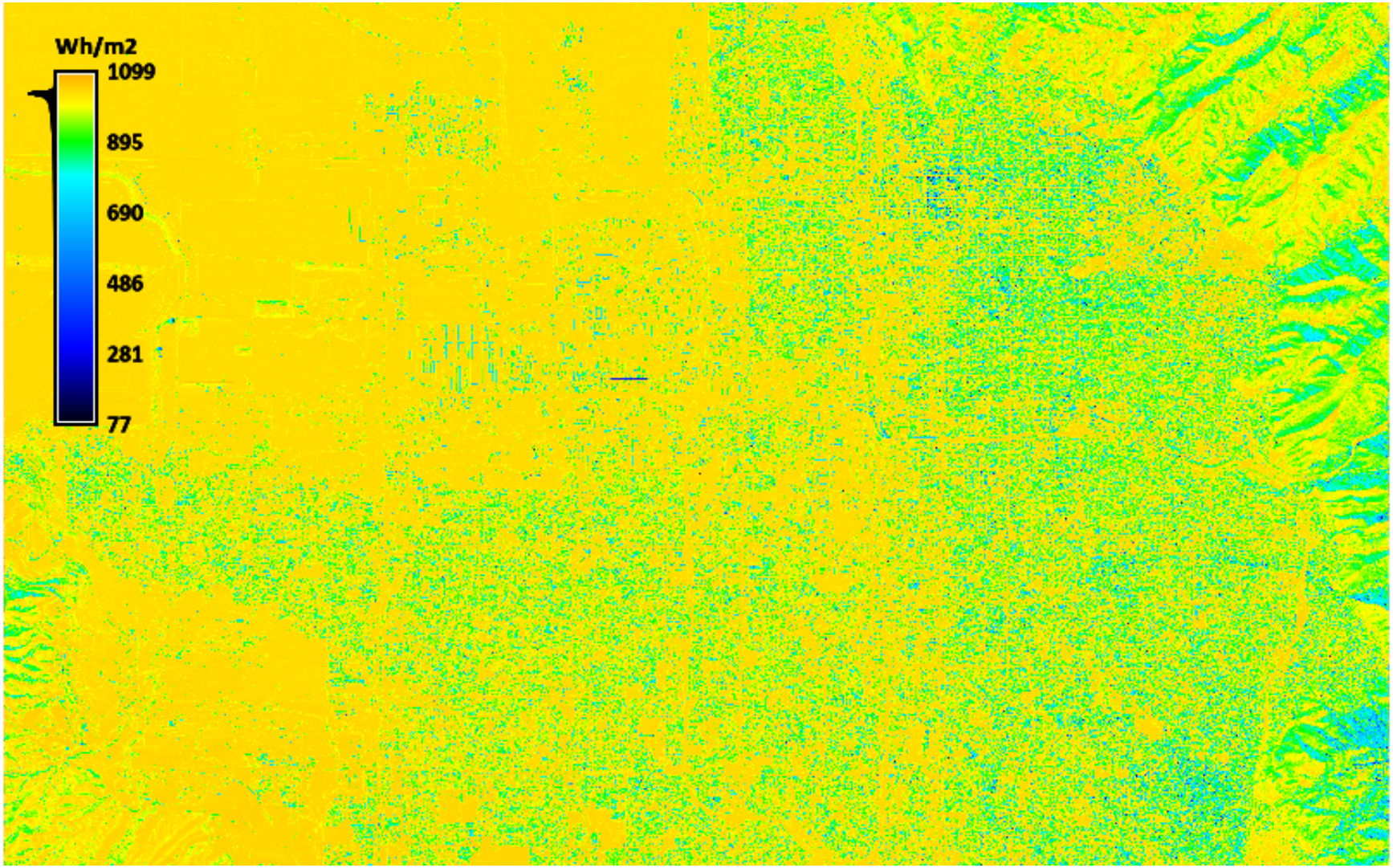

Figure 3.13. Figure showing the Salt Lake Valley PV electricity production at summer solstice using a tilt angle of 5^o.

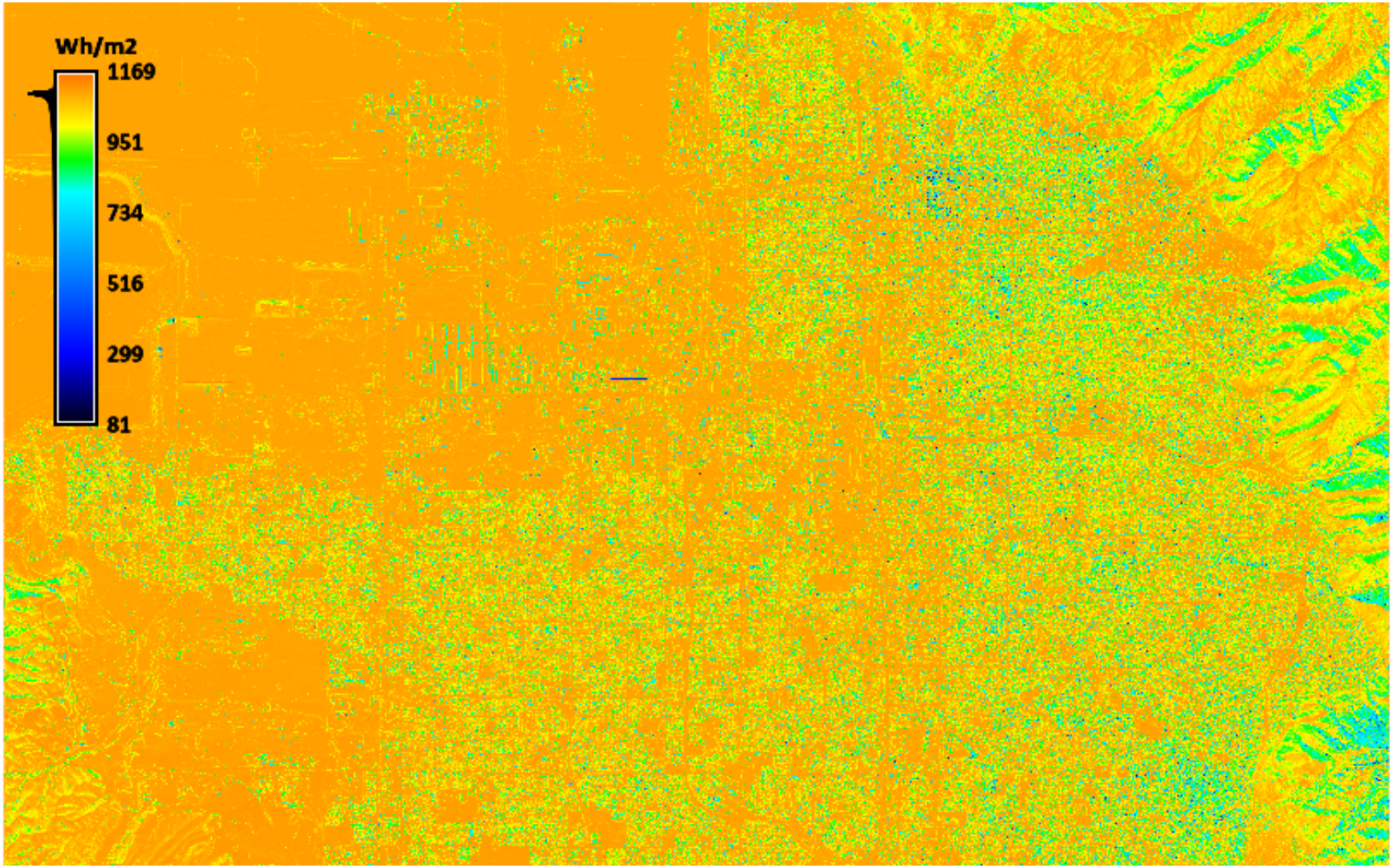

Figure 3.14. Figure showing the Salt Lake Valley PV electricity production at summer solstice using a tilt angle of 10^o.

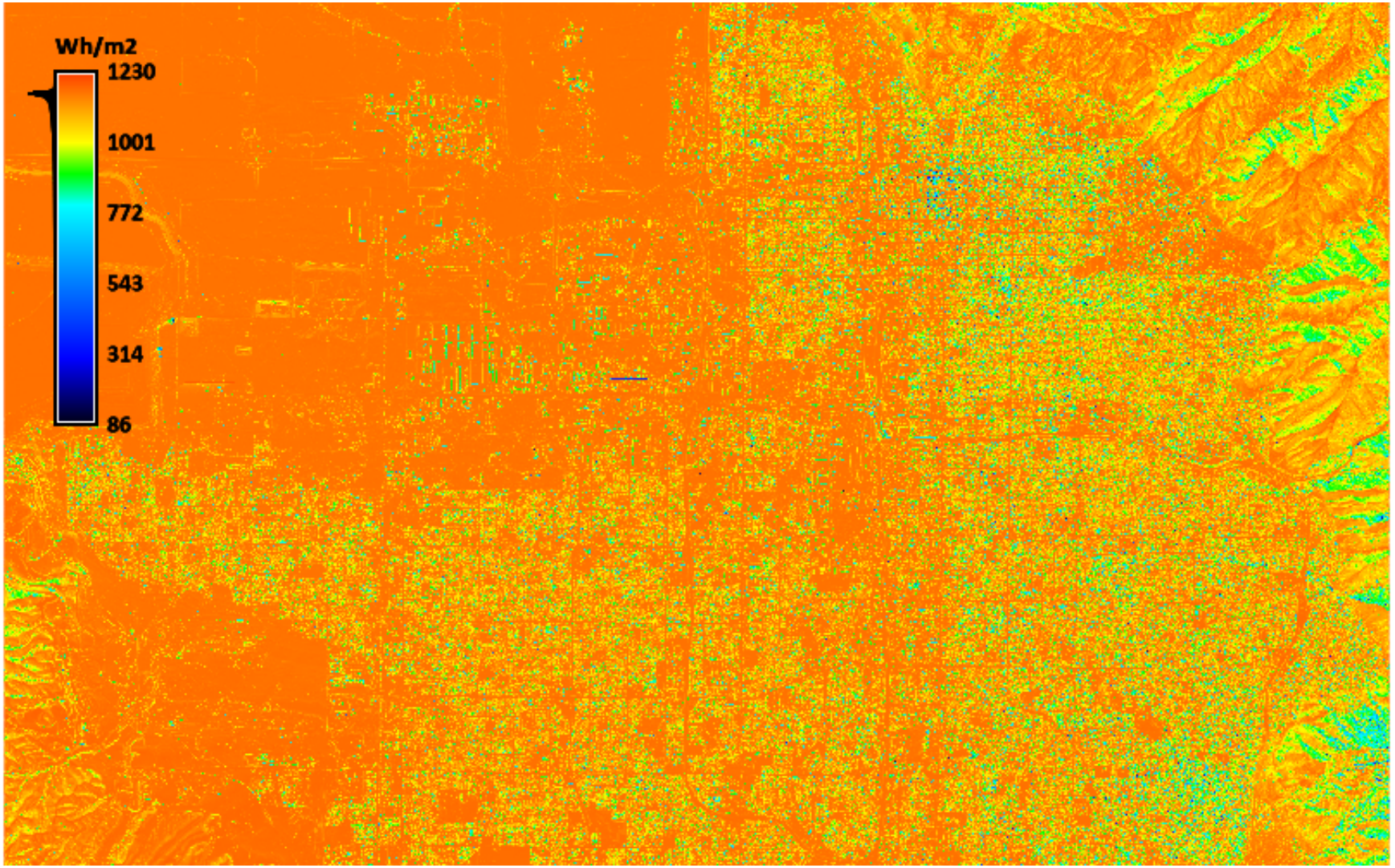

Figure 3.15. Figure showing the Salt Lake Valley PV electricity production at summer solstice using a tilt angle of 15^o.

Figure 3.16. Figure showing the Salt Lake Valley PV electricity production at summer solstice using a tilt angle of 20^o.

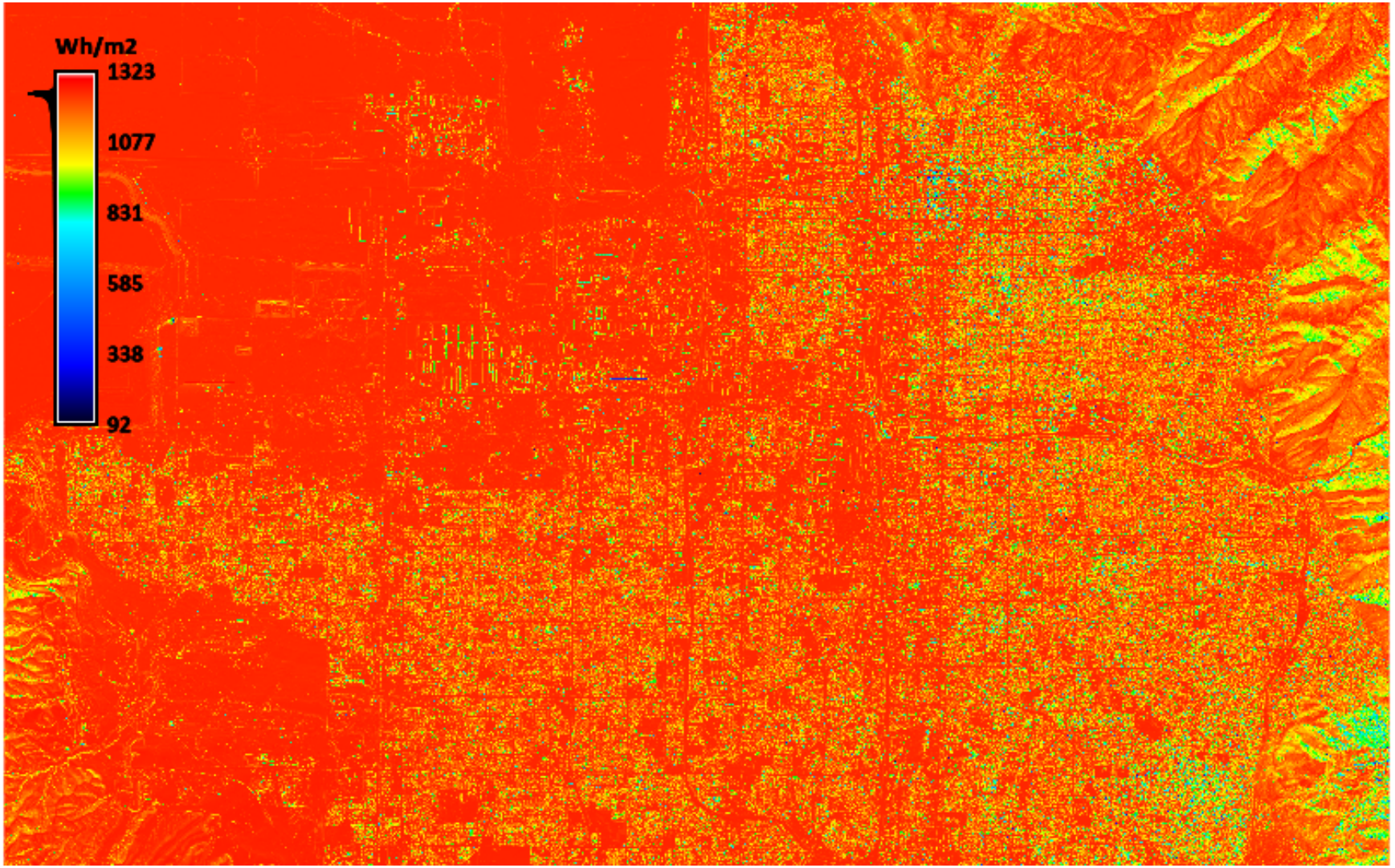

Figure 3.17. Figure showing the Salt Lake Valley PV electricity production at summer solstice using a tilt angle of 25^o.

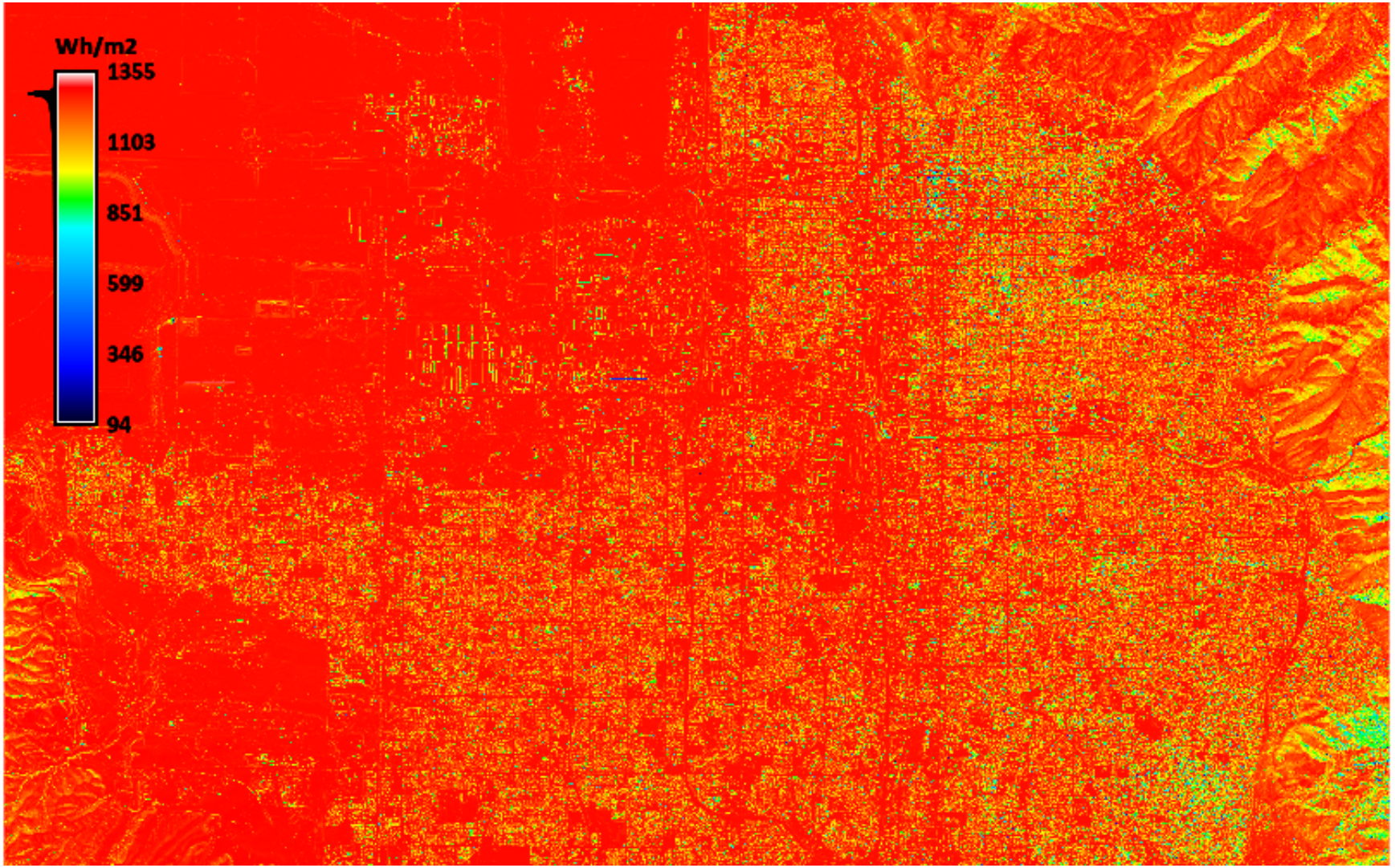

Figure 3.18. Figure showing the Salt Lake Valley PV electricity production at summer solstice using a tilt angle of 30^o.

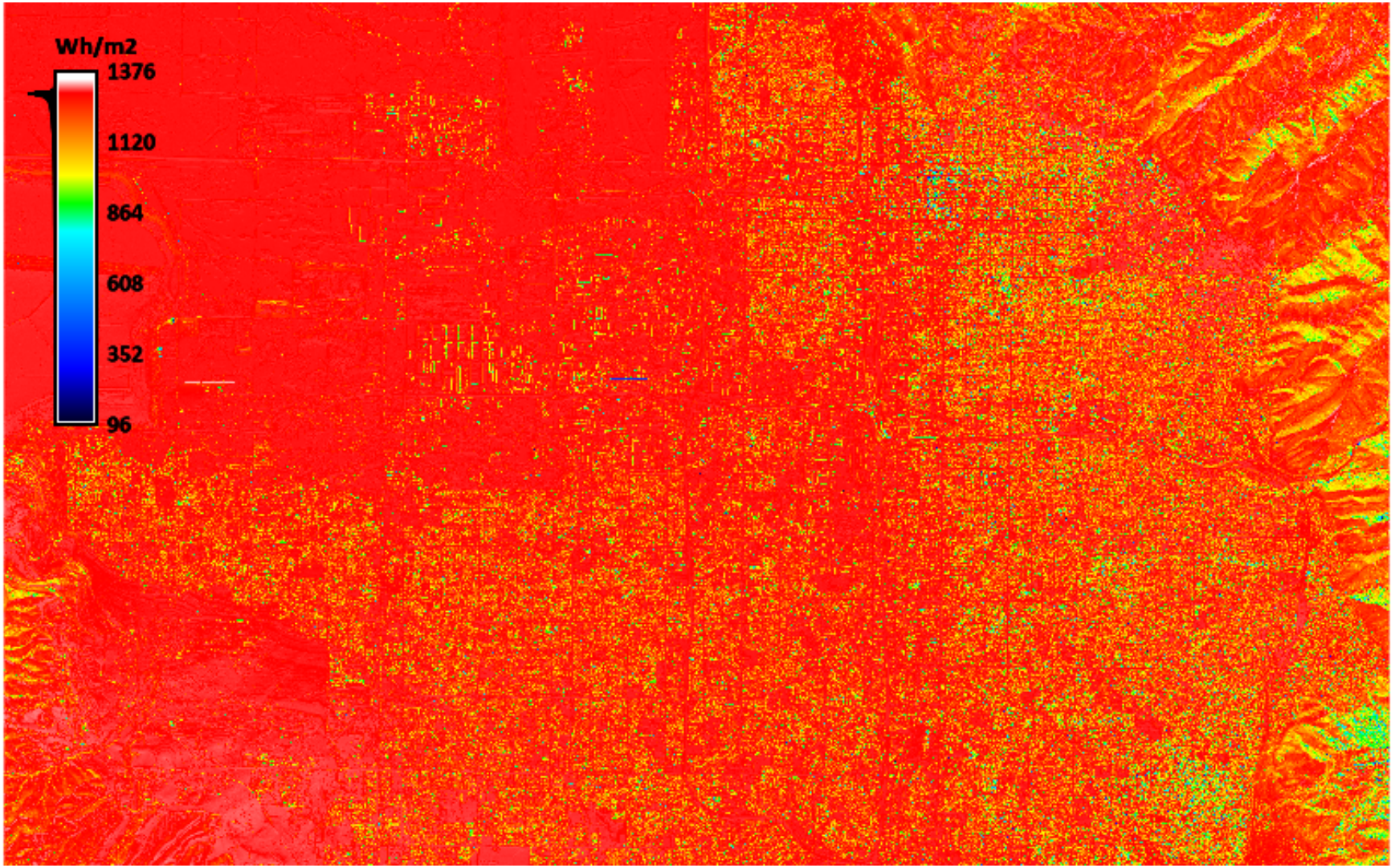

Figure 3.19. Figure showing the Salt Lake Valley PV electricity production at summer solstice using a tilt angle of 35^o.

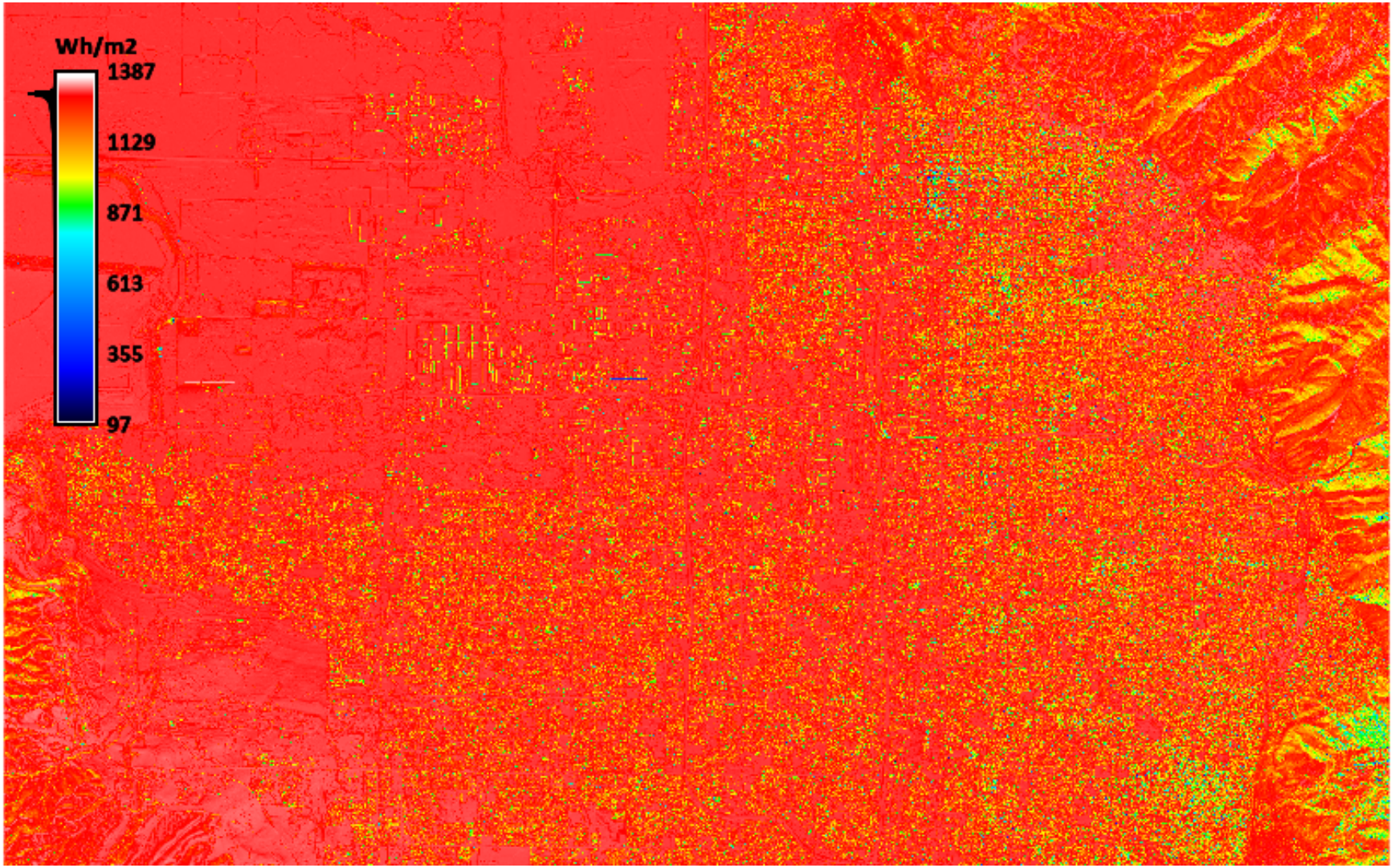

Figure 3.20. Figure showing the Salt Lake Valley PV electricity production at summer solstice using a tilt angle of 40^o.

solstice, yet the magnitude during summer solstice is larger because of the increased sun altitude angle allowing for more collection of incident irradiation.

The irradiation magnitude at a few sub-regions within the eastern region increases at a small rate with each incremental step. However, compared to winter solstice, many more sub-regions within the eastern region increase at a higher rate with each step. In this scenario, areas such as East Millcreek that utilize the natural ecosystem by building homes within the native vegetation are able to collect more incident irradiance due to the higher sun altitude angle. With the higher altitude angle, the shadowing of the local topography is far less dominant when compared to that at winter solstice. The density of the vegetation plays a lessened role in the impact of PV potential, and the duration of the mountainous morning shadow is lower. Similarly, in more mature areas such as Cottonwood, Holladay, and the eastern Salt Lake areas, the overgrown native and non-native landscape within these developments has less impact on PV potential. Again, the high sun altitude angle allows for less shadowing caused by the local topography and the irradiation magnitude increases with tilt angle. The sub-regions within the southwestern region experience similar topographical effects with respect to shading and altitude angle, yet the irradiation magnitude is slightly higher. The downtown Salt Lake City area shows the lowest potential in the valley at any given tilt angle due to the tall and closely spaced buildings. Although the sun altitude angle is high, the buildings are so closely spaced it results in topographical shadows for various parts of the area.

3.2.3 Varying Efficiencies at Winter Solstice with Tilt Angle of 10^o and 40^o

A broad range of PV cell efficiencies are available for electricity generation systems. It may be necessary for property owners to install higher efficiency panels in certain regions to meet the building load requirements. This is dependent upon the available area designated for PV array installation, as well as the designed tilt angle and surrounding topography. Sub-regions consisting of large installation areas or relatively low topographical density may benefit with respect to material cost by using less efficient PV cells but more arrays, while smaller installation areas or relatively high topographical density areas may require the more costly, yet highly efficient cells, for the needed power generation. The following figures are presented to illustrate the affects of varying efficiencies throughout

the valley. The analysis consists of 10^o and 40^o tilt angles while varying PV cell efficiencies at 2% increments ranging from 12% - 24% at winter solstice.

3.2.3.1 Efficiency at Winter Solstice Results

Figures 3.21 - 3.27 show the potential PV electricity generation for Salt Lake Valley at winter solstice as a function of the PV cell efficiency evaluated at a tilt angle of 10^o, while Figures 3.28 - 3.34 consist of a tilt angle of 40^o. In general, it is shown that the increase in cell efficiency is proportional to the increase in electricity potential. Similar to the previous case studies, the northwestern region has the highest PV potential within the valley at any given cell efficiency and tilt angle, while various sub-regions within the eastern and southern regions show the lowest potential. It is shown, at a tilt angle of 10^o, that the PV potential for most sub-regions within eastern and southern regions is low at each efficiency increment in comparison to the rest of the valley. At a tilt angle of 40^o, the PV potential becomes better for most of the sub-regions, even at a relatively lower efficiency.

The irradiance magnitude in the northwestern region continues to increase with each incremental step in PV cell efficiency at both tilt angles. The PV potential of the northwestern region is the highest in the valley due to its positioning with respect to the mountain ranges, the undeveloped land, and lower topographical density. These factors contribute to the high irradiation magnitude in comparison to the valley due to the lessened topographical shading. Most sub-regions within the northwestern region are eligible for utilizing each PV cell efficiency at either tilt angle that meets the requirements for a building's energy needs, because of the relatively low shading.

Various sub-regions within the eastern region may require a high PV cell efficiency at a tilt angle of 10^o, whereas these same sub-regions would require a lower cell efficiency at a tilt angle of 40^o to produce the same amount of energy annually. Areas such as East Millcreek that consist of high-density native landscape may require a larger cell efficiency to compensate for partial PV panel shading at low sun altitude angles. Similarly, the more mature areas such as Cottonwood, Holladay, and the eastern Salt Lake areas may require a larger PV cell efficiency to also compensate for the partial array shading, which is due to the overgrown native and non-native landscape. The landscape restricts the incidental irradiance, so the higher cell efficiency may be required to compensate for the partial

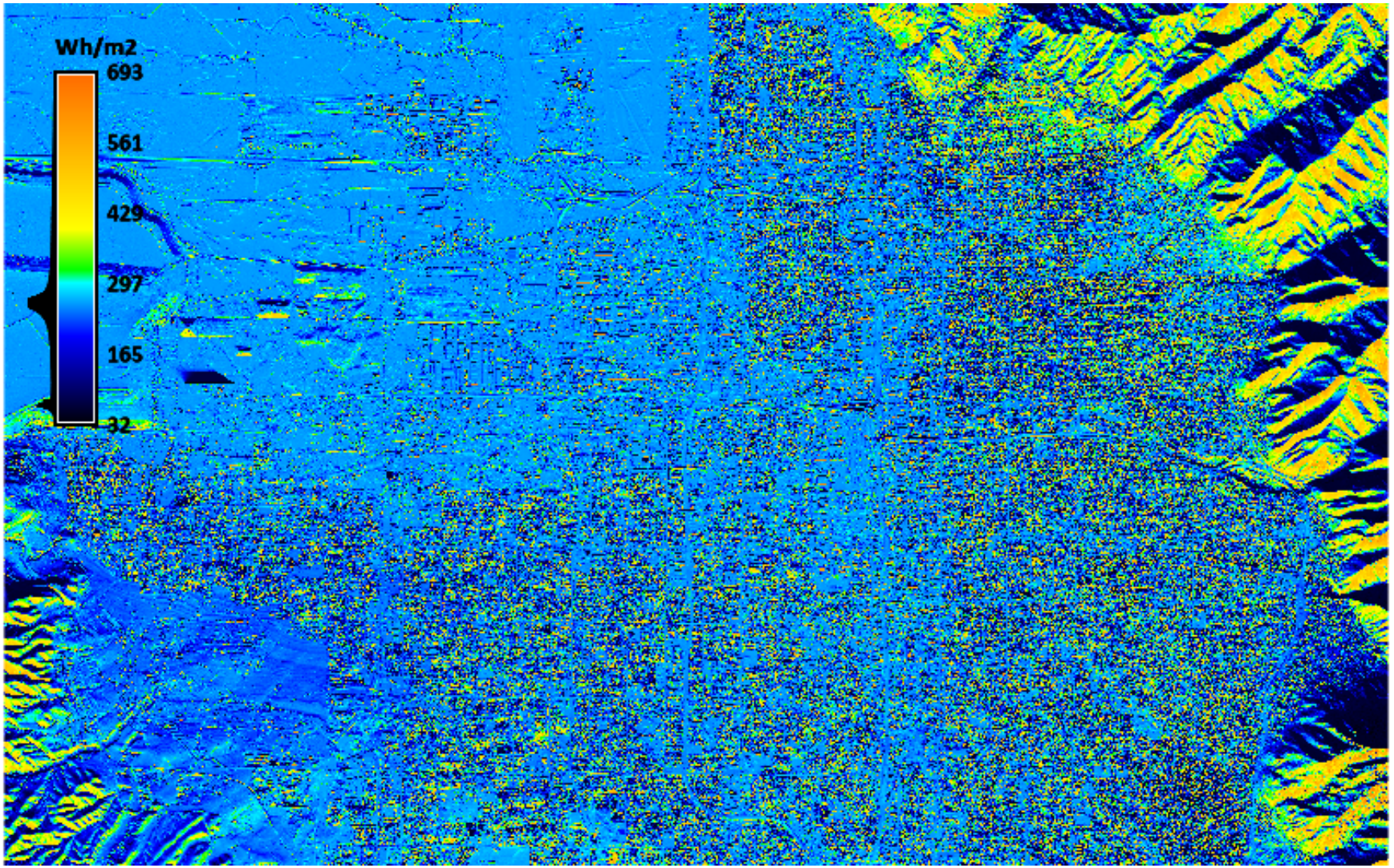

Figure 3.21. Figure showing the Salt Lake Valley PV electricity production at winter solstice with a 10^o tilt and $\eta_{PV} = 12\%$.

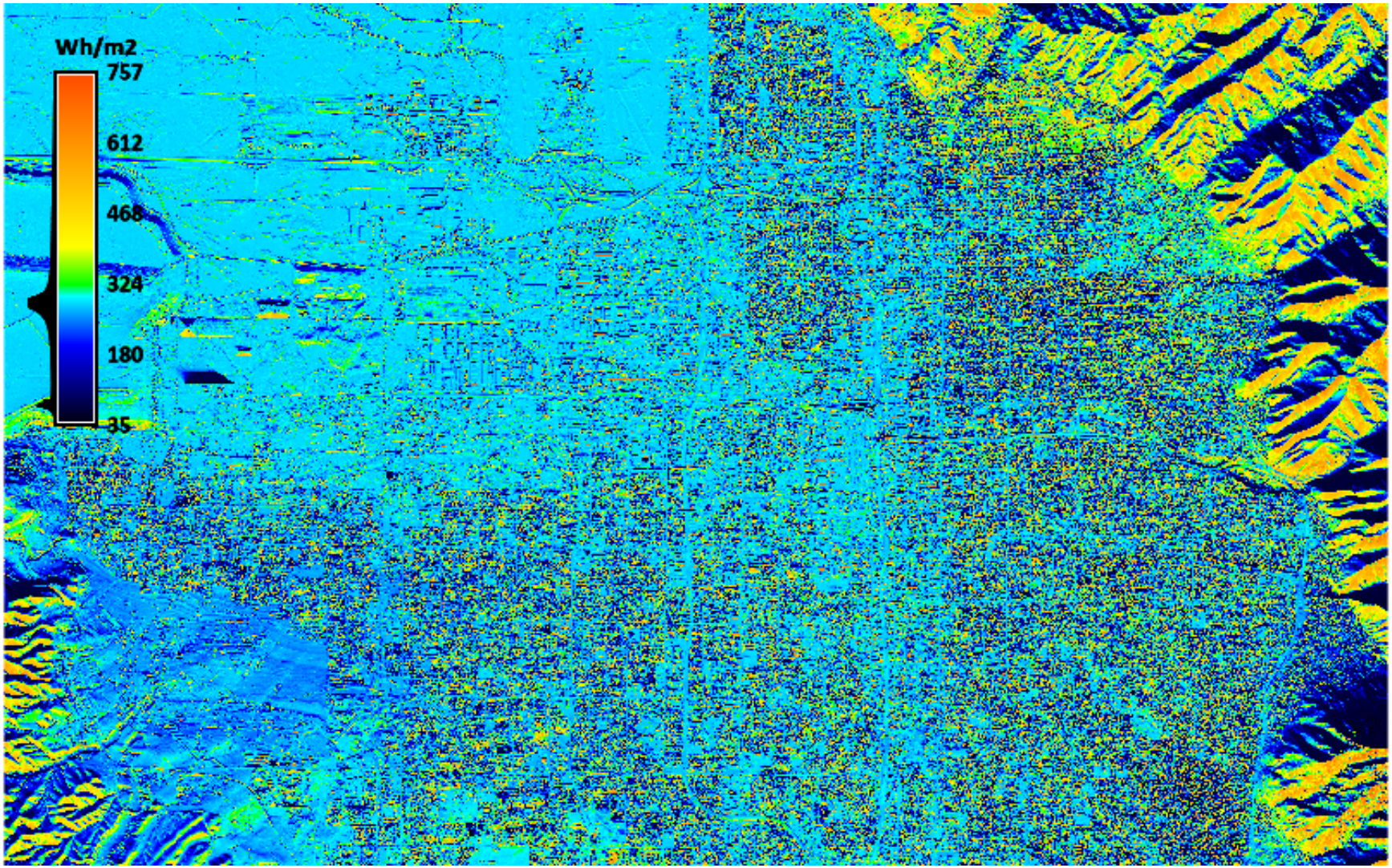

Figure 3.22. Figure showing the Salt Lake Valley PV electricity production at winter solstice with a 10^o tilt and $\eta_{PV} = 14\%$.

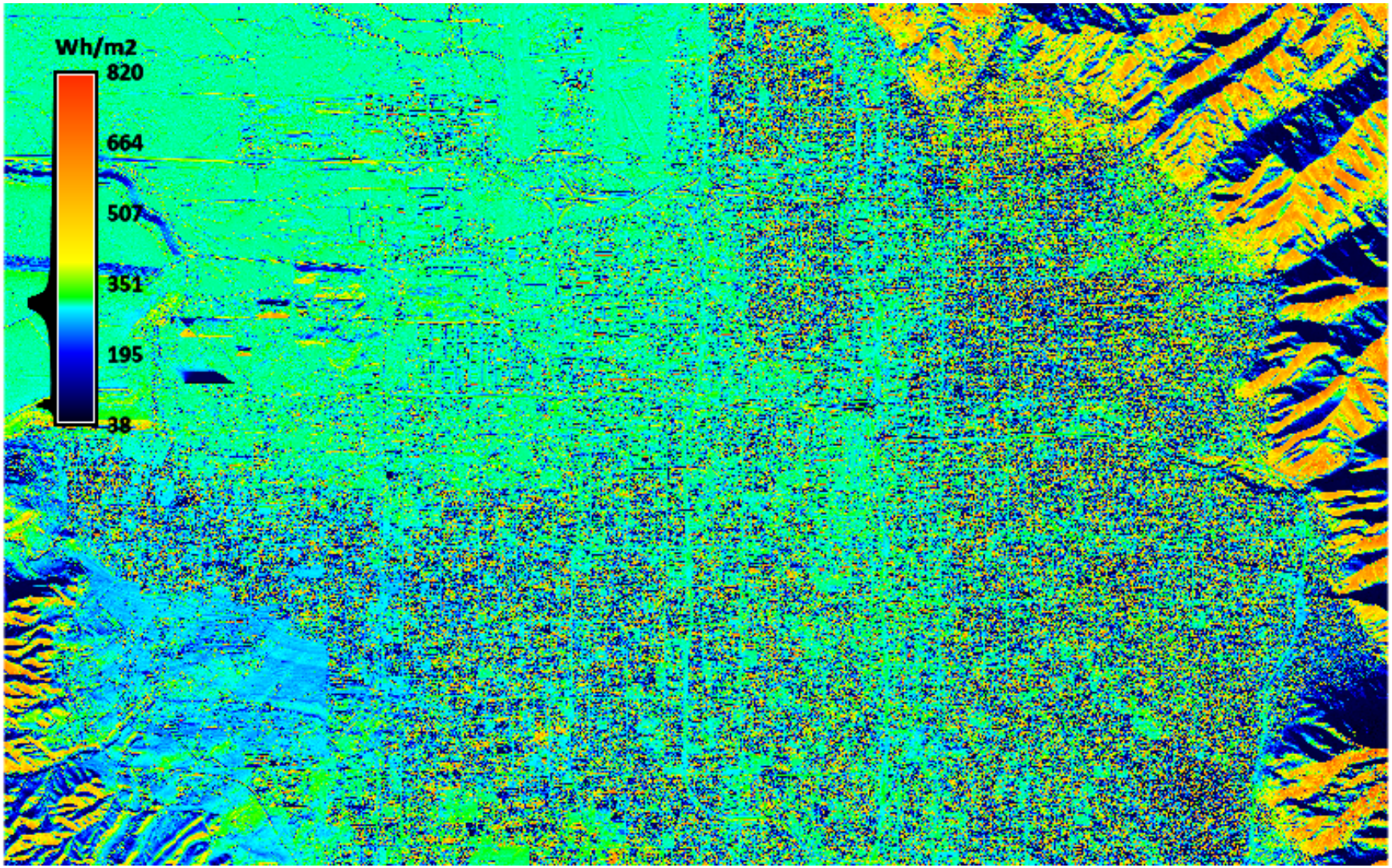

Figure 3.23. Figure showing the Salt Lake Valley PV electricity production at winter solstice with a 10^o tilt and $\eta_{PV} = 16\%$.

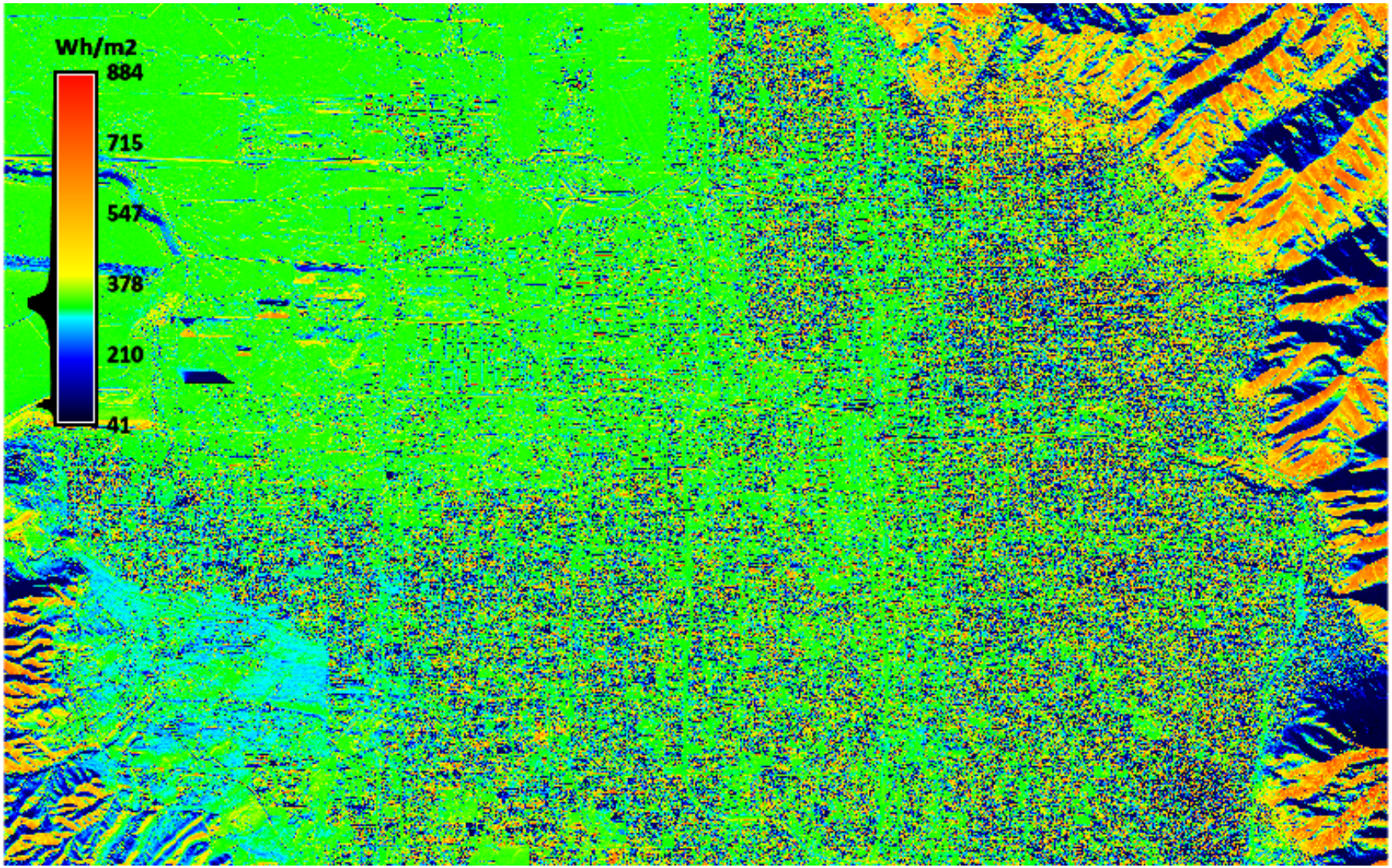

Figure 3.24. Figure showing the Salt Lake Valley PV electricity production at winter solstice with a 10^o tilt and $\eta_{PV} = 18\%$.

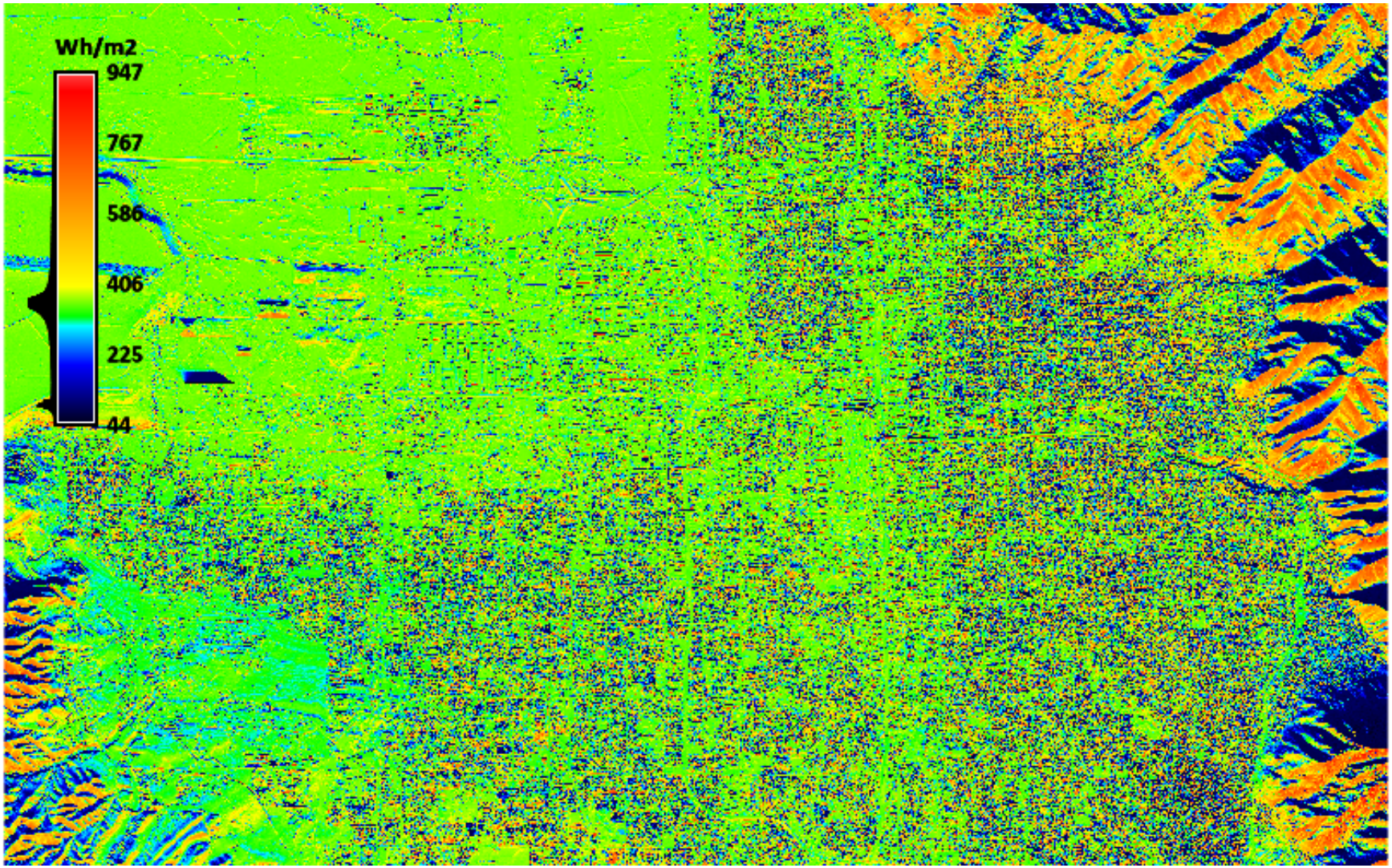

Figure 3.25. Figure showing the Salt Lake Valley PV electricity production at winter solstice with a 10^o tilt and $\eta_{PV} = 20\%$.

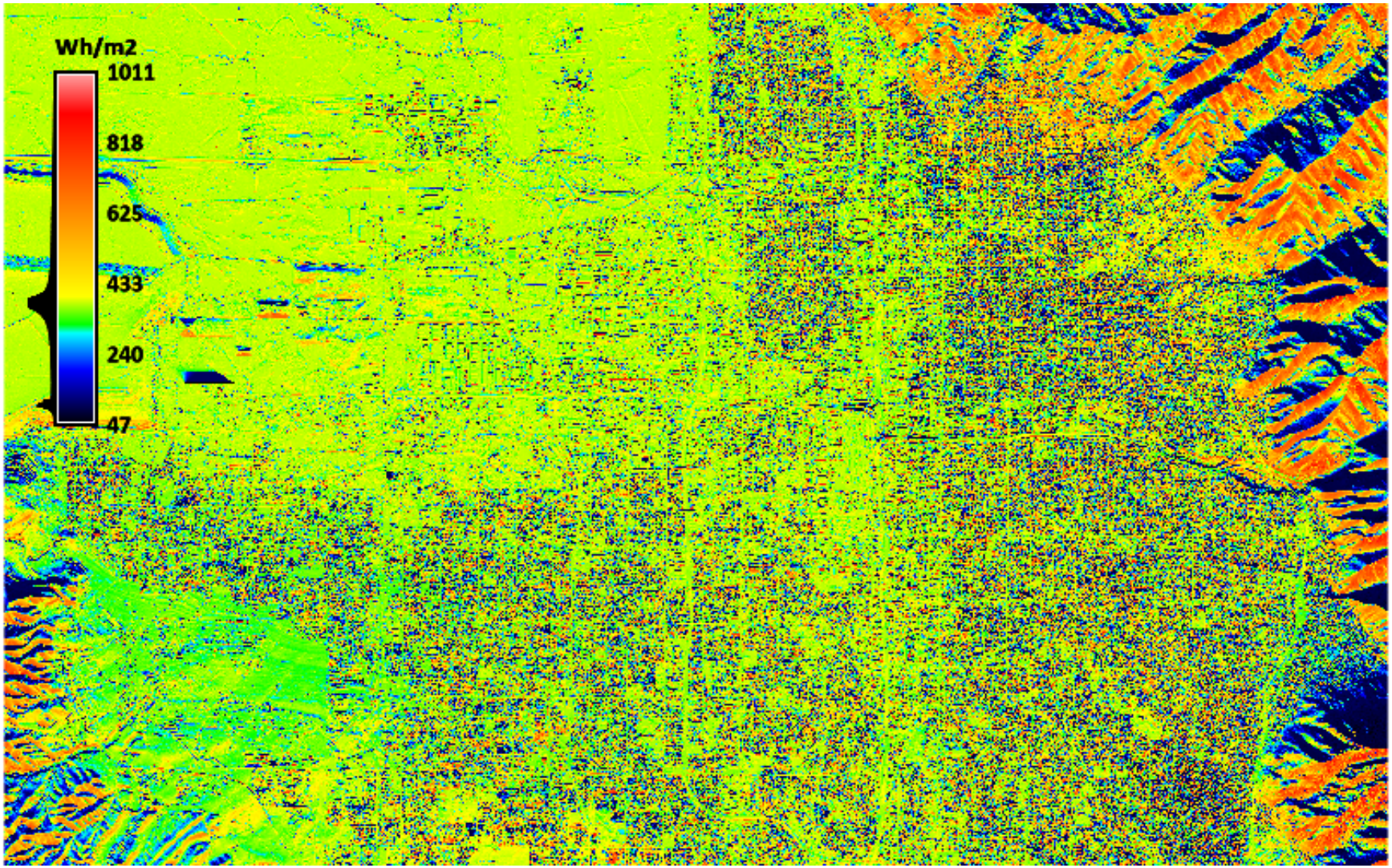

Figure 3.26. Figure showing the Salt Lake Valley PV electricity production at winter solstice with a 10^o tilt and $\eta_{PV} = 22\%$.

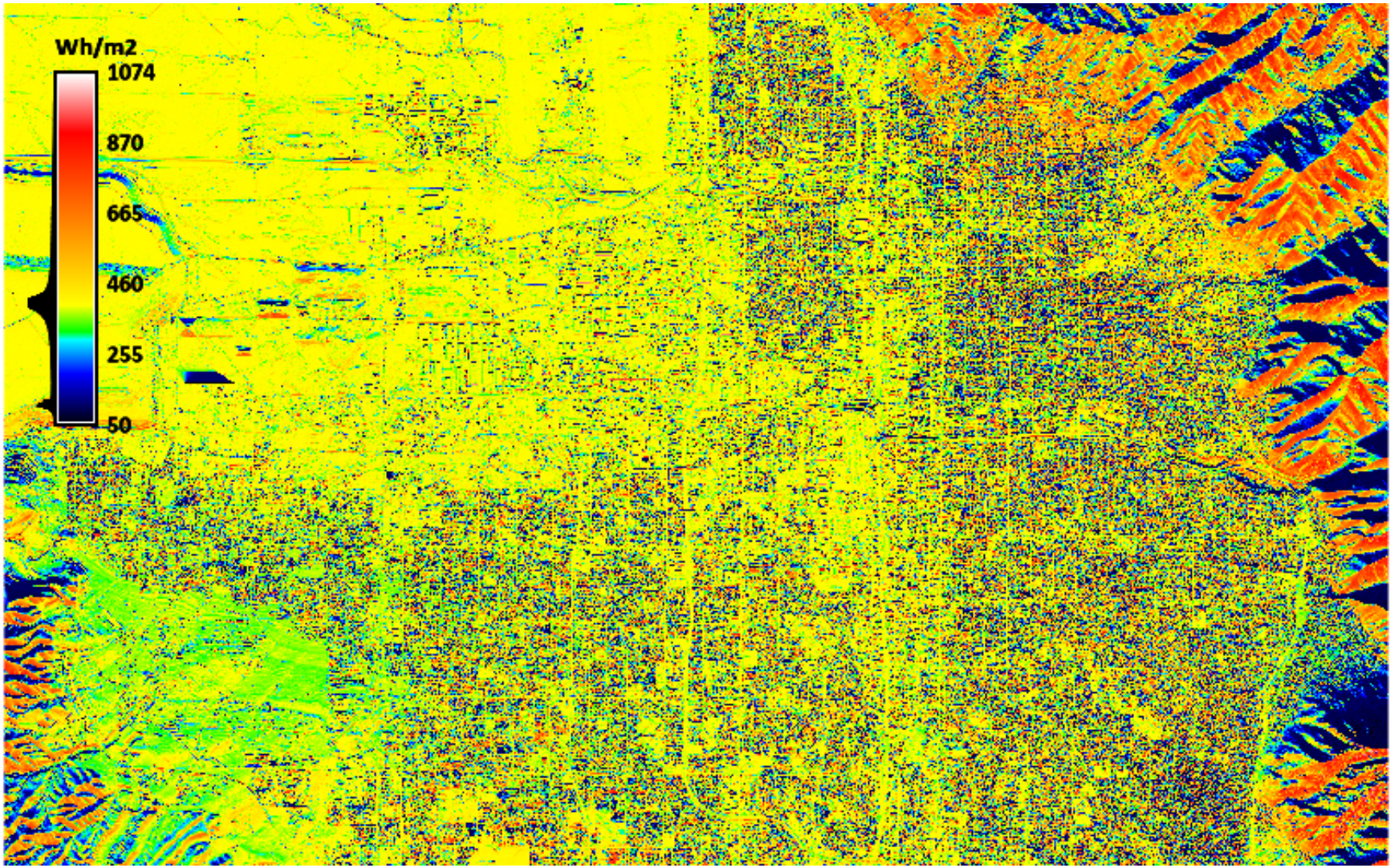

Figure 3.27. Figure showing the Salt Lake Valley PV electricity production at winter solstice with a 10^o tilt and $\eta_{PV} = 24\%$.

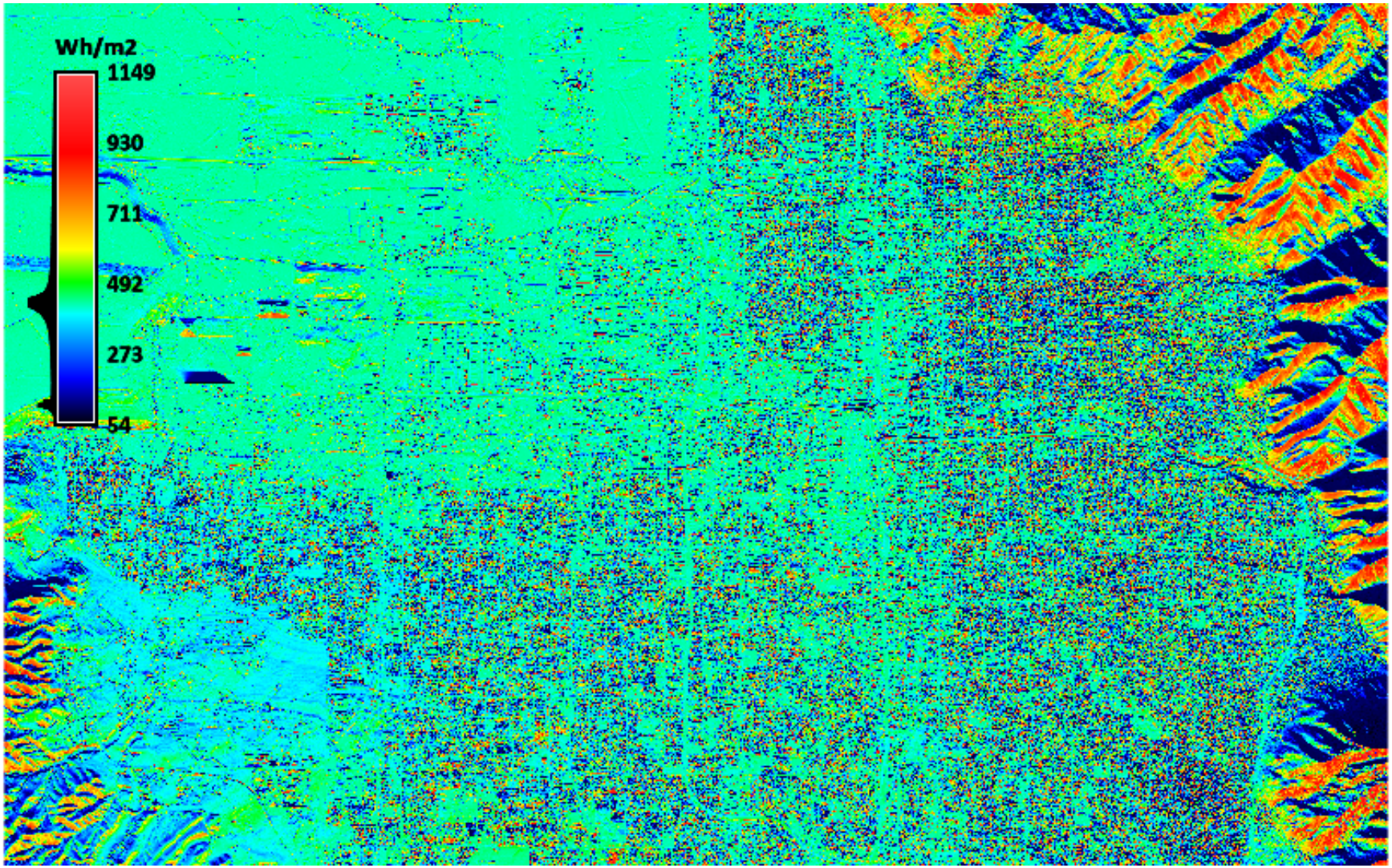

Figure 3.28. Figure showing the Salt Lake Valley PV electricity production at winter solstice with a 40^o tilt and $\eta_{PV} = 12\%$.

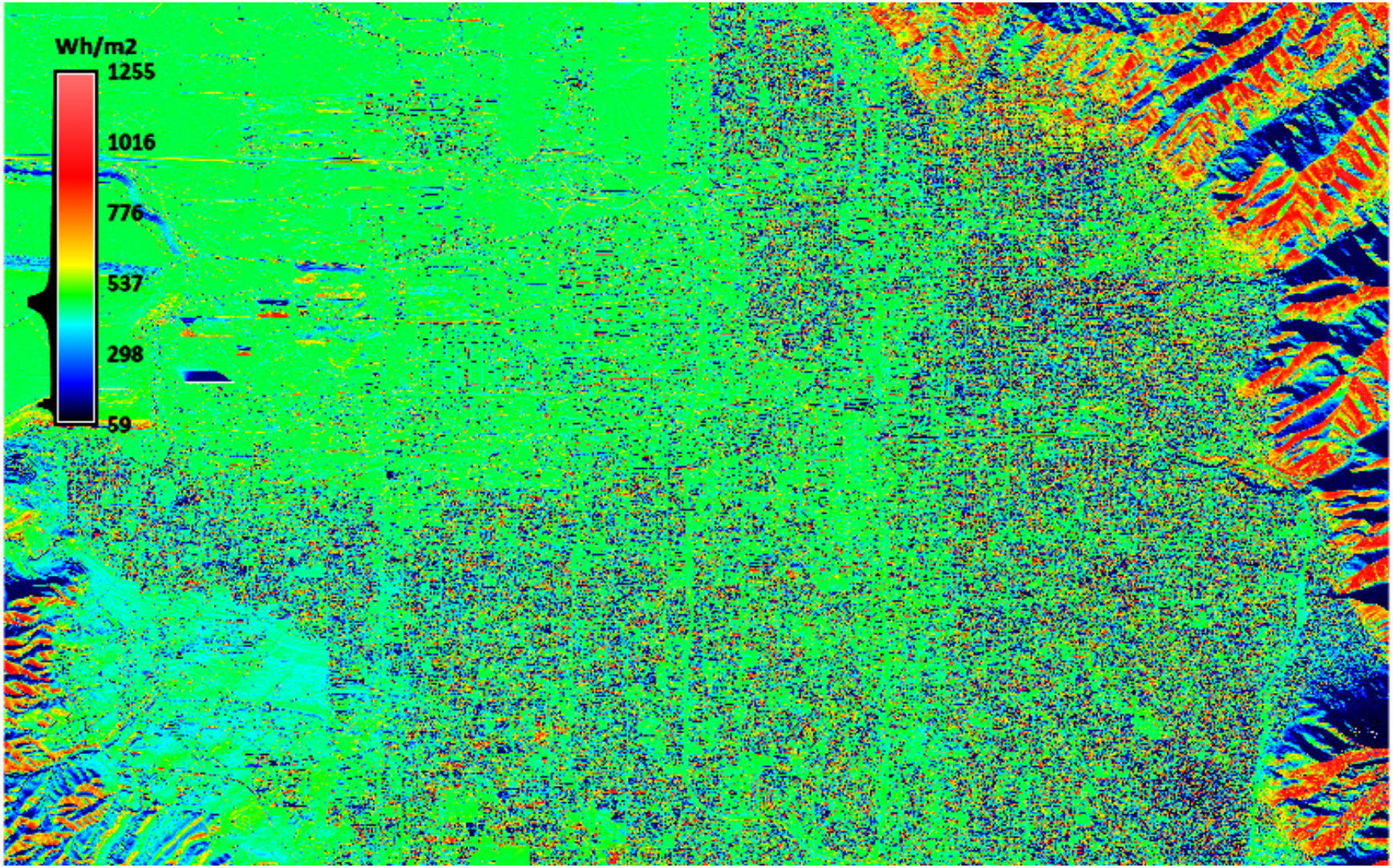

Figure 3.29. Figure showing the Salt Lake Valley PV electricity production at winter solstice with a 40^o tilt and $\eta_{PV} = 14\%$.

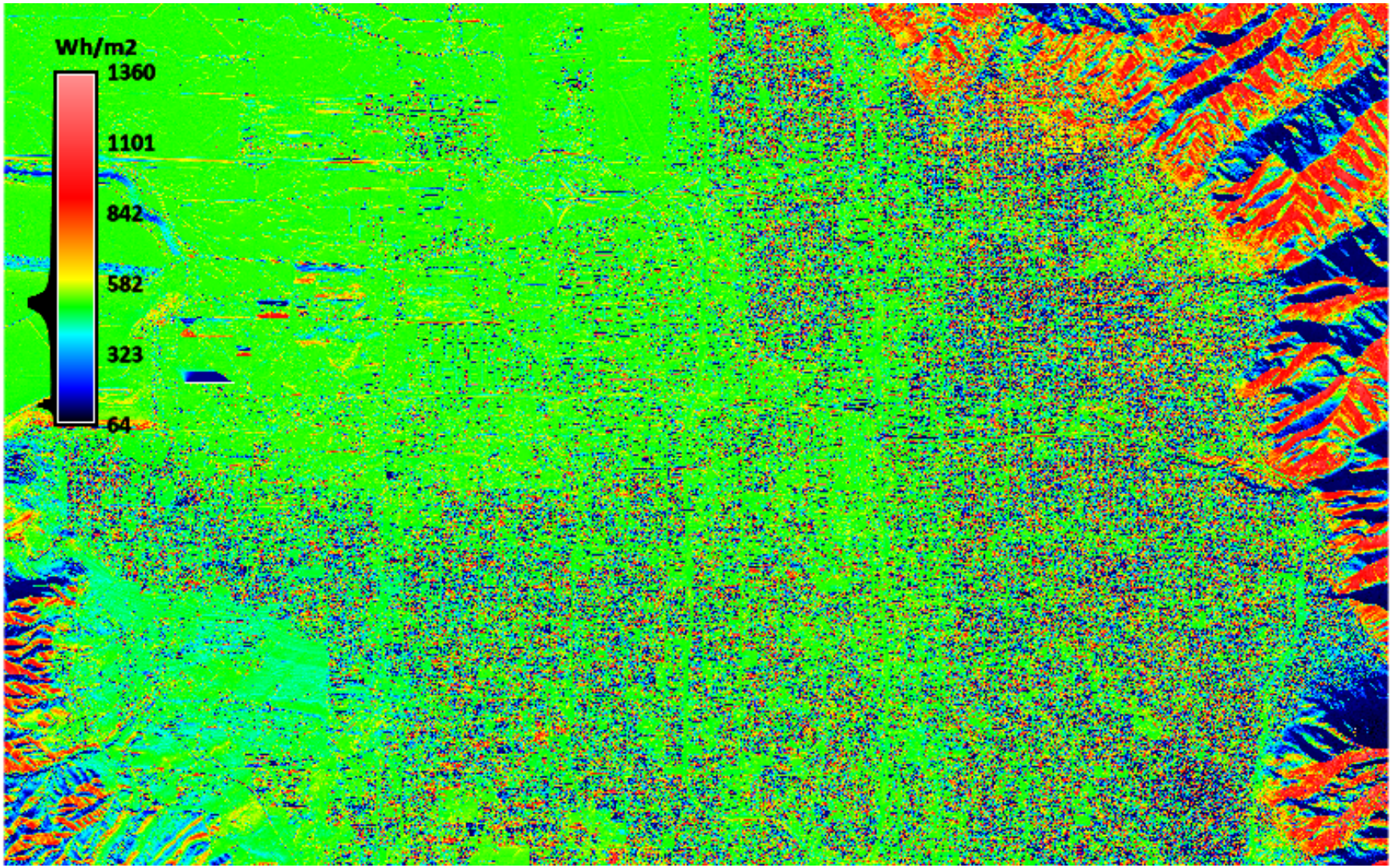

Figure 3.30. Figure showing the Salt Lake Valley PV electricity production at winter solstice with a 40^o tilt and $\eta_{PV} = 16\%$.

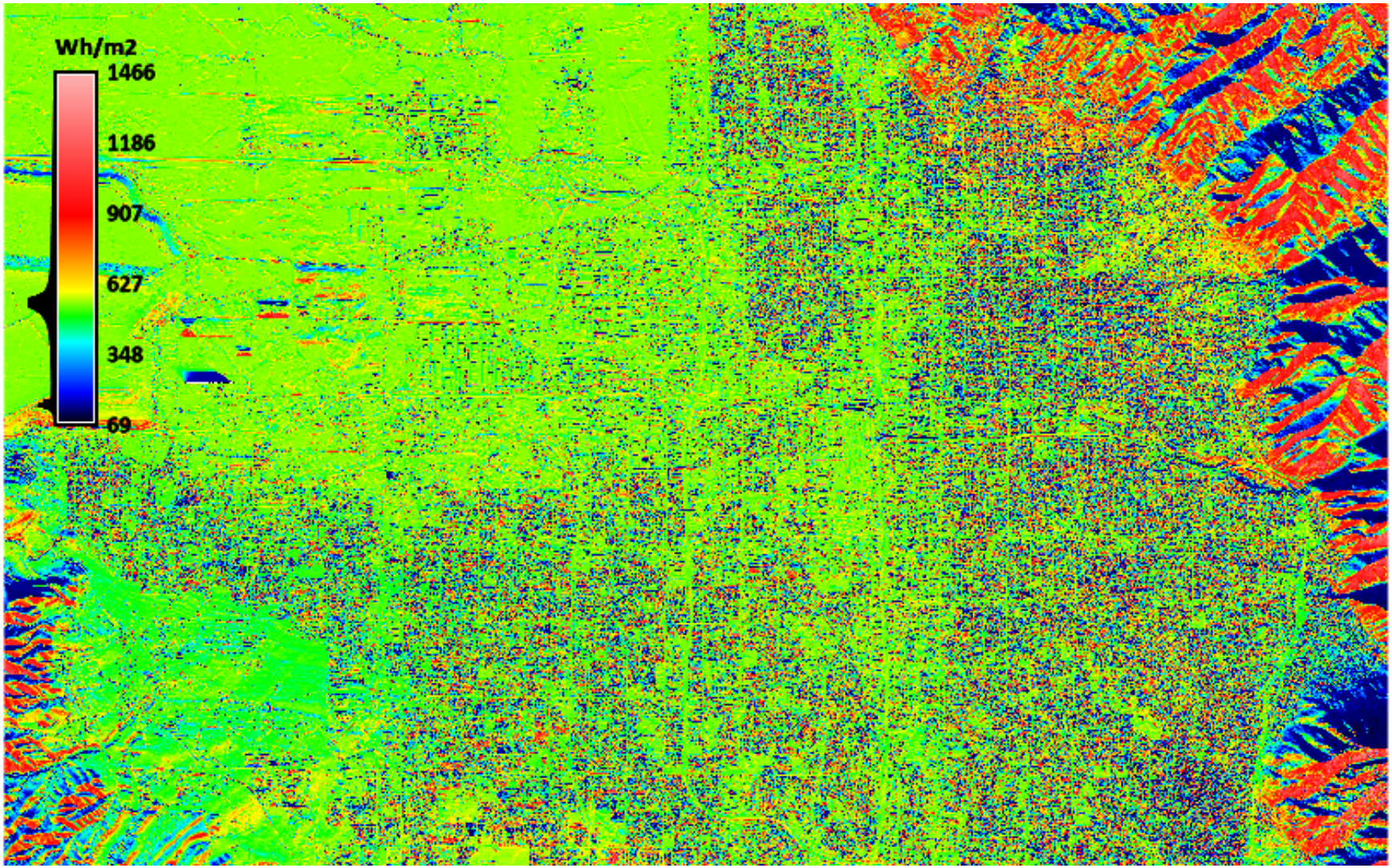

Figure 3.31. Figure showing the Salt Lake Valley PV electricity production at winter solstice with a 40^o tilt and $\eta_{PV} = 18\%$.

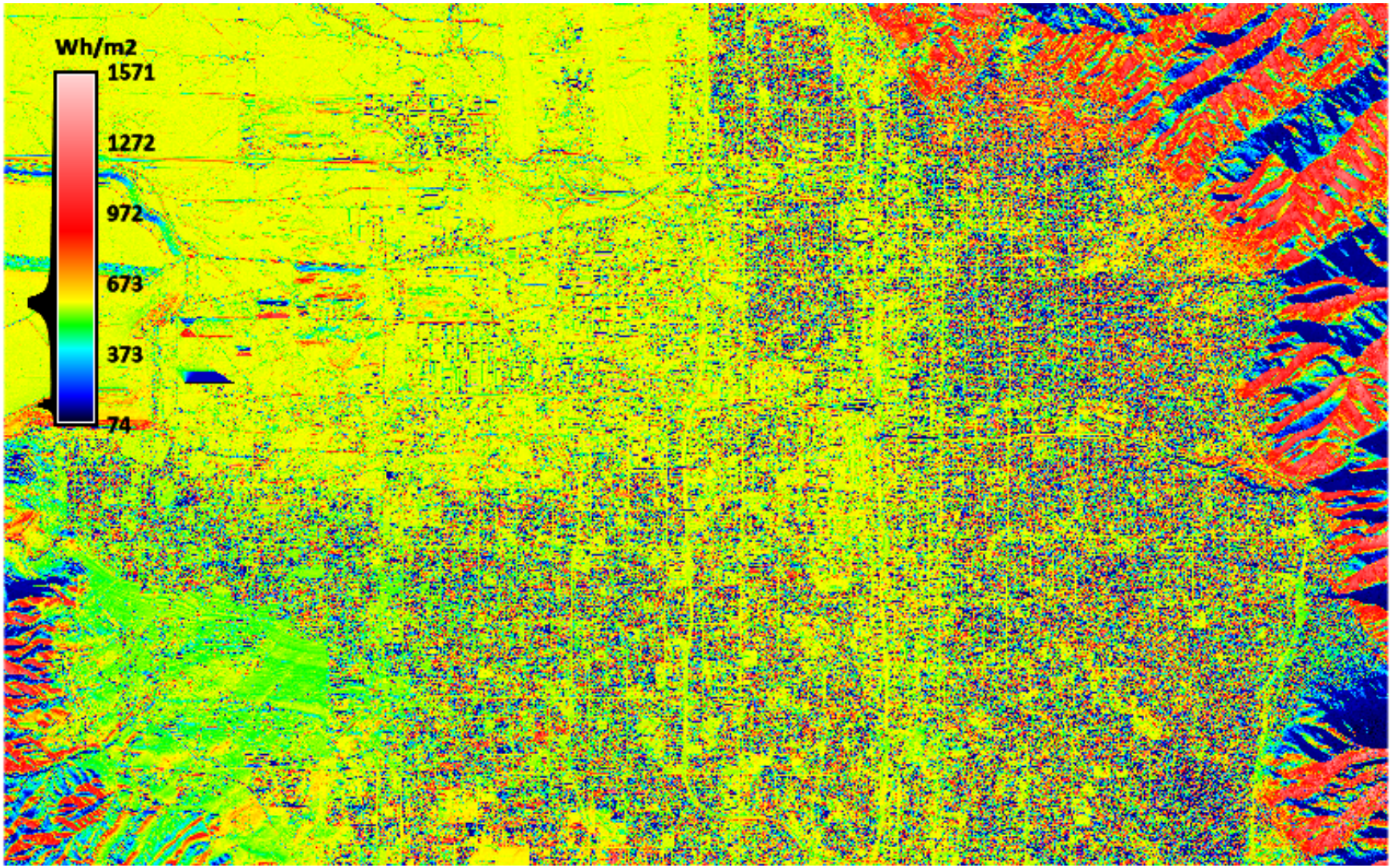

Figure 3.32. Figure showing the Salt Lake Valley PV electricity production at winter solstice with a 40^o tilt and $\eta_{PV} = 20\%$.

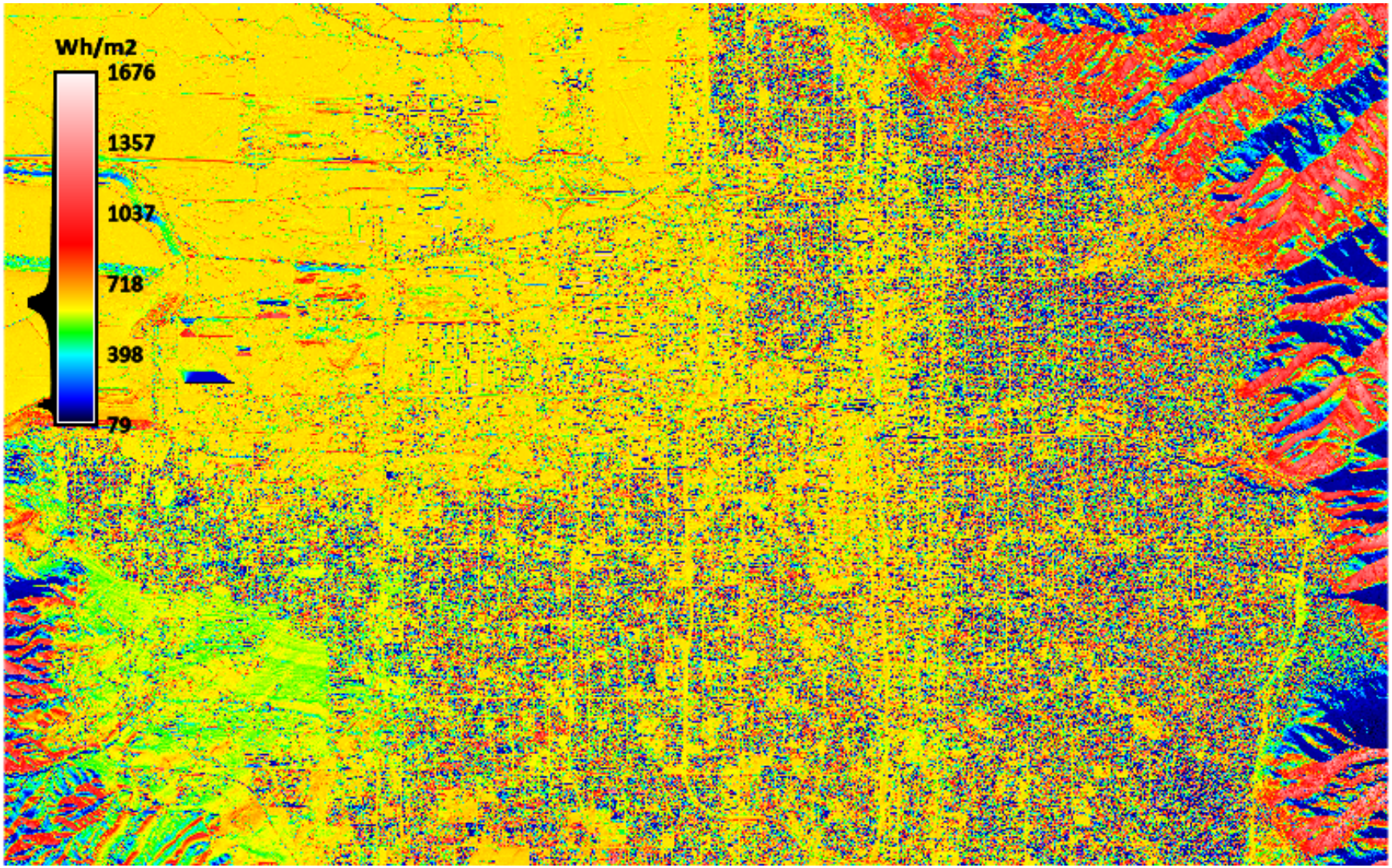

Figure 3.33. Figure showing the Salt Lake Valley PV electricity production at winter solstice with a 40^o tilt and $\eta_{PV} = 22\%$.

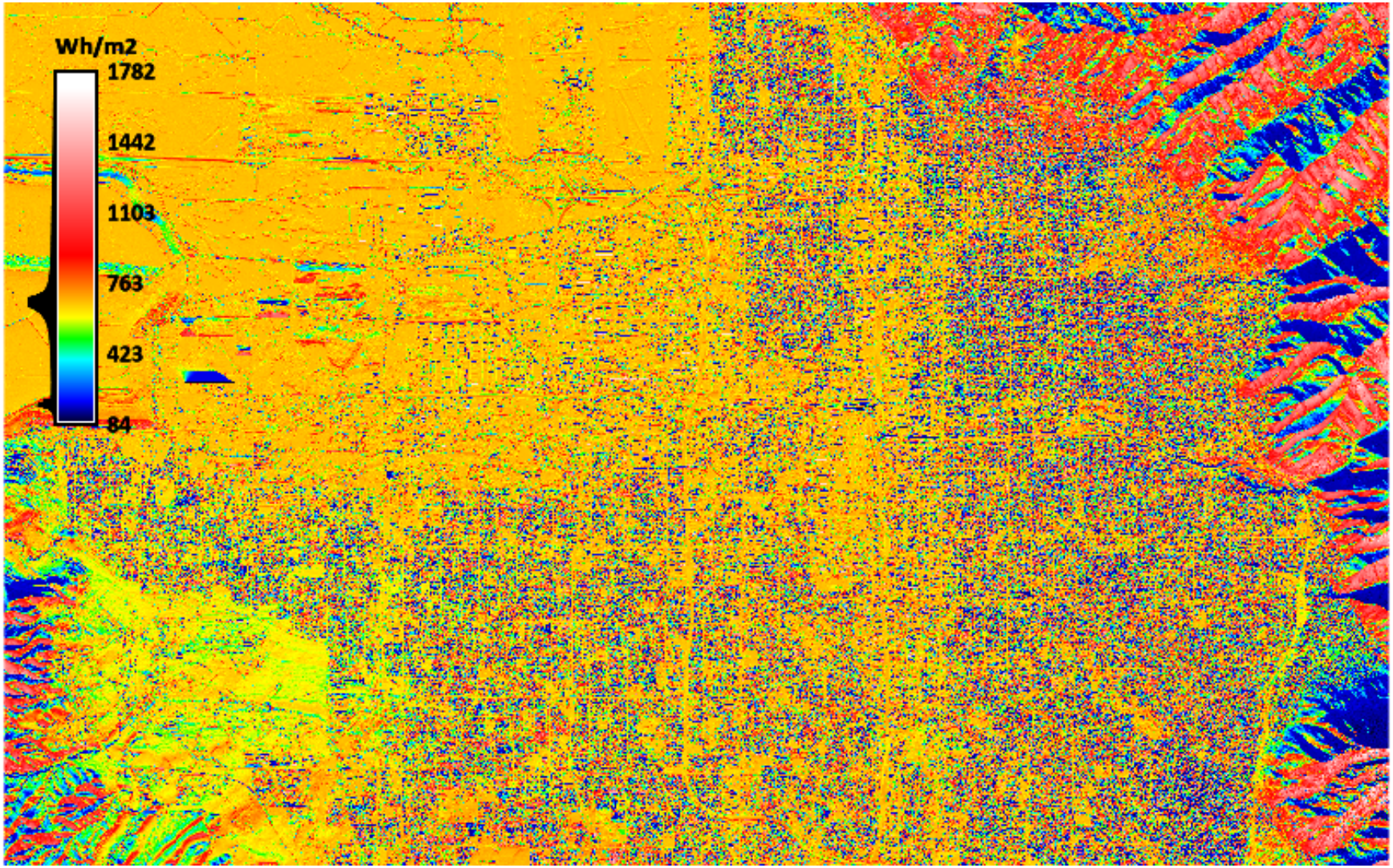

Figure 3.34. Figure showing the Salt Lake Valley PV electricity production at winter solstice with a 40^o tilt and $\eta_{PV} = 24\%$.

shading. The results are similar for each location with a tilt angle of 40^o, although because of the larger tilt, the irradiance is more normal to the intended surface, thus increasing the irradiance magnitude. Areas such as Taylorsville, West Valley, and Magna, which contain building developments consisting of more uniform building heights and relatively low vegetation, show similar results; however, the irradiance variation is less. The more uniform topography reduces the amount of shading within these areas. At a tilt angle of 10^o, many of these sub-regions may require larger cell efficiency, yet because of the more uniform topography, at a tilt angle of 40^o, these sub-regions may require a much less cell efficiency to produce the same amount of energy annually compared to the sub-regions within the eastern region. The downtown Salt Lake area contains buildings and structures consisting of nonuniform building heights that are closely spaced. Similar to the results in the previous sections, the PV potential for this area is lower at each tilt angle throughout the range of cell efficiency.

3.2.4 Varying Efficiency at Summer Solstice with Tilt Angle of 10^o and 40^o

Building power consumption during the summer months is typically much higher than that of the winter months. Human comfort in household and workplace environments is crucial for human well being and productivity. Typically, vapor compression air conditioning units are used during the summer months to cool the buildings within the desired temperature range. Not only do these air conditioning units require a tremendous amount of power, but the demand time is consistent for each sector in the valley; typically in the mid- to late afternoon, referred to as peak demand time [54]. Because of this high demand, utility grid electricity rates increase to a premium to compensate for the extra energy needed during these peak times [5, 60].

Considering utility programs such as net metering, building owners rely on PV electricity production during the summer months to supplement the extra power supply needed during the winter months. Therefore, excess PV power generation during the summer months is essential to not only meet the high demand loads required by the air conditioning units, but also to offset the needed supply during the winter months. With the different options for PV cell efficiency and the variability in tilt angle, a detailed analysis is crucial to meet the power generation requirements for the summer months. The following

figures are presented to illustrate the effects of varying efficiency throughout the valley. The analysis consists of 10^o and 40^o tilt angles while varying PV cell efficiencies at 2% increments ranging from 12% - 24% at summer solstice.

3.2.4.1 Efficiency at Summer Solstice Results

Figures 3.35 - 3.41 show the potential PV electricity generation for Salt Lake Valley at summer solstice as a function of the PV cell efficiency evaluated at a tilt angle of 10^o, while Figures 3.42 - 3.48 consist of a tilt angle of 40^o. In general, it is shown that the increase in cell efficiency is proportional to the increase in electricity potential, and as expected, the magnitude is much higher compared to that at winter solstice. Similar to each previous case study, the northwestern region has the highest PV potential within the valley at any given cell efficiency and tilt angle, while various sub-regions within the eastern and southern regions show the lowest potential. It is shown, at a tilt angle of 10^o, the PV potential for most sub-regions within eastern and southern regions is relatively low at each efficiency increment in comparison to the rest of the valley. At a tilt angle of 40^o, the PV potential becomes much better for most of the sub-regions.

The irradiation magnitude in the northwestern region continues to increase with each incremental step in PV cell efficiency at both tilt angles. The PV potential for the northwestern region is the highest in the valley due to its positioning with respect to the mountain ranges, the undeveloped land, and lower topographical density. These factors contribute to the high irradiance magnitude in comparison to the valley due to the lessened topographical shading. Most sub-regions within the northwestern region consist of PV potential that is high and reliable with respect to the local topography.

Similar to the previous results, various sub-regions within the eastern region may require a higher PV cell efficiency at a tilt angle of 10^o, whereas these same sub-regions would require a lower cell efficiency at a tilt angle of 40^o to produce the same amount of energy annually. Again, areas such as East Millcreek, Cottonwood, Holladay, and the eastern Salt Lake areas that consist of high density native and non-native landscape may require a larger cell efficiency to compensate for partial PV panel shading caused by the overgrown vegetation. The results are similar for each location with a tilt angle of 40^o, although because of the larger tilt, the irradiance is more normal to the intended surface,

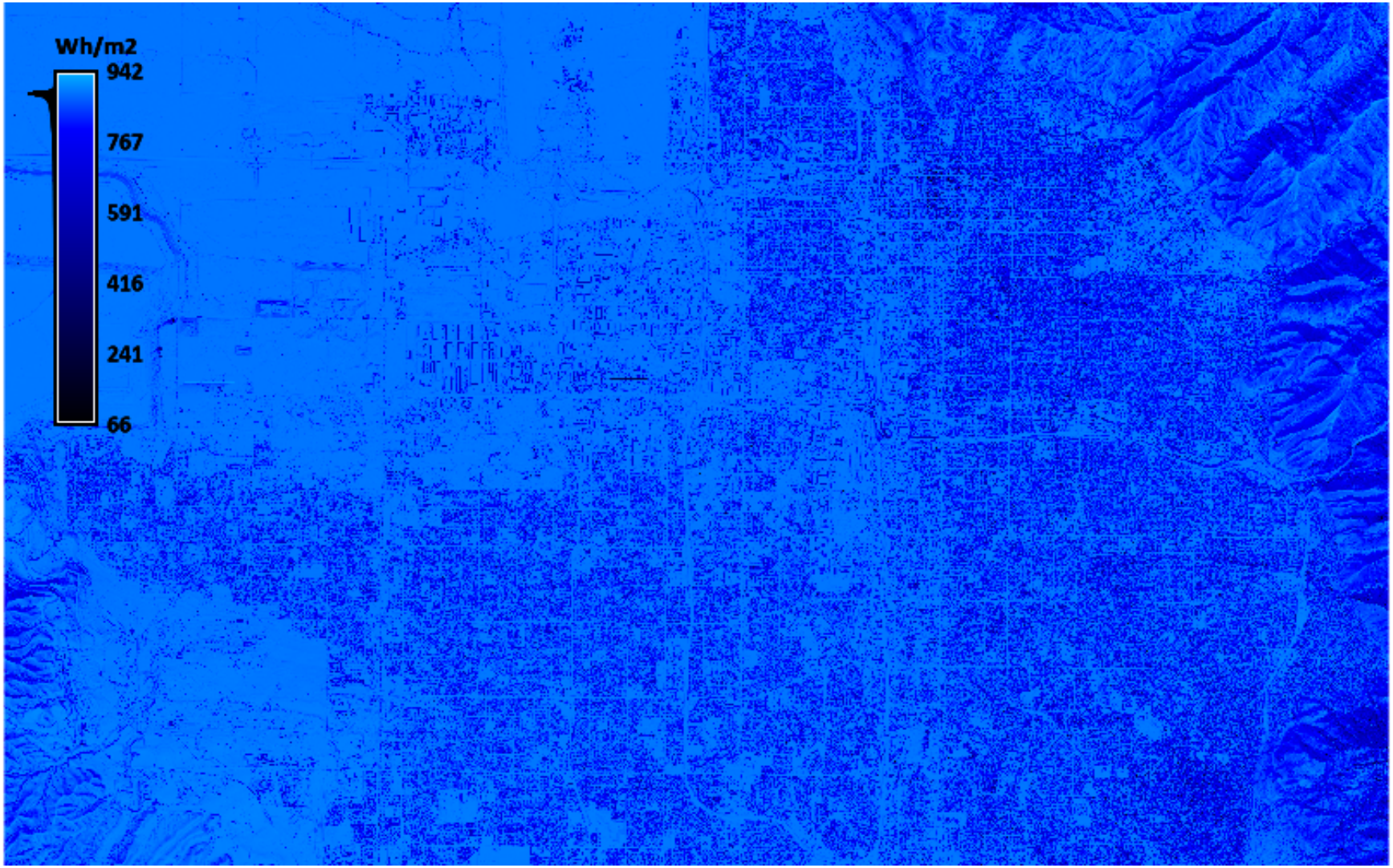

Figure 3.35. Figure showing the Salt Lake Valley PV electricity production at summer solstice with a 10^o tilt and $\eta_{PV} = 12\%$.

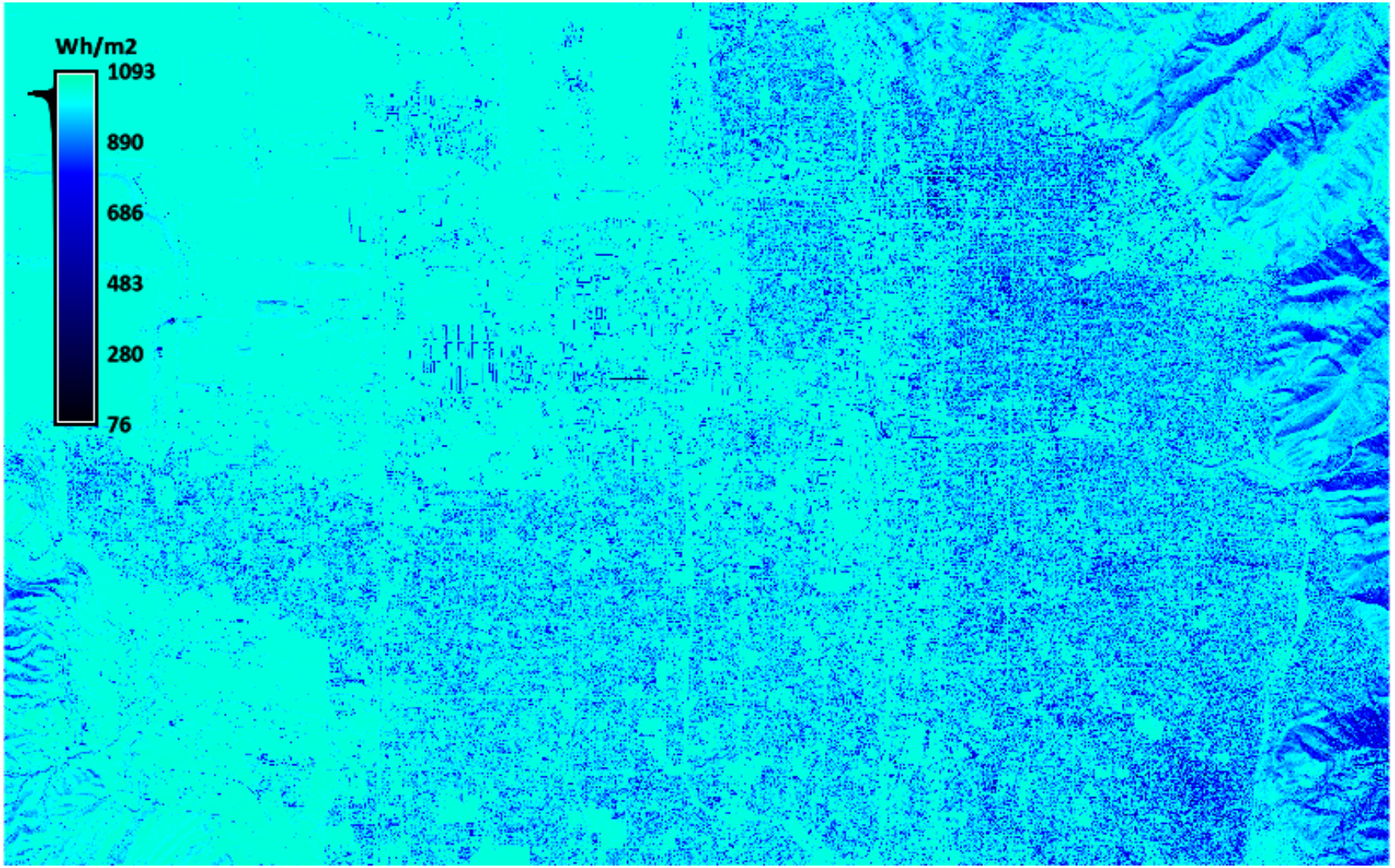

Figure 3.36. Figure showing the Salt Lake Valley PV electricity production at summer solstice with a 10^o tilt and $\eta_{PV} = 14\%$.

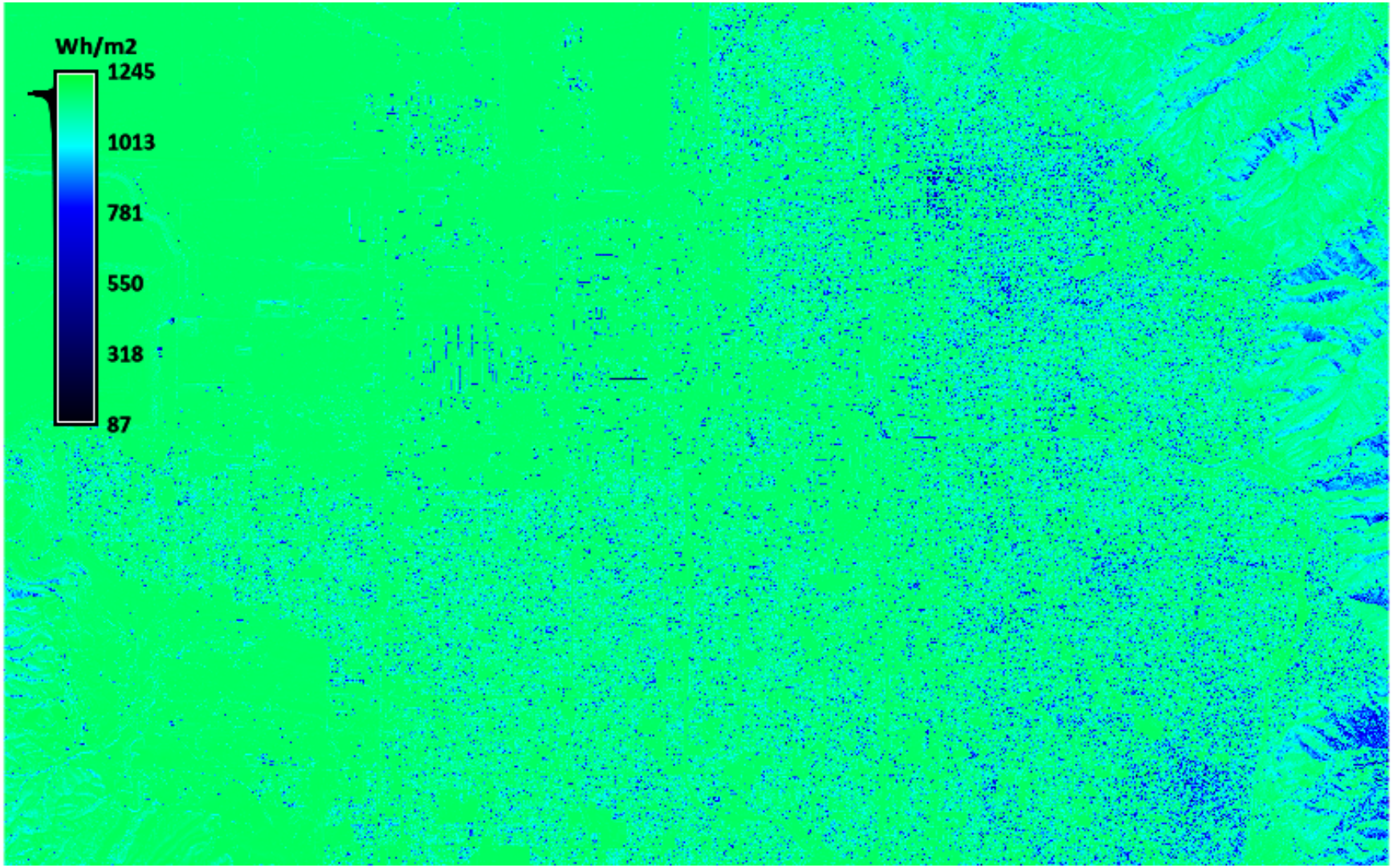

Figure 3.37. Figure showing the Salt Lake Valley PV electricity production at summer solstice with a 10^o tilt and $\eta_{PV} = 16\%$.

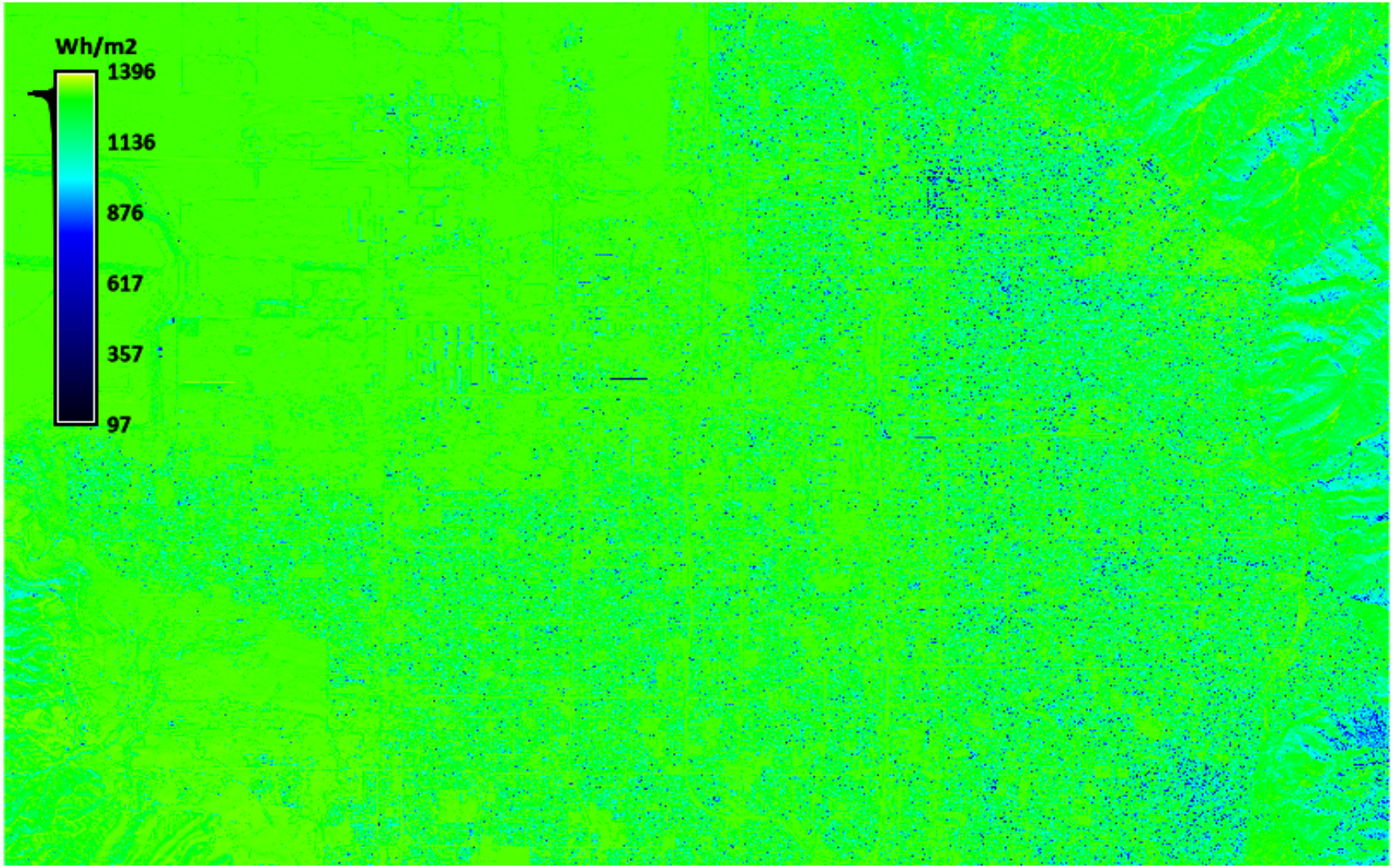

Figure 3.38. Figure showing the Salt Lake Valley PV electricity production at summer solstice with a 10^o tilt and $\eta_{PV} = 18\%$.

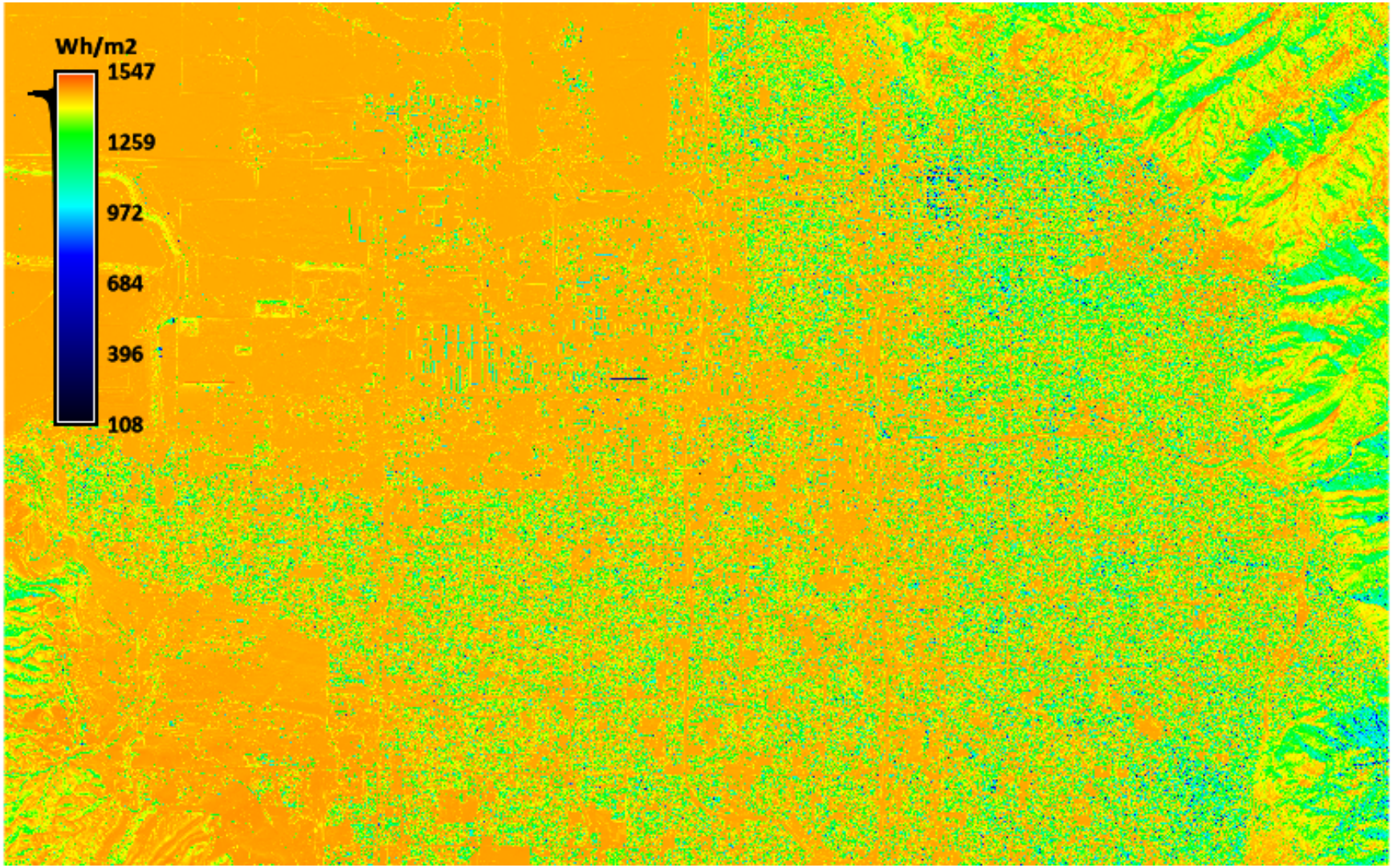

Figure 3.39. Figure showing the Salt Lake Valley PV electricity production at summer solstice with a 10^o tilt and $\eta_{PV} = 20\%$.

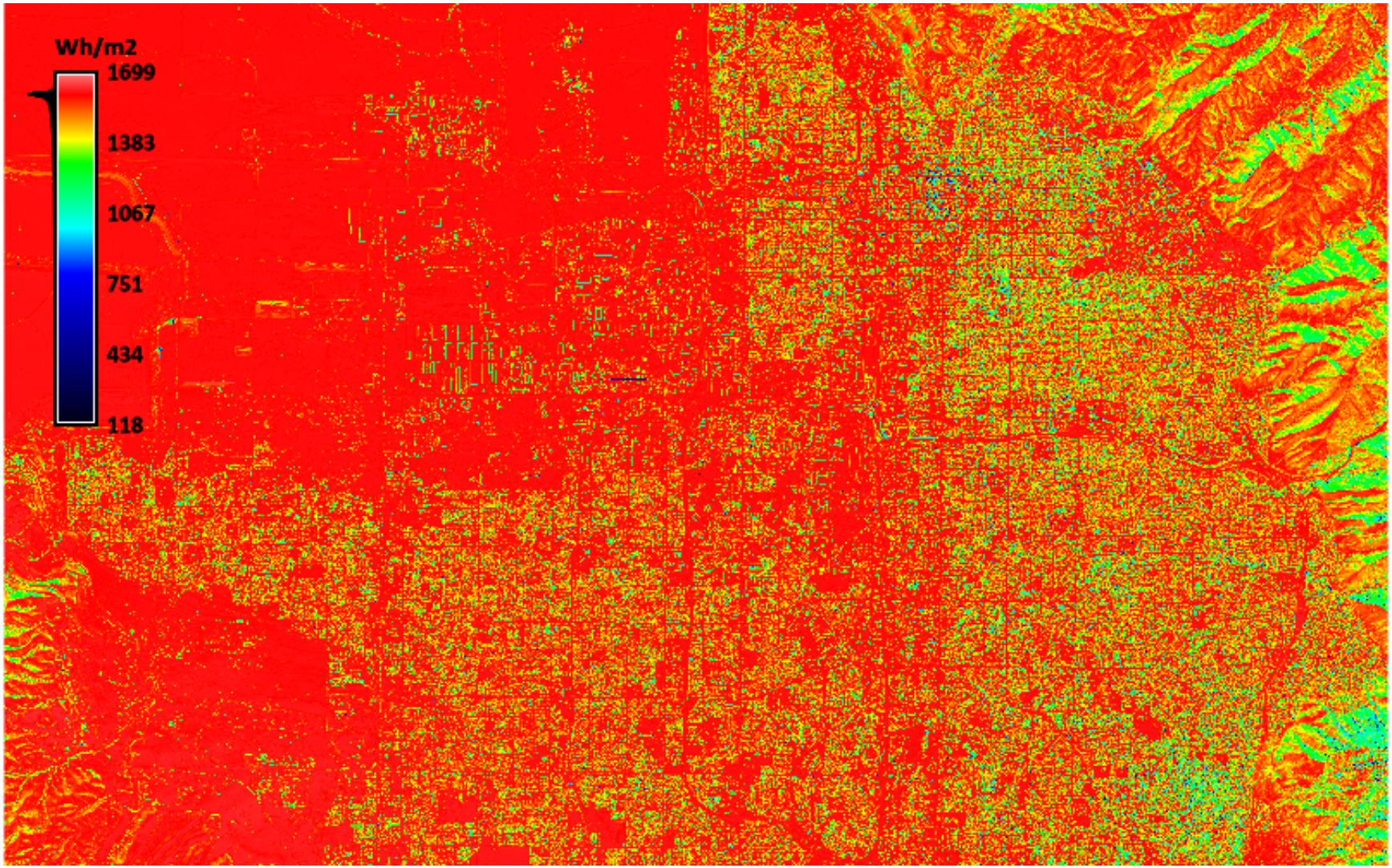

Figure 3.40. Figure showing the Salt Lake Valley PV electricity production at summer solstice with a 10^o tilt and $\eta_{PV} = 22\%$.

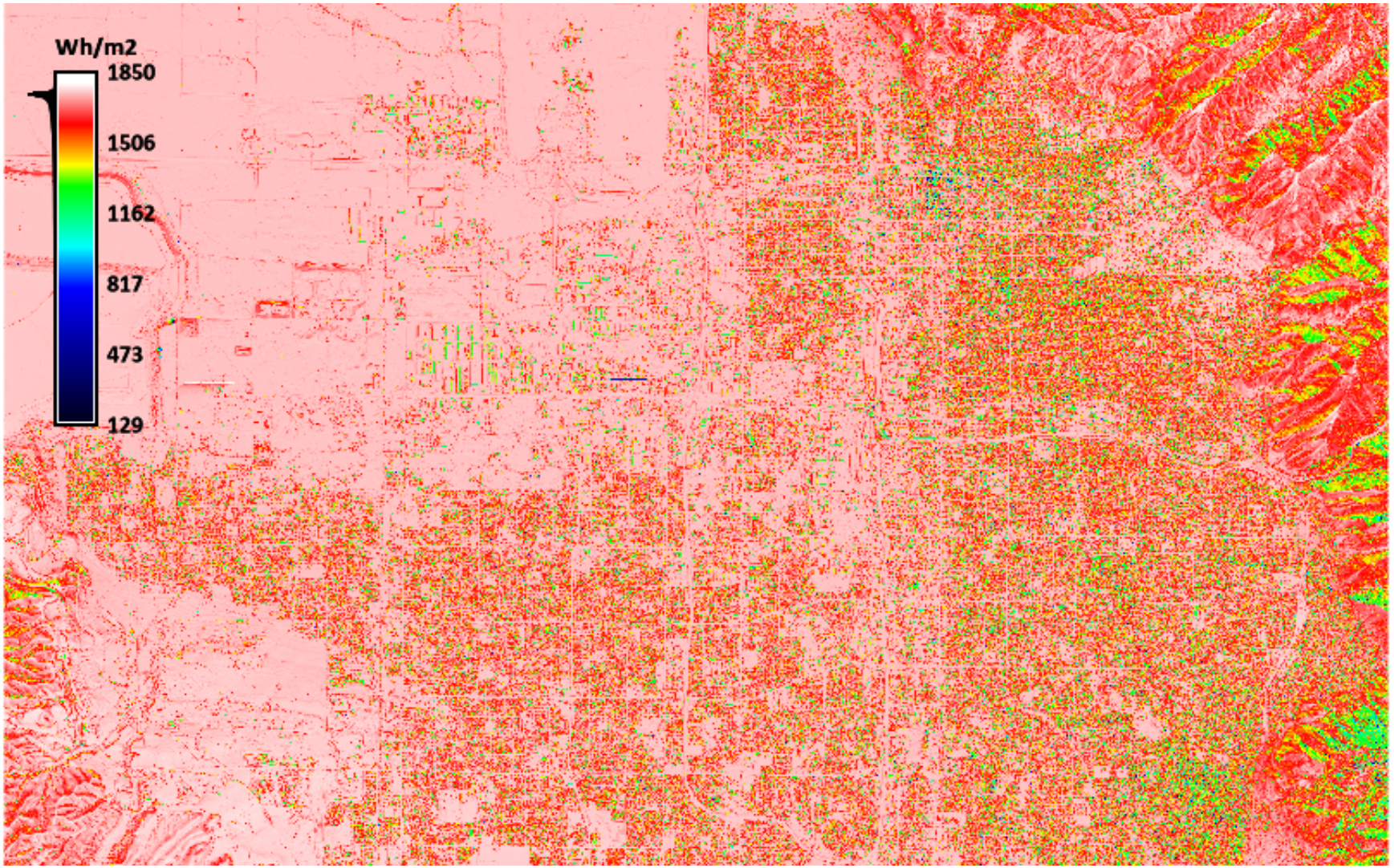

Figure 3.41. Figure showing the Salt Lake Valley PV electricity production at summer solstice with a 10^o tilt and $\eta_{PV} = 24\%$.

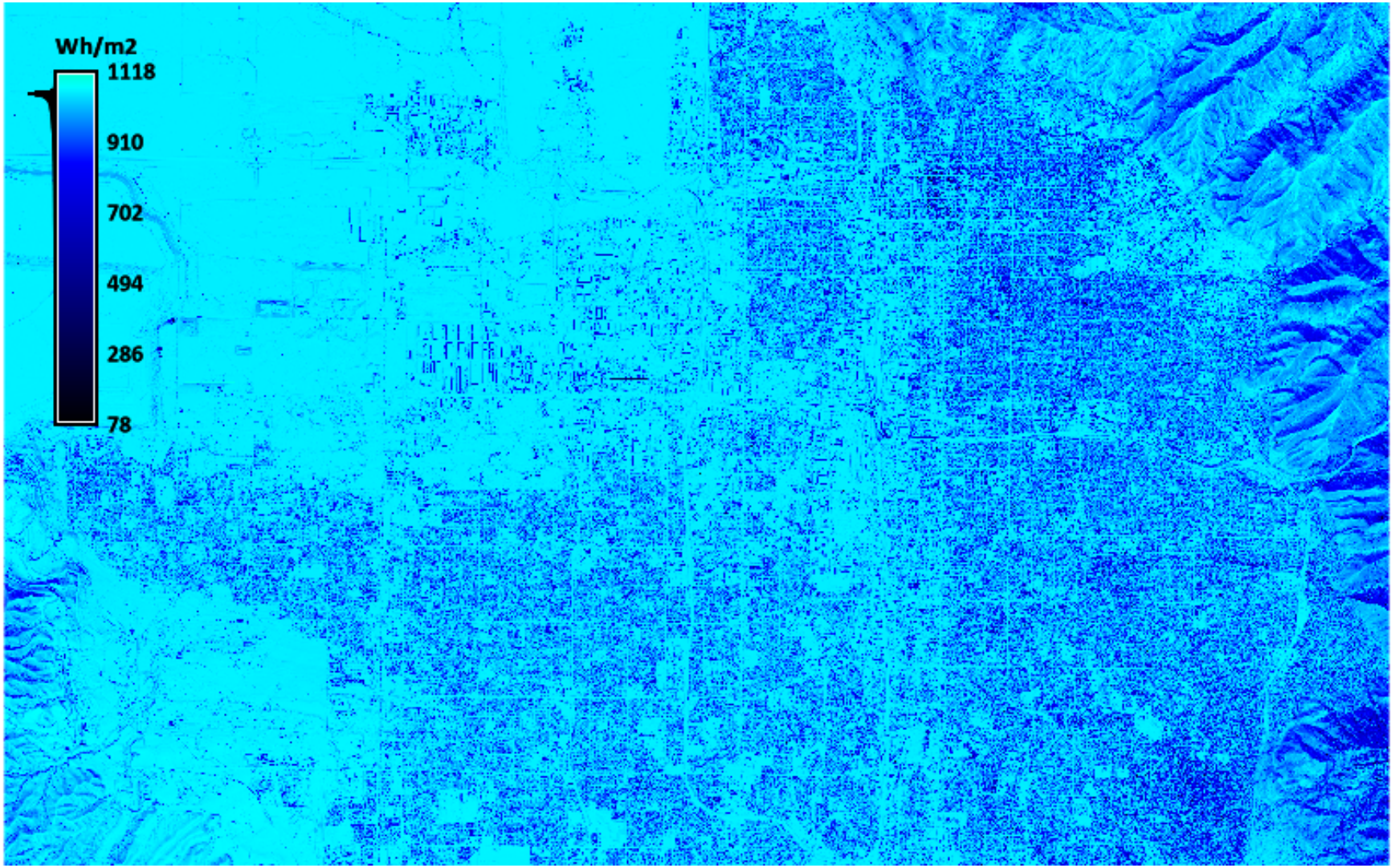

Figure 3.42. Figure showing the Salt Lake Valley PV electricity production at summer solstice with a 40^o tilt and $\eta_{PV} = 12\%$.

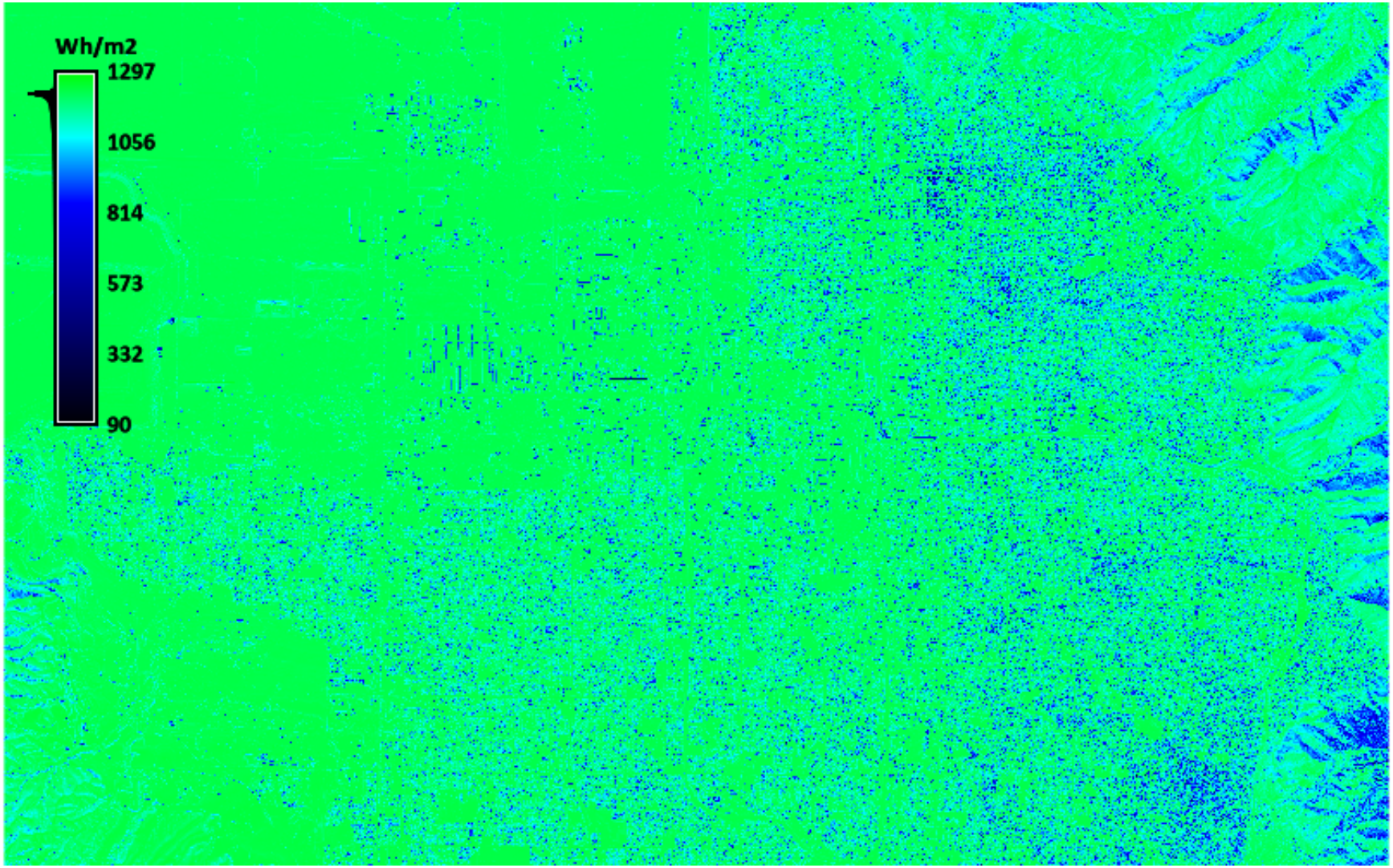

Figure 3.43. Figure showing the Salt Lake Valley PV electricity production at summer solstice with a 40^o tilt and $\eta_{PV} = 14\%$.

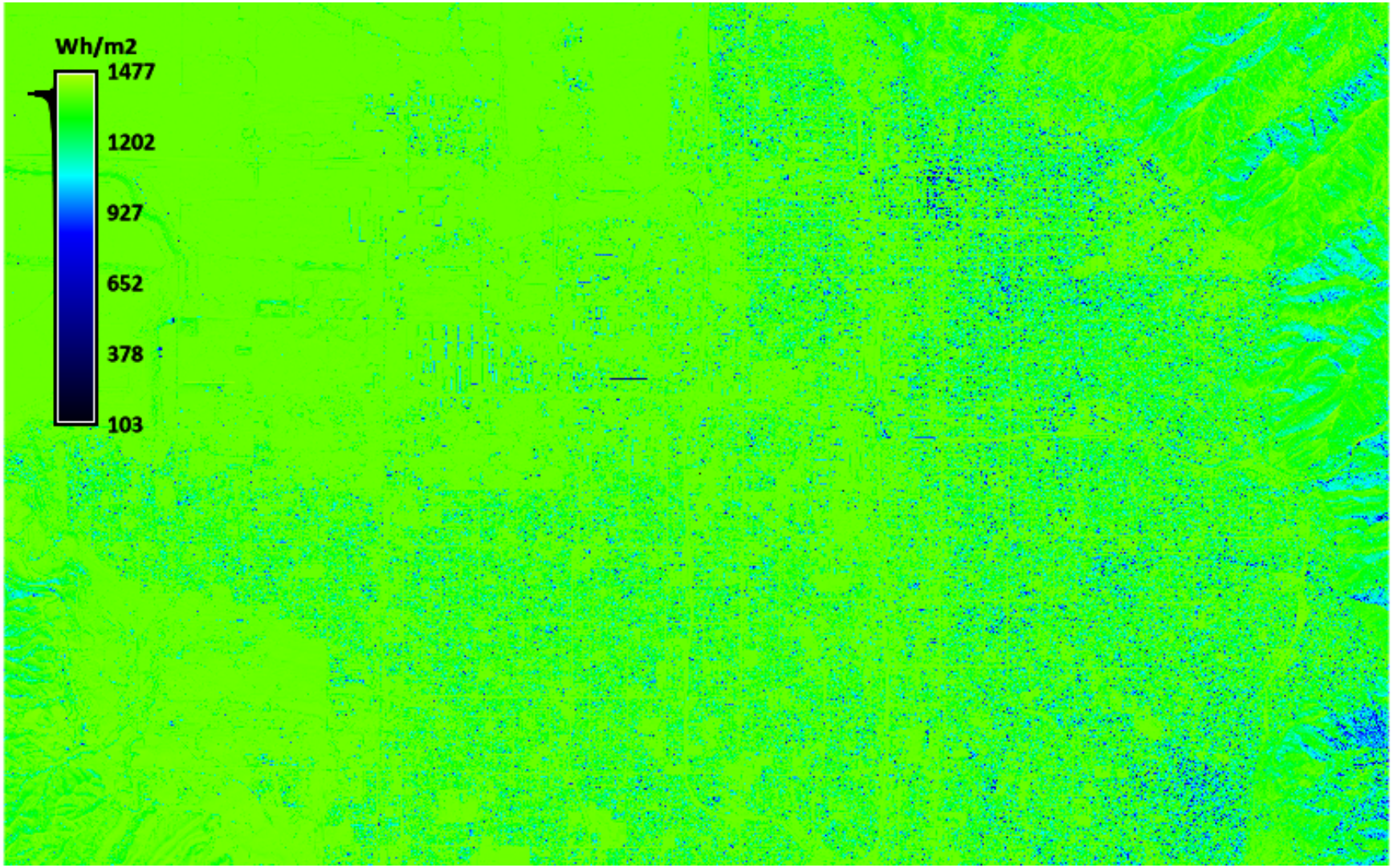

Figure 3.44. Figure showing the Salt Lake Valley PV electricity production at summer solstice with a 40^o tilt and $\eta_{PV} = 16\%$.

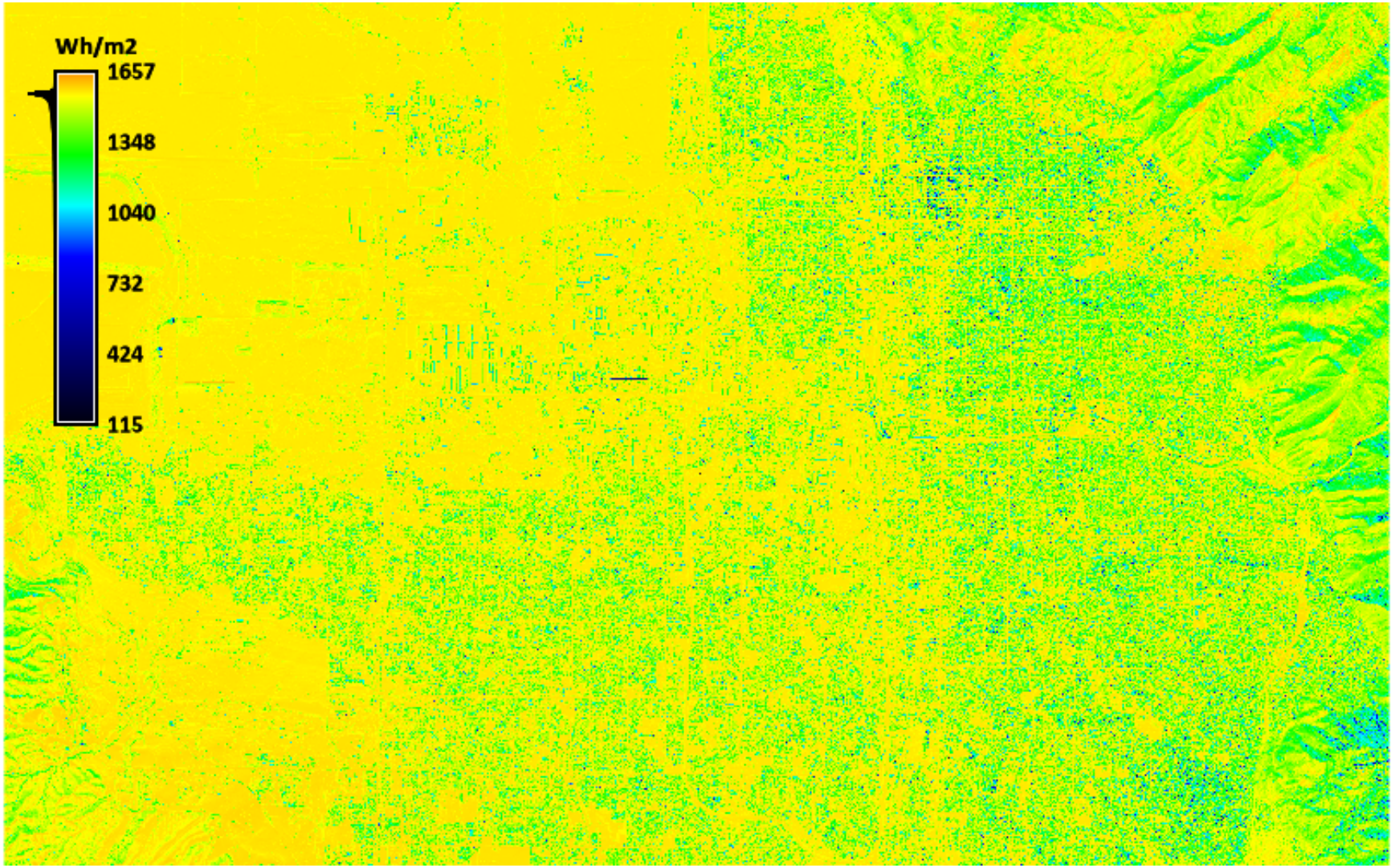

Figure 3.45. Figure showing the Salt Lake Valley PV electricity production at summer solstice with a 40^o tilt and $\eta_{PV} = 18\%$.

Figure 3.46. Figure showing the Salt Lake Valley PV electricity production at summer solstice with a 40^o tilt and $\eta_{PV} = 20\%$.

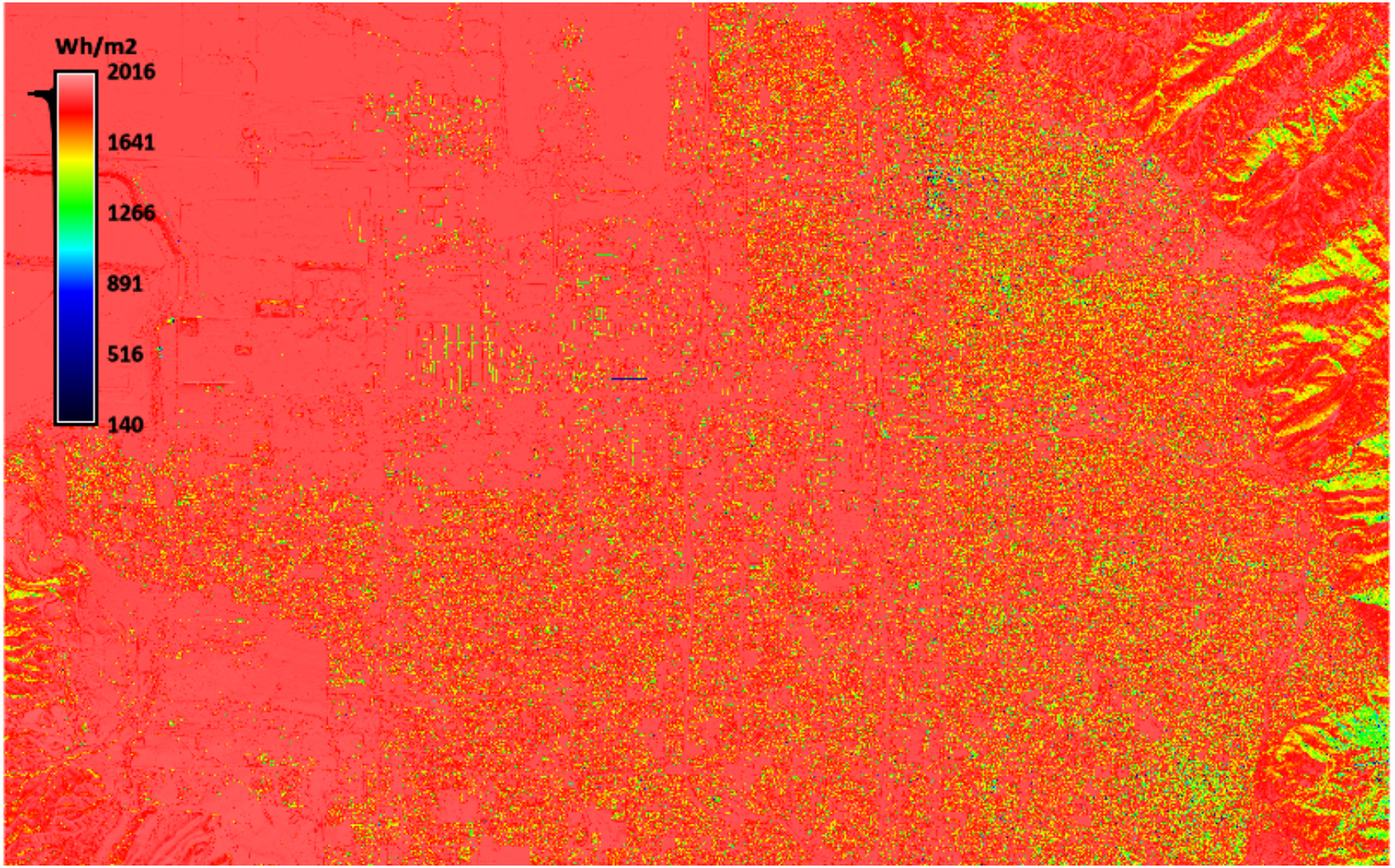

Figure 3.47. Figure showing the Salt Lake Valley PV electricity production at summer solstice with a 40^o tilt and $\eta_{PV} = 22\%$.

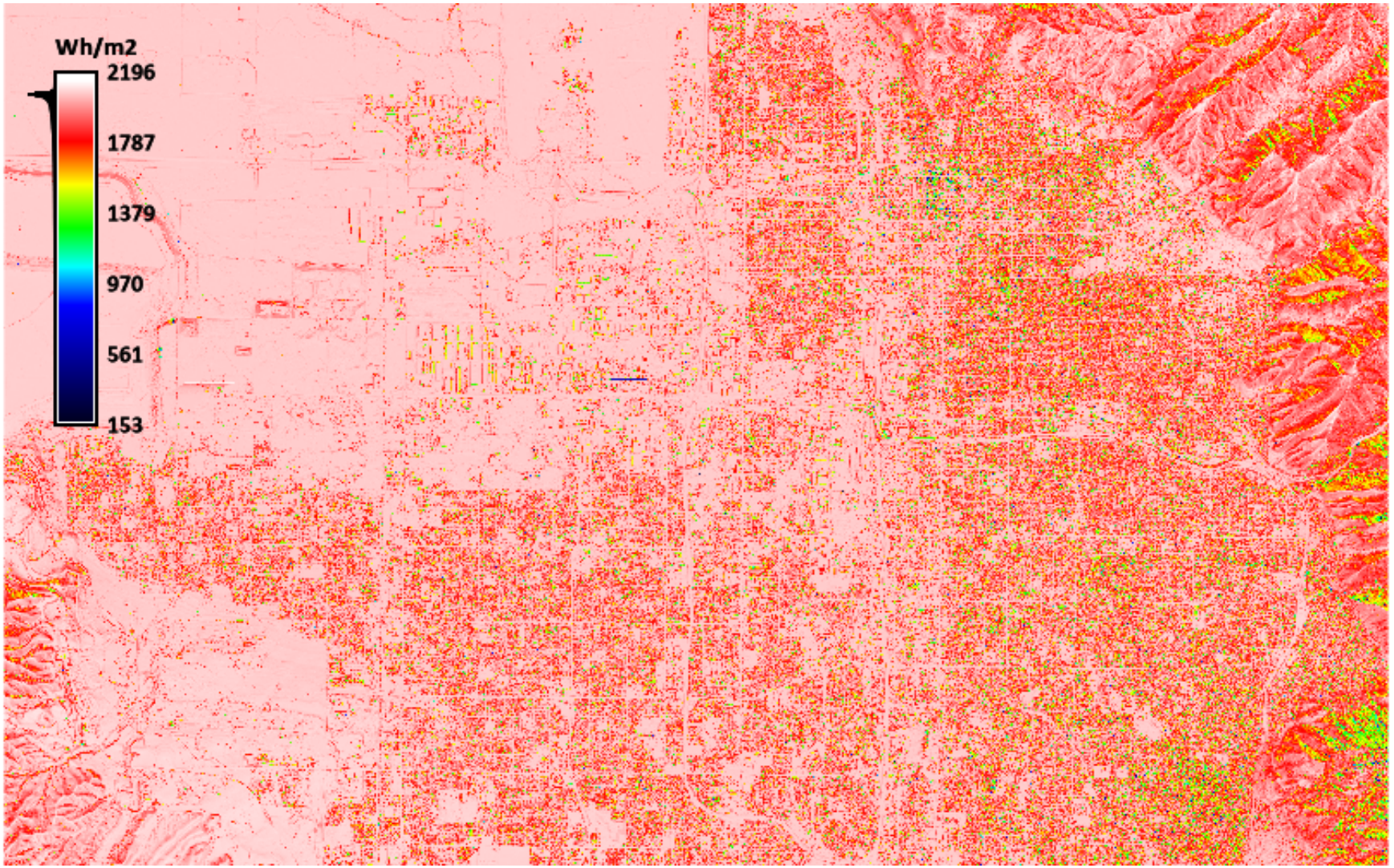

Figure 3.48. Figure showing the Salt Lake Valley PV electricity production at summer solstice with a 40^o tilt and $\eta_{PV} = 24\%$.

thus increasing the irradiation magnitude. Areas such as Taylorsville, West Valley, and Magna, which contain building developments consisting of more uniform building heights and relatively low vegetation, show similar results, yet the sub-regions within are fewer than that of the eastern region. At a tilt angle of 10^o, much of these sub-regions may require a larger cell efficiency, yet because of the more uniform topography, at a tilt angle of 40^o, these sub-regions may require a much lower cell efficiency to produce the same amount of energy annually compared to the sub-regions within the eastern region. The downtown Salt Lake areas show better PV potential compared to that at winter solstice because of the higher sun altitude angle that results in less shading, although in comparison with the rest of the valley, the area shows the lowest potential with each cell efficiency and tilt angle.

3.3 Levelized Cost of Electricity

To understand the economics and feasibility of a renewable energy technology, it is necessary to determine its cost effectiveness. Levelized cost of electricity (LCOE) is a bench-marking tool or method used to assess the economics of an energy technology, indicating a break even point when relating them to different energy sources [61]. The method considers the life cycle cost of an energy technology and the produced energy over the life cycle to obtain a cost per unit of energy, typically expressed as \$/kWh. The purpose of this tool is to compare renewable energy prices to that of fossil fuel energy purchased from the grid. Implementing this method in a renewable energy assessment is paramount to successfully identifying its feasibility, yet is difficult to achieve given the uncertainty of the inputs. The LCOE for a generic energy source is expressed as:

$$LCOE = \frac{Total\ Lifetime\ Cost}{Total\ Lifetime\ Energy\ Production} \tag{3.1}$$

The total lifetime cost of the system can include multiple parameters such as initial costs, which includes permitting, labor, materials, interest if financing, maintenance/operating, insurance (often required if financing), and government incentives [62–65]. These are often the main cost parameters associated to the LCOE of an energy system, although government incentives are not always applicable.

If the total cost includes parameters that incur future costs, a discount rate must be

included in the calculation that may vary with circumstance, location, and time. Because the LCOE methodology is very sensitive to the input parameters, the determination of a discount rate usually consists of a sensitivity analysis [62]. Another parameter to consider for projecting future LCOE values is the learning curve. Studies have shown that the cost associated with the production of goods tend to decline with time [63]. The learning curve is used to adjust the initial cost when projecting a LCOE for a future system, which is not useful for a current LCOE.

Site-to-site LCOE values for a given energy system may differ due to the variance of parameters. For a roof top PV system, the initial cost may vary depending on the mounting structure. Building code and permitting requires an analysis of the roof structure and its ability to support the load of the system [53]. Certain buildings may need reinforcement to maintain its structural integrity while supporting the load of an array. The maintenance cost will vary dependent upon the materials used, although only occasional cleaning is typically considered [64]. Insurance costs will vary depending on the surrounding structures and landscape. The energy produced by the system is dependent upon the mounting structure orientation and the surrounding topography. Each parameter in the LCOE method has the possibility to vary between locations, which shows that each potential system within a given region will consist of its own unique LCOE value.

Now consider the LCOE of a PV system with a typical life cycle of 25 years [62]. The assumption is made here that the only cost associated with the system is the initial cost (C_i) and the government incentives (I_G). In this case, the initial cost does not include financing, although it is necessary to include this in the analysis in such a scenario. The LCOE for a PV system can be expressed as:

$$LCOE = \frac{\sum_{t=0}^{25} C_i - I_G}{\sum_{t=0}^{25} E(1-d)} \tag{3.2}$$

Each PV panel is designated an annual degradation rate (d); PV power production reduces relatively linearly each year while rapidly reducing after 25 years or its specific warranty. The degradation rate is used to estimate PV power output (E) for each year. The summation of the annual energy production is determined by estimating PV power output each year over the technology's life cycle.

PV system costs have continually fallen as of 2016. The cost for residential, commercial, and utility scale systems were reported to be \$2.93, \$2.13, and \$1.42/W [46], which were based on a 5.6, 200, and 100,000 kW systems, respectively. Several factors contribute to these costs such as equipment, sizing, and labor. Residential PV systems are most costly due to the higher labor requirements and small purchase orders, whereas utility scale sites have a more streamlined approach and acquire discounted pricing for the large material orders. An acquisition of the LCOE for the residential and commercial sectors in the Salt Lake Valley was constructed and shown below. The installation cost as previously mentioned and government incentives discussed in Chapter 1 were used along with a $\eta_{PV} = 15\%$, $\eta_{In} = 95\%$, and data from a relevant retail PV panel [66]. Average residential and commercial grid electricity prices were reported to be \$0.111/kWh and \$0.0884/kWh [67], respectively, for the year 2016. These are the pricing set points that indicate the undesirable areas for potential PV power generation.

Figures 3.49 and 3.50 indicate the locations in Salt Lake Valley that are viable for PV power generation with respect to the residential and commercial sectors. The areas shown in red indicate locations that have a LCOE of half that of the average electricity pricing for the sector shown in 2016. Within the red to white transition spectrum, LCOE decreases accordingly, while the yellow to black transition spectrum indicates undesirable locations.

Sub-regions within the eastern and southern regions, show an elevated LCOE as expected due to the dense landscape and topography. Factors such as tilt angle and PV cell efficiency have implementation possibilities for theses sub-regions, thereby reducing the LCOE. The more open areas with a more uniform topographical distribution such as the northwestern region show a lower LCOE, indicating a more profitable system for utility owners or a less costly system for building owners. Although the results in the previous sections showed lower PV potential for the downtown Salt Lake area, the LCOE is relatively low with respect to the commercial sector. However, several other areas within the valley show poor LCOE values regarding the commercial sector, while increasing with the inclusion of the downtown Salt Lake area when considering the residential sector.

Because PV system installation pricing for commercial buildings is lower, and the government incentive package is larger, far more areas are feasible for the implementation of PV power generation systems in the commercial sector. The two figures shown in this

Figure 3.49. Figure showing the LCOE of Salt Lake Valley for the residential sector

Figure 3.50. Figure showing the LCOE of Salt Lake Valley for the commercial sector

section indicate the necessity for a thorough PV assessment when considering a power generation system. Failure to do so could result in a lower than anticipated economic benefit.

CHAPTER 4

CONCLUSION AND FUTURE WORK

The results obtained by this research describe the variability and cost effectiveness of potential PV power generation systems within Salt Lake Valley. The objectives specified in Chapter 1 were achieved and evaluated throughout this manuscript. Figure 2.3 shows the capabilities of GIS software when coupled with LiDAR data, in creating a model that captures the solar radiation potential for a given region, with inclusion of the local topography. The figure describes the effects of the unique topography found within Salt Lake Valley with respect to PV potential and its spatial variation. In comparison to Figure 2.2, it was shown that the model presented by NREL, and the database currently used for PV assessments, doesn't fully capture the true irradiation data for Salt Lake Valley.

The mountain ranges that surround the valley cast morning and evening shadows, which affects the magnitude of irradiation at various sub-regions along the far east and west side of the valley, as presented within Figures 3.1-3.46. Furthermore, the figures show the higher PV potential in the northwestern region that consists of reduced vegetation and a more uniform building height distribution, with distantly spaced building footprints. However, the results differ in various sub-regions found within the eastern and parts of the southern regions, which are highly developed and consist of dense native and non-native landscaping. However, most of these highly developed regions showed favorable results with an increased tilt angle, cell efficiency, or both. Similarly, the downtown Salt Lake area consisting of nonuniform building heights showed lower PV potential at any given tilt angle or PV cell efficiency in comparison to other regions within the valley.

The LCOE was presented for the residential and commercial sectors within the valley in Figures 3.47 and 3.48. The LCOE variation was shown throughout the valley presenting the sub-regions that fall below the current price point regime indicating undesirable locations for PV power generation systems. As expected, the results showed sub-regions

consisting of dense vegetation and nonuniform building height distributions comprising the highest LCOE and least economical locations for PV power generation systems. However, the LCOE was shown to be relatively low for both sectors within much of the valley, although the commercial sector showed better results due to the lower installation pricing and the higher PV system incentive package given at both the federal and state tax level.

The work presented in this manuscript has many opportunities for expansion, modification, and applications. The model was constructed at a 3 meter spatial resolution for computational purposes, yet the LiDAR data available for the Salt Lake Valley region consist of a half meter resolution. Utilizing multiple computers operating in a parallel scheme or allowing for longer simulation times would take advantage of this fine resolution and thus give more detailed results. This would allow for assessments in great detail regarding optimal panel placement with respective cell efficiency. For example, the assessment could include a single building in similar detail to that of Figure 2.1, which would indicate areas that receive the most irradiation. Using this approach, the assessment could include a cost-optimized rooftop PV generation design.

Cloud data are an optional input parameter to the model that contain atmospheric cloud properties and positioning. By using cloud data in the model, resulting irradiance values would better resemble the area of interest. However, these data are difficult to obtain as it takes years of measurements to accurately describe the phenomena, and considering the current climate change, future predictions are far from reach. However, if the data are unobtainable, the model has capabilities of calibration to local pyranometer data to give similar results, although this too is dependent on previous data. With the implementation of expected cloud cover, a user could obtain more accurate estimations of solar irradiance at the site of interest, which would allow for better estimations of predicted power generation and LCOE.

Salt Lake Valley is unique and interesting because of the surrounding mountain ranges, foothills, and local topography. However, this is the scenario in many regions within Utah and the surrounding states. This modeling approach could be implemented into any region that has the availability of spatial geographical data. With the increase in utility scale installations, utility companies may benefit by commissioning a study to obtain this data for the region of interest. This would allow for a better understanding of the power

production on a temporal basis.

With the transition of fossil fuels toward renewable energy, it is paramount that a thorough PV assessment is conducted to better predict power generation. With the exponential growth of PV installations and continuing outlook, a method such as this could better assist utility grid management teams in fossil fuel power generation demand, thus lowering primary emissions. Although the manuscript was focused toward PV power generation, the same method is applicable for solar thermal technology assessments. This transition may be a difficult challenge, but a healthy future is at risk, which necessitates the pioneering in power generation technology.

REFERENCES

[1] U. Desa, "World urbanization prospects, the 2011 revision," *Final Report with Annex Tables. New York, NY: United Nations Department of Economic and Social Affairs*, 2012.

[2] E. L. Glaeser and M. E. Kahn, "The greenness of cities: Carbon dioxide emissions and urban development," *Journal of Urban Economics*, vol. 67, no. 3, pp. 404–418, 2010.

[3] J. Laird, "PV's falling costs: In the U.S., the DOE is pioneering research in order to reduce the cost of installed PV to below a dollar-per-Watt by 2017.," *Renewable Energy Focus*, vol. 12, no. 2, pp. 52–56, 2011.

[4] N.C. Clean Energy Technology Center, *DSIRE*, 2017. http://www.dsireusa.org/.

[5] Solar Energy Industries Association, *Solar Industry Data*, January 2017. http://www.seia.org/research-resources/solar-industry-data.

[6] Salt Lake City, *Solar PV Information*, 2016. http://www.slcgov.com/building/solar-pv-information.

[7] PV-Tech, *SunEdison to develop 262MW of solar in Utah*, 2016. http://www.pv-tech.org/news/sunedison-to-install-262mw-of-solar-in-utah .

[8] National Renewable Energy Laboratory, *National Solar Radiation Database*, 2016. https://nsrdb.nrel.gov.

[9] P. Redweik, C. Catita, and M. Brito, "Solar energy potential on roofs and facades in an urban landscape," *Solar Energy*, vol. 97, pp. 332–341, 2013.

[10] H. T. Nguyen and J. M. Pearce, "Incorporating shading losses in solar photovoltaic potential assessment at the municipal scale," *Solar Energy*, vol. 86, pp. 1245–1260, May 2012.

[11] J. R. Simpson, "Improved estimates of tree-shade effects on residential energy use," *Energy and Buildings*, vol. 34, pp. 1067–1076, Nov 2002.

[12] L. Wiginton, H. Nguyen, and J. Pearce, "Quantifying rooftop solar photovoltaic potential for regional renewable energy policy," *Computers, Environment and Urban Systems*, vol. 34, pp. 345–357, jul 2010.

[13] Y.-w. Sun, A. Hof, R. Wang, J. Liu, Y.-j. Lin, and D.-w. Yang, "GIS-based approach for potential analysis of solar PV generation at the regional scale: A case study of Fujian Province," *Energy Policy*, vol. 58, no. 2013, pp. 248–259, 2013.

[14] J. Hofierka and M. Suri, "The solar radiation model for Open source GIS: implementation and applications," 2002.

[15] J. Hofierka and J. Kauk, "Assessment of photovoltaic potential in urban areas using open-source solar radiation tools," *Renewable Energy*, vol. 34, pp. 2206–2214, 2009.

[16] T. Santos, N. Gomes, S. Freire, M. C. Brito, L. Santos, and J. A. Tened??rio, "Applications of solar mapping in the urban environment," *Applied Geography*, vol. 51, pp. 48–57, 2014.

[17] GRASS Development Team, *Geographic Resources Analysis Support System (GRASS GIS) Software*. Open Source Geospatial Foundation, USA, 2015. http://grass.osgeo.org.

[18] Open Topography, *High-Resolution Topography Data and Tools*, 2016. http://opentopo.sdsc.edu/datasets.

[19] M. Weiss and A. M. Newman, "A guide to writing articles in energy science," *Applied Energy*, vol. 88, no. 11, pp. 3941–3948, 2011.

[20] GRASS Development Team, *GRASS GIS*. Open Source Geospatial Foundation, 2015. https://en.wikipedia.org/wiki/GRASSGIS.

[21] GRASS Development Team, *LiDAR*. Open Source Geospatial Foundation, 2016. https://grasswiki.osgeo.org/wiki/LIDAR.

[22] J. Krcho, "Morphometric analysis and digital models of georelief," *Veda, Bratislava*, vol. 432, 1990.

[23] M. Jenco, "Distribution of direct solar radiation on georelief and its modelling by means of complex digital model of terrain," *Geograficky casopis*, vol. 44, pp. 342–355, 1992.

[24] R. Kittler and J. Mikler, "Basis of the utilization of solar radiation," *VEDA, Bratislava*, p. 150, 1986.

[25] J. Greif and K. Scharmer, "European solar radiation atlas," *Commission of European Communities, Directorate general, science, research and development. École des Mines de Paris, Paris*, 2000.

[26] M. Šúri and J. Hofierka, "A new gis-based solar radiation model and its application to photovoltaic assessments," *Transactions in GIS*, vol. 8, no. 2, pp. 175–190, 2004.

[27] M. Šúri, T. A. Huld, and E. D. Dunlop, "Pv-gis: a web-based solar radiation database for the calculation of pv potential in europe," *International Journal of Sustainable Energy*, vol. 24, no. 2, pp. 55–67, 2005.

[28] S. Liang, C. J. Shuey, A. L. Russ, H. Fang, M. Chen, C. L. Walthall, C. S. Daughtry, and R. Hunt, "Narrowband to broadband conversions of land surface albedo: Ii. validation," *Remote Sensing of Environment*, vol. 84, no. 1, pp. 25–41, 2003.

[29] NASA, *Moderate Resolution Imaging Spectroradiometer*, 2017. https://modis.gsfc.nasa.gov/.

[30] A. Cescatti, B. Marcolla, S. K. Santhana Vannan, J. Y. Pan, M. O. Román, X. Yang, P. Ciais, R. B. Cook, B. E. Law, G. Matteucci, M. Migliavacca, E. Moors, A. D. Richardson, G. Seufert, and C. B. Schaaf, "Intercomparison of MODIS albedo retrievals and in situ measurements across the global FLUXNET network," *Remote Sensing of Environment*, vol. 121, pp. 323–334, 2012.

[31] E. G. Moody, M. D. King, S. Platnick, C. B. Schaaf, and F. Gao, "Spatially complete global spectral surface albedos: Value-added datasets derived from terra modis land products," *IEEE Transactions on Geoscience and Remote Sensing*, vol. 43, no. 1, pp. 144–158, 2005.

[32] K. W. Oleson, G. B. Bonan, C. Schaaf, F. Gao, Y. Jin, and A. Strahler, "Assessment of global climate model land surface albedo using modis data," *Geophysical Research Letters*, vol. 30, no. 8, 2003.

[33] F. Gao, C. B. Schaaf, A. H. Strahler, A. Roesch, W. Lucht, and R. Dickinson, "Modis bidirectional reflectance distribution function and albedo climate modeling grid products and the variability of albedo for major global vegetation types," *Journal of Geophysical Research: Atmospheres*, vol. 110, no. D1, 2005.

[34] H. Akbari, S. Menon, and A. Rosenfeld, "Global cooling: increasing world-wide urban albedos to offset CO2," *Climatic Change*, vol. 94, pp. 275–286, Jun 2009.

[35] F. Linke, "Transmissions-koeffizient und Trübungsfaktor," *Beiträge zur Physik der freien Atmosphäre*, no. 10, pp. 91–103, 1922.

[36] P. Ineichen and R. Perez, "A new airmass independent formulation for the Linke turbidity coefficient," *Solar Energy*, vol. 73, no. 3, pp. 151–157, 2002.

[37] M. Chaâbane, M. Masmoudi, and K. Medhioub, "Determination of Linke turbidity factor from solar radiation measurement in northern Tunisia," *Renewable Energy*, vol. 29, no. 13, pp. 2065–2076, 2004.

[38] F. Kasten, "Linke turbidity factor based on improved values of the integral rayleigh optical thickness," *Solar Energy*, vol. 56, no. 3, pp. 239–244, 1996.

[39] P. Ineichen, "Conversion function between the Linke turbidity and the atmospheric water vapor and aerosol content." 2008.

[40] National Renewable Energy Laboratory, "U.S. Data — National Solar Radiation Database (NSRDB)," tech. rep., National Renewable Energy Laboratory.

[41] J. Hofierka, M. Suri, and T. Huld, "GRASS GIS manual: r.sun," tech. rep., 2007.

[42] M. A. Green, K. Emery, Y. Hishikawa, W. Warta, and E. D. Dunlop, "Solar cell efficiency tables (Version 45)," *Progress in Photovoltaics: Research and Applications*, vol. 23, pp. 1–9, jan 2015.

[43] S. White, *Solar photovoltaic basics : a study guide for the NABCEP entry level exam*.

[44] C. Bianchi and A. D. Smith, "Effects of irradiance and ambient temperature on a decision-making tool for rooftop PV array sizing for commercial buildings," 2016.

[45] National Renewable Energy Laboratory Weather Data, *Salt Lake City International Airport TMY3 Weather Data*, 2015. https://energyplus.net/weather.

[46] R. Fu, D. Chung, T. Lowder, D. Feldman, K. Ardani, and R. Margolis, "U.S. Solar Photovoltaic System Cost Benchmark: Q1 2016," tech. rep., NREL, 2016.

[47] Solar Edge, *Power Optimizer*, 2017. https://www.solaredge.com/us/products/power-optimizer/.

[48] Enphase, *Micro Inverter*, 2017. https://enphase.com/en-us/products-and-services/microinverters.

[49] I. H. Rowlands, B. P. Kemery, and I. Beausoleil-Morrison, "Optimal solar-PV tilt angle and azimuth: An Ontario (Canada) case-study," *Energy Policy*, vol. 39, no. 3, pp. 1397–1409, 2011.

[50] A. K. Yadav and S. S. Chandel, "Tilt angle optimization to maximize incident solar radiation: A review," *Renewable and Sustainable Energy Reviews*, vol. 23, pp. 503–513, 2013.

[51] S. M. Lucich, *Modeling Carbon Dioxide Emissions Reductions for Three Commercial Reference Buildings in Salt Lake City*. PhD thesis, 2015.

[52] F. Kreith and S. Krumdieck, *Principles of Sustainable Energy Systems*. CRC Press, 2014.

[53] B. Brooks, *Solar America Board for Codes and Standards*, 2015. http://www.solarabcs.org/about/publications/reports/expedited-permit.

[54] M. Hummon, P. Denholm, and R. Margolis, "Impact of photovoltaic orientation on its relative economic value in wholesale energy markets," 2012.

[55] J. D. Rhodes, C. R. Upshaw, W. J. Cole, C. L. Holcomb, and M. E. Webber, "A multi-objective assessment of the effect of solar PV array orientation and tilt on energy production and system economics," *Solar Energy*, vol. 108, pp. 28–40, 2014.

[56] T. A. Deetjen, J. B. Garrison, J. D. Rhodes, and M. E. Webber, "Solar PV integration cost variation due to array orientation and geographic location in the Electric Reliability Council of Texas," 2016.

[57] Rocky Mountain Power, *Net Metering Service*, 2015. https://www.rockymountainpower.net/content/dam/rocky_mountain_power.

[58] Solar Simplified, *Net Metering in Utah*, 2015. http://solarsimplified.org/connecting-to-the-grid/net-metering-in-utah.

[59] Salt Lake City Planning Commission, *Salt Lake City Zoning Ordinance*, 2011. http://www.slcdocs.com/Planning/Projects/Sust/Ord20.pdf.

[60] Rocky Mountain Power, *Rocky Mountain Power Energy Charges Billing Terms*, February 2015. https://www.rockymountainpower.net/ya/kyb/dbt.html.

[61] T. T. D. Tran, K. Park, and A. D. Smith, "System scaling approach and thermoeconomic analysis of a pressure retarded osmosis system for power production with hypersaline draw solution: A Great Salt Lake case study," 2017.

[62] K. Branker, M. Pathak, and J. Pearce, "A review of solar photovoltaic levelized cost of electricity," *Renewable and Sustainable Energy Reviews*, vol. 15, pp. 4470–4482, dec 2011.

[63] J. Hernández-Moro and J. Martínez-Duart, "Analytical model for solar PV and CSP electricity costs: Present LCOE values and their future evolution," *Renewable and Sustainable Energy Reviews*, vol. 20, pp. 119–132, apr 2013.

[64] M. Campbell, J. Blunden, E. Smeloff, and P. Aschenbrenner, "Minimizing utility-scale PV power plant LCOE through the use of high capacity factor configurations," in *2009 34th IEEE Photovoltaic Specialists Conference (PVSC)*, pp. 000421–000426, IEEE, jun 2009.

[65] S. B. Darling, F. You, T. Veselka, and A. Velosa, "Assumptions and the levelized cost of energy for photovoltaics," *Energy & Environmental Science*, vol. 4, p. 3133, Aug 2011.

[66] Canadian Solar, *Canadian Solar CS6k Series PV Cells*, 2017. https://canadiansolar.com.

[67] U.S. Energy Information Administration, *Average Retail Price of Electricity*, March 2017. https://www.eia.gov/electricity/data/browser.